공학박사 학위논문

Characteristics of High Viscous Oil-Gas Flow in Downward Vertical Pipes

수직 하방 관내 고점성 오일-가스 2상 유동 특징 연구

2016년 2월

서울대학교 대학원

에너지시스템공학부

정 성 훈

Characteristics of High Viscous Oil-Gas Flow in Downward Vertical Pipes

지도교수 강 주 명

이 논문을 공학박사 학위논문으로 제출함

2015년 12월

서울대학교 대학원

에너지시스템공학부

정 성 훈

정성훈의 공학박사 학위논문을 인준함

2016년 1월

위 원 장 _____ (인)

부위원장 _____ (인)

위 원 _____ (인)

위 원 _____ (인)

위 원 _____ (인)

Abstract

Characteristics of High Viscous Oil-Gas Flow in Downward Vertical Pipes

Sunghoon Chung

Department of Energy Systems Engineering

The Graduate School

Seoul National University

There is a recent interest on the production of medium to heavy oils in offshore environments. The use of multiphase pumps located in platforms has been proposed to ensure the transport of the fluids to the shoreline facilities. After the platform, the multiphase flow stream is redirected to the sea floor using a down comer. Thus, the understanding of the viscosity effect in downward vertical flow becomes critical for the system design.

An experimental study on the viscosity effect has been carried out using a 2-in. ID multiphase flow facility. The viscosity of the oil ranged from 127 to 586 mPa·s. The superficial gas and liquid velocities varied from 0.3 to 7 m/s and 0.05 to 0.7 m/s, respectively. Flow pattern, pressure gradient and liquid holdup data were acquired and compared with previous

air-water experiments.

Three different flow patterns have been identified based on visual observations and capacitance sensor readings. Flow pattern, superficial velocities and viscosity effects on pressure gradient and liquid holdup are presented. Comparisons with available mechanistic models and simulators are reported. Existing mechanistic models dominantly predicts flow pattern as slug flow, and over-predicts average liquid holdup especially low liquid viscosity condition.

To ensure applicability of existing annular flow model, experimental data of upward flow for high viscosity oil. As a result, closure relationship is affordable for vertical upward flow due to its low liquid entrainment fraction, while it shows disappointing prediction performance in vertical downward flow.

Keywords : two-phase flow, vertical downward flow, high viscosity, pipe flow, flow pattern, pressure gradient, average liquid holdup

Student Number : 2010-30260

Table of Contents

List of Tables

List of Figures

Chapter 1 Introduction

The petroleum production system consists of vertical and horizontal pipe networks and thereby the accurate analysis of multiphase flow, e.g. oil, water, and gas, have been essential to accomplish the optimality in production and transportation. A large number of experimental and modeling studies on multiphase flow have been carried out owing to its importance in industrial applications.

1.1 Multiphase Flow of Heavy Oil in Vertical Downward Pipes

Flow characteristic of multiphase flow is highly affected by the pipe inclination due to the effect of gravity. Pipe inclination determines the direction of gravity. The difference of densities among the phases causes the buoyant force, resulting the slippage between gas and liquid. Thus flow characteristics of vertical downward flow are quite different from those of vertical upward flow due to the difference of gravity direction. Flow patterns appearing in vertical pipes are shown in Figure 1.1.

In vertical upward flow, the gravity obstructs the flow of fluids and buoyant force helps the gas to flow faster. Accordingly, it has a tendency of high liquid holdup and pressure drop comparing horizontal condition. A dominant flow pattern is slug flow. In downward flow, however, as the

orientation of gravity is towards mean flow direction, heavier phase (i.e. liquid phase) becomes easy to flow resulting relatively lower liquid holdup. As potential energy of fluids can compensate frictional energy loss and could have small or negative pressure drop.

There is a recent interest on the production of medium to heavy oils in offshore environments (Table 1.1). The heavy oil is defined to have the range from 100 to 10,000 mPa·s. In offshore field, the use of multiphase pumps located in platforms has been proposed to ensure the transport of the fluids to the shoreline facilities or FPSO (Floating production storage and offloading) units. After the platform, the multiphase flow stream is redirected to the sea floor using a down comer. In heavy oil field, to overcome the limited oil mobility, the multiphase flow of oil-gas mixture are considered as an option for transportation.

As the water depths of offshore heavy oil fields vary from hundreds to thousands of feet, the understanding of the viscosity effect in downward vertical flow becomes critical for the system design. Unlike any light oil, any multiphase transportation and production system controlling high viscous and dense liquid requires facilities with high specifications that overcomes high frictional pressure drop, which is frequently challenging in offshore field owing to the spatial limitations of platform. Hence the recent concern of heavy oil and multiphase flow increases the necessity to evaluate two factors, i.e. the pressure drop and the liquid holdup, accurately (Wang et al., 2014). In spite of its importance in heavy oil production, however, commonly used laboratory liquids in most of studies on vertical downward two-phase flow

have viscosities less than 20 mPa·s.

The quantitative analysis related to liquid viscosity in pipes have been limited at experimental observations and the development of a mechanistic model that shows poor accuracy with experimental results (Gokcal, 2008; Kora, 2010). As the liquid viscosity increases, slug liquid hold up, translational velocity, and slug frequency are changed.

Table 1.1 List of offshore heavy oil fields

Field	**Status**	**Depth (ft)**	**Operator**	**Country**	**Viscosity (mPa·s)**
Captain	Producing	350	Chevron	UK	50-150
Mariner	Under Dev.	363	Statoil	UK	67 & 508
Bentley	Under Dev.	373	Xcite Energy	UK	1,500
Kraken	Under Dev.	386	EnQuest PLC	UK	78-161
Bressay	Discovered	337	Statoil	UK	540
Pazflor	Producing	2,369-3,399	Total	Angola	3,000 (dead oil)
Jubarte	Producing – Under Dev.	4,505	Petrobras	Brazil	3,000 (dead oil)

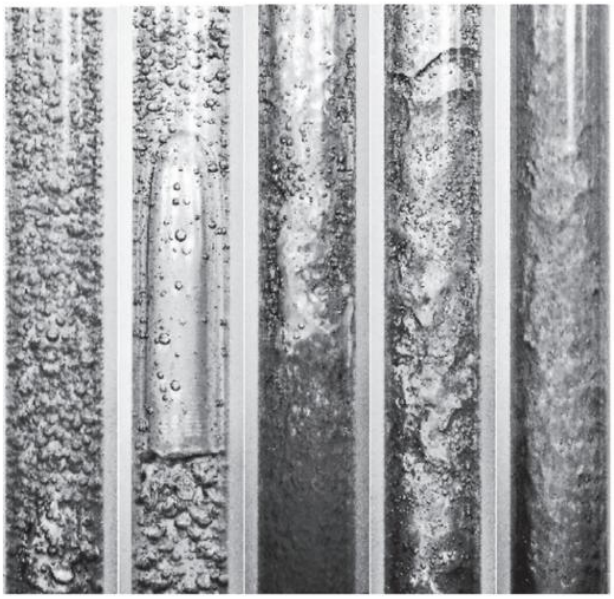

(a) Vertical upward flow (Godbole et al., 2011)

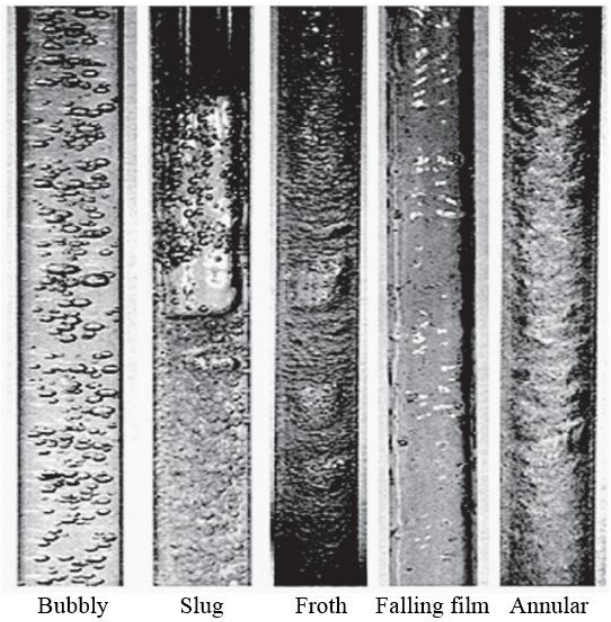

(b) Vertical downward flow (Bhagwat and Ghajar, 2011)

Figure 1.1 Flow patterns in vertical two phase flow

1.2 Motivation

In petroleum industries, relatively few investigations in vertical downward two-phase flow have been reported. Downward flow has been traditionally encountered in relatively short length of pipes in offshore production operations while vertical upward flow can be easily encountered in production wells and risers. Most of the studies on vertical downward flow are based on chemical and nuclear engineering scheme with air-water two-phase conditions and small pipe diameter. The major concern of these studies is to predict gas void fraction instead pressure drop of the pipe. But in petroleum industry, pressure gradient should be considered as one of main parameter.

The motivation of this research divides into two necessities: to examine the prediction performance of existing mechanistic model and to analyze the influenced factors to determine both of pressure drop and liquid holdup integrating experimental and numerical studies, quantitatively.

Some mechanistic models have been developed for various flow inclination of angle (Barnea, 1987; Zhang, et al, 2003; Gokcal, 2008; Kora, 2010). These models show dissatisfied matching for two-phase flow containing high viscous liquid but they fail to find the causes and remain quantitative investigations based on experimental results with high viscous oil and gas flow. However, as can be seen in previous studies by the University of Tulsa (Gokcal, 2008; Kora, 2010), existing mechanistic models show dissatisfied performance for two-phase flow with high viscosity liquids. Similarly, prediction performance for vertical downward flow with high

viscosity liquid is still unclear. As Troniewski and Spisak (1987) reported, however, high liquid viscosity has a possibility to result different flow characteristics.

1.3 Objectives of Study

The main objective of this project is to perform experimental and modeling study for two-phase downward flow in vertical pipes with high-viscosity-oil. A 50.8-mm-ID (2-in.) and 22.72-m-long horizontal test section was used in this experimental study. The experiments were conducted with various oil viscosities, namely, 586 mPa·s, 401 mPa·s, 213 mPa·s, and 127 mPa·s, corresponding to oil temperatures of 70 °F, 80 °F, 100 °F, and 120 °F. The selected oil viscosities cover medium to high oil viscosities.

The effect of high viscosity oil on two-phase behavior was investigated. The targeted flow parameters are flow pattern, pressure drop and average liquid holdup. Specific features were analyzed from experimental measurements. And the performance of existing correlations and models for different parameters as flow patterns, pressure gradient, and average liquid holdup are evaluated against acquired experimental data. Finally, existing closure relationship are quantitatively examined on its applicability on various flow conditions.

1.4 Structure of the Dissertation

This study is divided into 6 chapters as described below and some other related information is provided in appendices:

Chapter 1 provides an introduction to the dissertation, defining the problems, objectives of the study and structure of the dissertation.

Chapter 2 contains a review of published work on vertical downward flow and effect of liquid viscosity on two-phase flow.

Chapter 3 gives the description of details on test fluids, test matrix, a description of the experimental facility, instrumentation, data acquisition and processing, and an uncertainty analysis.

Chapter 4 contains the results from the experiment and findings.

Chapter 5 provides the discussion on model comparison and applicability of existing correlations.

Chapter 6 pieces together all the key conclusions from this study. And, recommendations for further work are also provided.

Chapter 2 Literature Review

2.1 Gas-Liquid Two-phase Vertical Downward Flow

Many empirical correlations and mechanistic models have been developed for two-phase downward flow in vertical pipes. The empirical correlations are developed by obtaining mathematical relations between known parameters and design variables, such as pressure gradient and liquid holdup, based on experimental data. Empirical correlations are often limited by the range of data used in the development of the correlation.

The mechanistic models are based on fundamental principles (conservation of mass, momentum and energy). These models require the prediction of the flow pattern to model multiphase flow in pipes. Consequently, for the predicted flow pattern, a hydrodynamic model can be used to predict both of pressure gradient and liquid holdup. If a mechanistic model can predict the flow behavior in all the flow patterns at a given inclination angle, it is called a comprehensive mechanistic model. On the other hand, when a mechanistic model can predict the flow behavior in all flow patterns and for all inclination angles is referred to as a unified model.

In this section, a summary of well-known two-phase vertical downward flow empirical correlations is reviewed first. Then a review of the unified models for two-phase flow is presented.

2.1.1 Comprehensive correlations

For vertical downward concurrent flow, most of the studies are based on chemical and nuclear engineering scheme with air-water two-phase conditions and small pipe diameter. As the major concern of these studies is to predict gas void fraction accurately, most of them did not consider the calculation of pressure gradient.

Oshinowo and Charles (1974) experimentally investigated flow pattern correlation, liquid holdup and pressure drop in vertical downward flow. They suggested empirical correlations for flow pattern transition and claimed that Lockhart-Martinelli scheme met with limited success while the scheme was satisfactory in correlating frictional pressure drop and holdup in upward flow.

Yamazaki and Yamaguchi (1979) experimentally studied transition of flow pattern in vertical downward flow. They also suggested empirical correlations for void fraction and pressure drop prediction.

Barnea et al. (1982) and Usui (1989) identified transition criteria of flow patterns for two-phase downward flow. Barnea et al. divided downward flow with three patterns; annular, slug and dispersed bubble while Usui subdivided annular flow into annular flow and falling film flow.

Mukherjee and Brill (1985) investigated empirical equations to predict flow patterns transition for different inclination angles including horizontal and vertical flow. They claimed that flow regime map for downward flow conformed more to the Mandhane et al. (1974) while the

transition of upflow were similar to those proposed by Duns and Ros (1963).

Barnea (1987) combined different mechanistic models proposed for horizontal, near horizontal, upward vertical, downward vertical, upward inclined, and downward inclined to propose a unified model for predicting flow pattern transitions for the whole range of pipe inclinations. In addition to pipe geometry, the model considers fluid properties and flow conditions.

Usui and Sato (1988) investigated correlation to predict the average void fraction for each flow regime including falling film and annular drop flow.

A set of studies investigating the prediction of void fraction in vertical downward flow are based on similar drift flux concept; Goda et al (2003), Hibiki et al. (2004), Ishii et al. (2004), and Sun et al. (2004).

Kim et al. (2003) experimentally investigated flow pattern correlation. It was found that the flow regimes in the co-current downward flow strongly depend on the channel size.

Bhagwat and Ghajar (2012) compared characteristics of Vertical Upward and Downward Flow. They tested the performance of the Void Fraction Correlations and proposed top five performing correlations.

2.1.2 Unified Models

Gomez et al. (2000a) proposed a unified steady-state two-phase flow mechanistic model for the prediction of flow pattern, liquid holdup and pressure drop that is applicable to the range of inclination angles from

horizontal to vertical. The model adapts Barnea et al. (1987) unified model for flow pattern prediction. For slug flow, Gomez et al. used Taitel and Barnea (1990) slug flow model with a new developed slug liquid holdup closure relationship. For annular flow, Gomez et al. extended Alves et al. (1991) model to the entire range of inclination angles.

Zhang et al. (2003a and 2003b) developed a unified hydrodynamic model (TUFFP unified model) to predict flow pattern transitions, pressure gradient, and liquid holdup for all inclination angles from -90° to 90°. The model is based on the dynamics of slug flow and is applicable to all pipe geometries and fluid properties. The momentum equations for slug flow were used to predict flow pattern transitions from intermittent flow to other flow patterns. In this model, the defined flow patterns are bubble, intermittent, and stratified/annular flows. This classification is based on hydrodynamic characteristics of each flow pattern. Model prediction was compared with experimental data that included different pipe diameters, flow patterns, inclination angles, fluid physical properties, and gas-liquid flow rates. The comparisons showed agreement for both flow pattern and hydrodynamic behavior predictions.

2.2 Effect of Liquid Viscosity on Two-Phase Flow

Ros (1961) conducted a dimensional analysis study and eliminated irrelevant dimensionless groups characterizing pipe inclination angle, wall contact angle, gas viscosity, and wall roughness. The retained dimensionless groups characterize liquid viscosity, pipe diameter, velocity ratio, liquid velocity and gas-liquid density ratio. It was reported that at higher oil viscosities (51.5, 290 and 337 mPa·s) the increase in pressure gradient is not only due to an increase in friction factor but also due to the higher slippage between gas and liquid, especially at low liquid flow rates.

Nadler and Mewes (1995) conducted experiments with viscosity range of 1.0 to 37.0 mPa·s, and investigated the effect of liquid viscosity on slug flow for horizontal pipes keeping other fluid physical properties constant. Their experimental results indicated that when viscosity of liquid increased, the average liquid holdup increased.

Nuland (1999) experimentally studied the effect of liquid viscosity on slug liquid holdup. Experiments were conducted with liquid viscosity of 50 mPa·s to 400 mPa·s in horizontal pipes. Nuland (1999) concluded that the effect of viscosity on slug liquid holdup is weak in comparison to the effect of flow rates.

Furukuwa & Fukano (2001) experimentally studied the effect of liquid viscosity on flow patterns in upward vertical gas-liquid two-phase flow. Water and two different concentrations of aqueous glycerol solutions with viscosities up to 15 mPa·s were used in a 19.2 mm ID vertical pipe. They

concluded that flow pattern transitions are dependent on liquid viscosity.

Colmenares et al. (2001) studied pressure drop and flow pattern models for horizontal slug flow for viscous oils. Their experimental results suggested that the slug flow region in the flow pattern map enlarged when the oil viscosity increased. They also evaluated existing slug models, and concluded that the Taitel and Barnea (1990) model was the best candidate to be used for high viscosity oils. A modified model was developed by using experimental data for a liquid viscosity of 480 mPa·s. They concluded that slug frequency and liquid film height increased, and the slug length decreased as the liquid viscosity increased.

Shosho and Ryan (2001) conducted an experimental study with Newtonian and non-Newtonian fluids to investigate the effects of viscosity and tube size on drift velocity for vertical and inclined tubes. The drift velocity was correlated in terms of three dimensionless numbers; Froude, Eötvös, and Morton numbers. For non-Newtonian fluids with high Morton number, Froude number was affected by both viscous forces and tube size.

Shosho and Ryan (2003) experimentally studied the effects of a high liquid viscosity on two-phase flow in vertical pipe. Water and glycerin solutions were used as test liquids. The liquid viscosities were 1.0, 50, 200, and 550 mPa·s. Mostly, annular flow was observed in their study. They concluded that low viscosity correlations for entrained liquid fraction and interfacial friction factor were not suitable for the highly viscous liquids. A new correlation for the interfacial friction factor was developed based on collected high viscosity data.

Rosa et al. (2004) experimentally investigated the influence of liquid viscosity on gas-liquid slug flow in horizontal pipes. Air-water and air-glycerin (27 mPa·s) were used 32 as the two pairs of test fluids. Bubble shape, velocity and void fraction, bubble and slug lengths, slug frequency and coalescence rate were studied. They concluded that as liquid viscosity increased, the average slug length and coalescence rate decreased, while the bubble front velocity and slug frequency increased.

Gokcal (2005) performed an experimental investigated the effect of high viscosity oil (181 mPa·s - 587 mPa·s) on two-phase flow behavior in a 50.8 mm ID horizontal pipe. For flow pattern prediction, Gokcal concluded that, as liquid viscosity increases within his investigation range of viscosities, the data did not show a significant effect of the oil viscosity on the transition boundaries. On the other hand, considerable difference has been observed with respect to low viscosity oil data. The study also showed that the pressure gradient increased with the increase in liquid viscosity. This became more pronounced with increasing superficial oil and gas velocities. The comparison of the pressure drop experimental data against the TUFFP unified model predictions showed an unsatisfactory performance for high viscosity oil conditions. Gokcal et al. (2006) modified the closure relationships in the TUFFP unified model resulting in improved predictions of the experimental data for flow pattern transition, pressure gradient, and liquid holdup.

Schmidt et al. (2008) experimentally studied the phase and velocity distributions in vertically upward high-viscosity (up to 7000 mPa·s) two-phase flow. Void fraction measurements were made using a gamma-densitometer.

Pressure gradient was not reported in their experimental study. They concluded that existing void fraction correlations do not predict the average void fraction properly.

Akhiyarov et al. (2010) experimentally studied the effect of high oil viscosity on two-phase behavior in upward vertical flow. Oil viscosity of 120 - 510 mPa·s and Tulsa City Natural gas were used as the two-phase fluid system in a 52.5 mm ID pipe. Flow pattern, pressure gradient, and average liquid holdup were recorded. Comparing the obtained experimental data with model predictions showed poor performance of the models for high oil viscosity.

Jeyachandra (2011) experimentally studied the effect of high viscosity oil (181 mPa·s - 587 mPa·s) on two-phase flow behavior in a 50.8 mm ID slightly inclined ($\pm 2^{o}$) pipes. Flow pattern, pressure gradient, average liquid holdup, and slug characteristics were measured and analyzed. The obtained experimental results agreed with Gokcal (2005) observations. As oil viscosity increased, pressure gradient and slug frequency increased, slug length decreased, and no significant change in average liquid holdup or slug liquid holdup was observed within the viscosity range used in the experiments.

Brito (2012) experimentally studied the effect of medium oil viscosity (39 mPa·s - 166 mPa·s) on two-phase flow behavior in a 50.8 mm ID horizontal pipe. Flow pattern, pressure gradient, average liquid holdup, translational velocity, slug liquid holdup, film holdup, slug length, and slug frequency were measured and analyzed. The obtained experimental results were compared with Gokcal (2005). It was found that pressure gradient and

average liquid holdup increased with increasing oil viscosity.

Farsetti et al. (2014) experimentally investigated the flow of high viscosity oil (900 mPa·s) and gas in a 22.8 mm ID horizontal and slightly inclined (-10^{o} to $+15^{o}$) pipes. Pressure gradient, translational velocity, slug frequency, slug length, and average liquid holdup were measured using capacitance probes. They concluded that correlations 34 available in literature (validated for the low viscosity liquid case) cannot be extended to the high viscosity case.

Kim (2014) experimentally studied the the pipe diameter effects in high viscosity oil (181 mPa·s - 587 mPa·s) and gas two-phase condition with a 76.2 mm ID horizontal pipes. Flow pattern, pressure gradient, average liquid holdup and slug characteristics (translational velocity, slug frequency, slug length, slug liquid holdup and film liquid holdup) were measured using capacitance probes. They concluded that the slug liquid holdup and slug frequency increase, and the film liquid holdup and slug length decrease as the pipe diameter increases.

2.3 **Summary**

Only limited experimental studies of low viscosity oil-gas two-phase flow in vertical downward pipes are available in literature. And also most of them are focused on transition of flow pattern and prediction of volume fractions of each phase. Furthermore, studies of high viscosity oil-gas two-phase flow commonly claim that existing mechanistic models must be verified with

higher viscosity liquid-gas two-phase flow experimental data. If models show poor predictions with high viscosity data, the existing models need to be investigated quantitatively on its applicability.

Chapter 3 Experimental Facility

The experimental study was conducted on a TUFFP three phase flow facility. ND-50 mineral oil and compressed air were used as a liquid and a gas, respectively. The following sections present facility description, fluids properties and details of instruments.

3.1 Facility Description

The experimental work was conducted using the TUFFP 2-in. ID three-phase flow facility located at the University of Tulsa North Campus Research Complex. Figure 3.1 depicts the schematic of the facility loop. A coated steel oil storage tank with an internal baffle was used for oil and gas separation. The capacity of oil tank is 2,900 gallons. The tank is equipped with an electrical heater and a recirculation pump to increase and maintain oil temperature. Oil tank is connected to the progressive cavity pump Robbins-Myers R&M 1000 to circulate the oil. Maximum working pressure of pump is 290 psi. Thus, a pressure relief valve, which open at 100 psi, is connected at the pump discharge to control excessive pressure over test section. The oil density and mass flow rate is measured with a CMF100 coriolis flow meter from Micro Motion™ with RTF9739 transmitter. Maximum mass flow rate is 1,000 lb/min. Finally, pressure and temperature are measured to monitor the oil properties.

A dry rotary screw compressor supplies compressed air with a

capacity of 1,030 cubic feet at 100 psig. A pair of Endress-Hauser Promass 83F coriolis flow meter are installed to measure gas mass flow rate. Before the each coriolis meter, an automatic control valves are connected to control gas flow rate. These valves can be operated in parallel or individually. A feedback control, using the valve opening, is utilized to maintain gas flow rate constant. The phases flow through the mixing tee at the inlet section of test section. Liquid-gas mixture flows through upward section which consists of 22.72-m-long and 2-inch ID pipe. Bended 2-inch steel pipe links upward and downward flow sections. Downward section has three part; 15.85-m-long steel pipe, 3.59-m-long transparent polycarbonate pipe and 3.28-m-long steel pipe. End of downward flow section is connected to oil tank with flexible hose.

Figure 3.2 shows schematics of test section. Test section is mounted on a boom with a hoisting lift system and can be inclined at any angle between horizontal and vertical. Two capacitances were used to examine flow patterns. A Resistance Temperature Detector (RTD) temperature transducer and a pressure transducer are installed to measure temperature and pressure of fluids. A pair of Quick-Closing Valves (QCV) are used to measure the average liquid holdup combined with differential pressure transmitter. Differential pressure transmitter also provides pressure drop with flow. A surveillance camera was installed to collect video of flow for flow pattern identification. Length of trapping section and pressure drop measurement are 6.09 m (L/D = 120) and 5.36 m (L/D = 105), respectively.

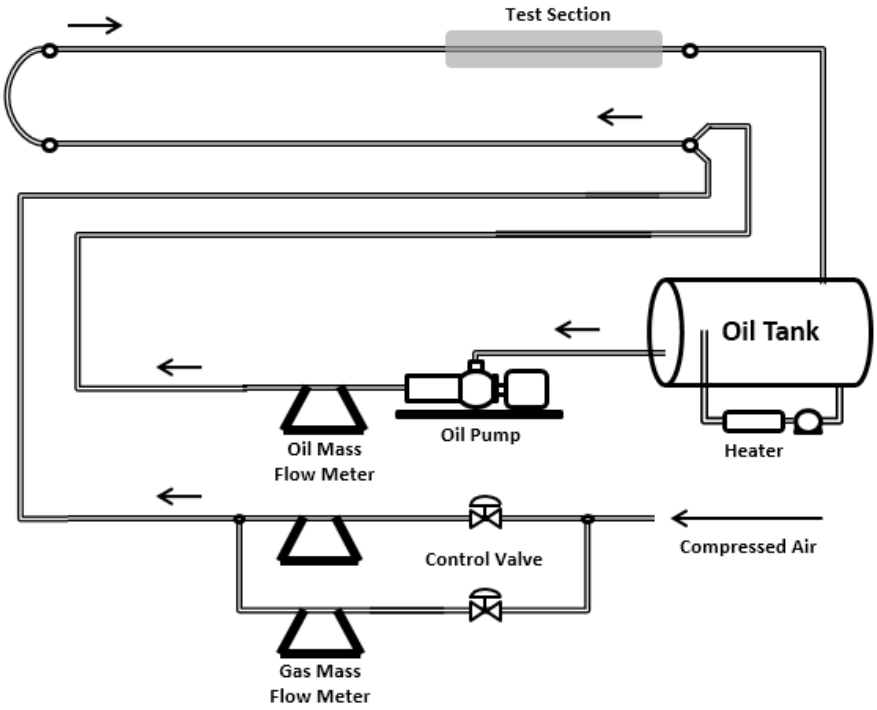

Figure 3.1 Facility Schematic.

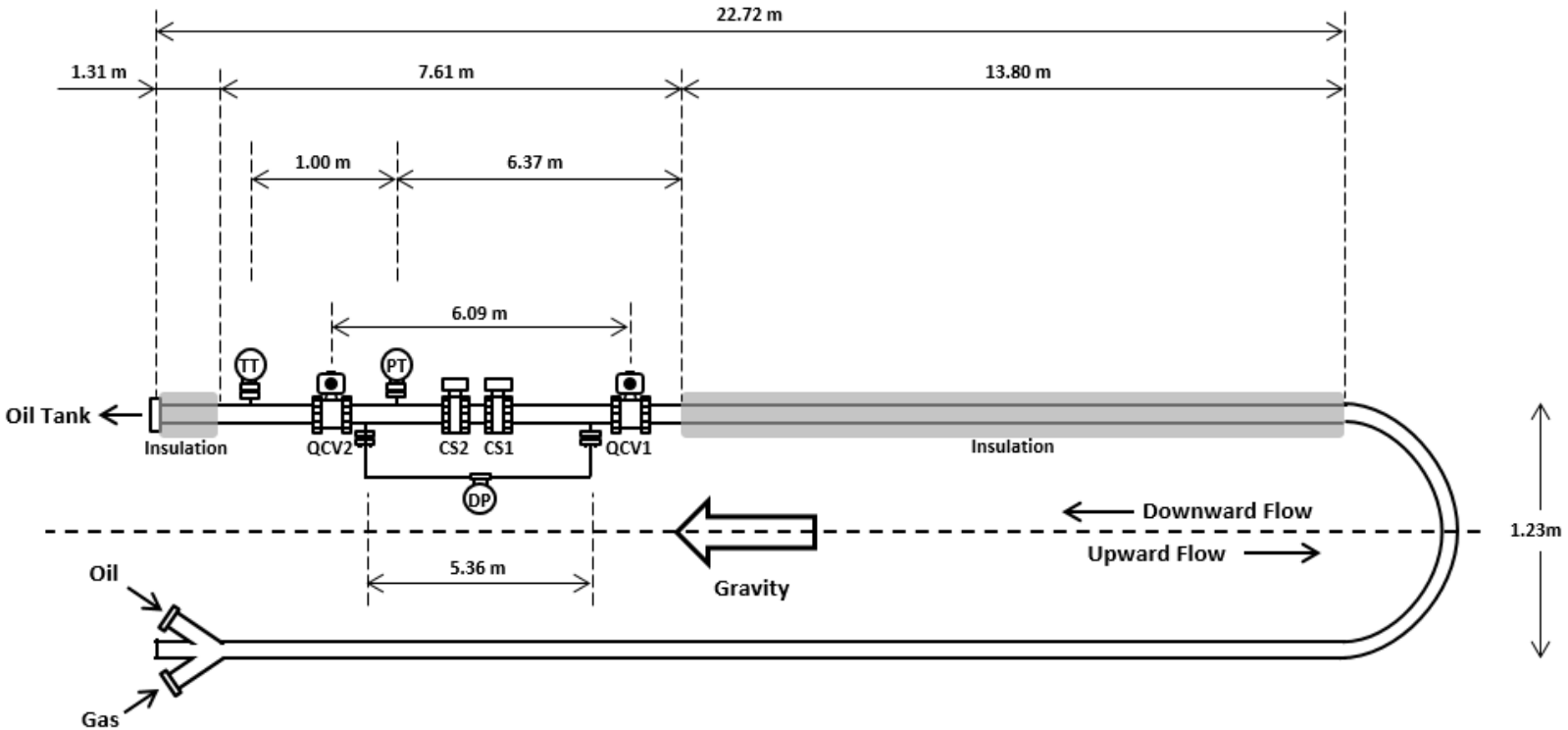

Figure 3.2 Schematic of Test Section.

3.2 Fluids

3.2.1 Air Properties

Compressed air was used as the gas phase. Since properties of gas are very sensitive to pressure and temperature because of high compressibility, they were calculated from known correlations. Air density was calculated using revised CIPM-2007 formula for moisture air (Picard et al., 2008) as follows:

$$\rho_{air} = 3.48349 \times 10^{-3} \frac{p}{ZT}(1 - 0.378X_v), \tag{3-1}$$

where p is the pressure in Pascal, T is the temperature in Kelvin, Z is the compressibility factor, and X_v is the mole fraction of water vapor. X_v is calculated from equation (3-2).

$$X_v = h\frac{p_{sv}}{p} f(p, T_t). \tag{3-2}$$

h is the relative humidity. It is assumed 0.6 in this study. $f(p, T_t)$ is the enhancement factor at the ambient pressure and temperature:

$$f(p, T_t) = 1.00062 + 0.0000000314p + 0.00000056T_t^2, \tag{3-3}$$

where T_t is the temperature in degree Celsius. p_{sv} in equation (3-2) is saturation vapor pressure in Pascal at ambient temperature. It is calculated by equation (3-4).

$$p_{sv} = Exp(1.2378 \times 10^{-5} T^2 - 0.01912T + 33.937 - 6343T^{-1}) \quad (3\text{-}4)$$

The correlation for compressibility factor (Z) and coefficients are as given:

$$Z = 1 - \frac{p}{T}\left[a_0 + a_1 T_t + a_2 T_t^2 + (b_0 + b_1 T_t) X_v + (c_0 + c_1 T_t) X_v^2\right]$$

$$+ \left(\frac{p}{T}\right)^2 (d + e X_v^2), \quad (3\text{-}5)$$

$a_0 = 1.58123 \times 10^{-6}$ K Pa^{-1}, $a_1 = -2.9331 \times 10^{-8}$ Pa^{-1},

$a_2 = 1.1043 \times 10^{-10}$ K^{-1}Pa^{-1}, $b_0 = 5.707 \times 10^{-6}$ K Pa^{-1},

$b_1 = -2.051 \times 10^{-8}$ Pa^{-1}, $c_0 = 1.9898 \times 10^{-4}$ K Pa^{-1},

$c_1 = -2.376 \times 10^{-6}$ Pa^{-1}, $d = 1.83 \times 10^{-11}$ K^2 Pa^{-2},

$e = -0.765 \times 10^{-8}$ K^2 Pa^{-2}.

The air viscosity was calculated with Sutherland's Law (1893). Air viscosity is the function of temperature as follows:

$$\mu = \mu_0 \frac{T_0 + C}{T + C} \left(\frac{T}{T_0}\right)^{3/2}. \quad (3\text{-}6)$$

In Sutherland's formula, μ_0, T_0 and C are the reference viscosity in mPa·s, the reference temperature in $^{\circ}K$ and Sutherland's constant for air, respectively.

For air, $\mu_0 = 1.827 \times 10^{-2}$ mPa · s, $T_0 = 291.15$ K and C = 120 $^{\circ}K$.

3.2.2 Oil Properties

Lubsoil ND-50 mineral oil was selected as the test oil due to the high viscosity and Newtonian behavior in the testing range. The viscosity of oil was measured 7 times using the rheometer, a RheoScope 1™. For each measurements, oil temperature was changed from 60 to 120 $^{\circ}F$. The obtained oil viscosity correlation is as given:

$$\mu_{oil} = 1.0134 \times 10^8 \, T^{-2.839} \quad (3\text{-}7)$$

where T is in $^{\circ}F$, and μ_{oil} is in mPa·s. Figure 3.3 depicts correlation curve

between oil viscosity and oil temperature.

As oil is assumed incompressible, oil density which was measured from coriolis flow meter can be used. Additional physical properties of ND-50 are as follows:

- API gravity: 28.5°.
- Density: 884.4 kg/m3 @ standard condition.
- Pour and flash point temperatures: -15 ℃ (5 ℉) and 265 ℃ (510 ℉), respectively.
- Surface tension: 35.75 dynes/cm at 19.8 ℃ (68 ℉) and atmospheric pressure.

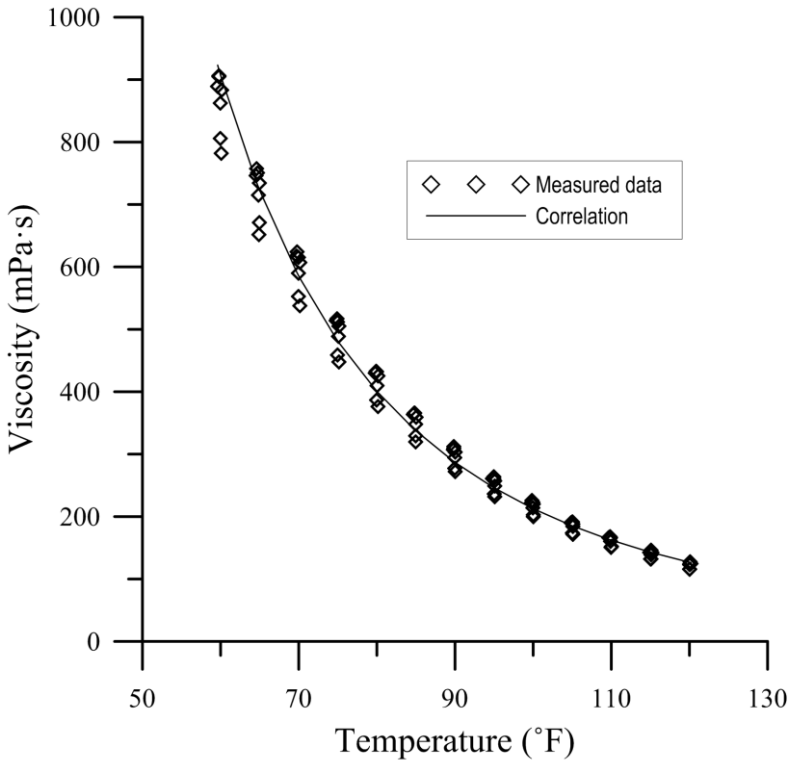

Figure 3.3 Viscosity vs. Temperature of oil.

3.3 Instrumentation

The following instrumentation was used to perform the identification of flow pattern, and the measurement of pressure gradient and liquid holdup.

3.3.1 Basic Instrumentation

Temperature data was collected by calibrated resistance temperature detector (RTD) temperature transducers. They were installed oil metering section, gas metering section and test section, being calibrated to have $\pm 0.25\,℃$ of uncertainty. To measure pressure of test section, a Rosemount gauge pressure transducer was mounted between the Quick Closing Valves. Uncertainty of pressure transducer is $\pm 0.15\%$.

Rosemount differential pressure transducer was installed to measure pressure drop in flowing condition and liquid holdup in trapped condition. It has a systematic uncertainty of ±0.055%. The impulse line of differential pressure system, divided into two sections connected by pressure transducer, is designed for real-time measure of the pressure differences between two different points. It is filled with silicon oil to catch the small change in pressure drop of the flow. As the test section is raised up to vertical position, however, the hydrostatic pressure of silicon oil occurs significant pressure difference, zero-DP, even the pipe is empty. To obtain the pressure differences between two points accurately, measured zero-DP in vertical position was

subtracted from the measured pressure drop readings.

CMF100 coriolis flow meter from Micro Motion™ with RTF9739 transmitter was used to measure oil mass flow rate and oil density. The known uncertainties of density and mass flow rate measurement are ±0.5kg/m^3 and ±0.1%, respectively. For measurement of gas mass flow rate, two Endress-Hauser Promass 83F coriolis flow meters are used. They are reported to have uncertainty of ±0.1% of their readings.

3.3.2 Quick Closing Valve System

A pair of Quick Closing Valves are installed to measure an average liquid holdup with a differential pressure transducer. The measured pressure difference varies with liquid level of trap section due to hydrostatic pressure of liquid column. To obtain liquid holdup-pressure difference correlation, a special type of calibration was conducted. First, trap section was filled with water, and the pressure difference in trap condition (DP_{trap}) was recorded repeatedly after draining predetermined volume of water. Figure 3.4 shows the correlation between total drained volume and DP_{trap}.

While this calibration was conducted with water as liquid phase, the correlation should be modified with liquid density. When we drained predetermined volume of water, *DP* changes as follows:

$$\Delta DP_{trap} = \rho_L g \Delta h_L = \rho_L g \Delta H_L h_{trap} \text{ and}$$
$$\Delta H_L = 1 - (\Delta V_{drain}/V_{QCV}) = \Delta h_L / h_{trap} \quad (3\text{-}8)$$

where ρ_L, h_L, H_L, h_{trap}, V_{drain} and V_{QCV} are density of liquid, height of liquid column, liquid holdup, total length of trap section, volume of drained water and volume between QVCs, respectively (Figure 3.5). From equation (3-8), we can obtain

$$H_L \, \alpha \, (DP_{trap}/\rho_L g) \quad (3\text{-}9)$$

regardless the liquid density. Figure 3.6 depicts the correlations between liquid holdup and $DP_{trap}/\rho_L g$. Following equations can be used to calculate liquid holdup from the DP_{trap} reading:

$$H_L = -0.0041 \, (DP_{trap}/\rho_L g) + 0.0694. \quad (3\text{-}10)$$

As DP_{trap} changes when from 945 ml to 12,058 ml and V_{QCV} is 12,952 ml from the measurement, equation (3-10) can be applied for the range between 0.069 and 0.926.

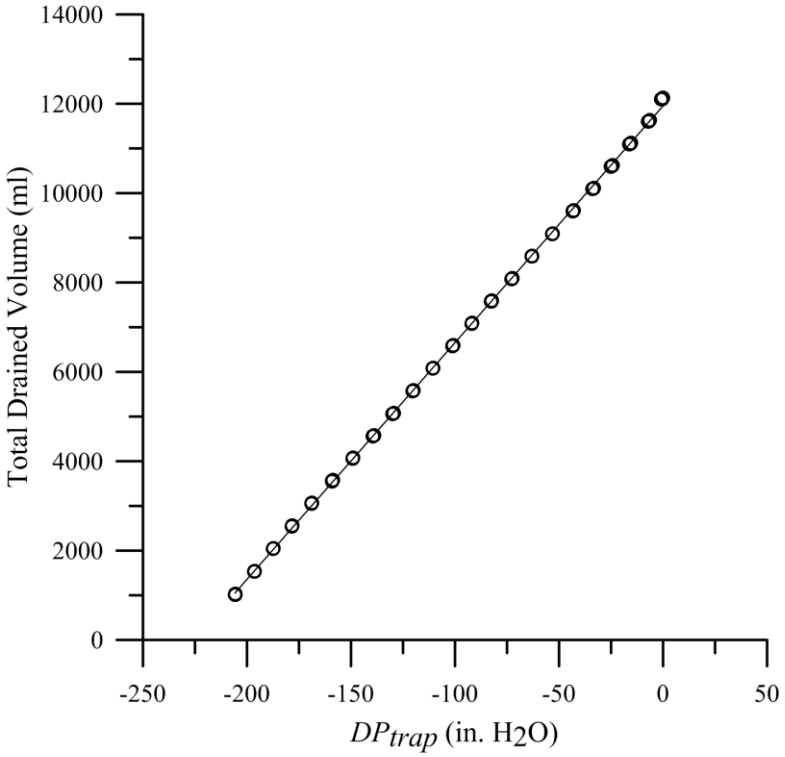

Figure 3.4 Total drained water volume vs. DP_{trap}.

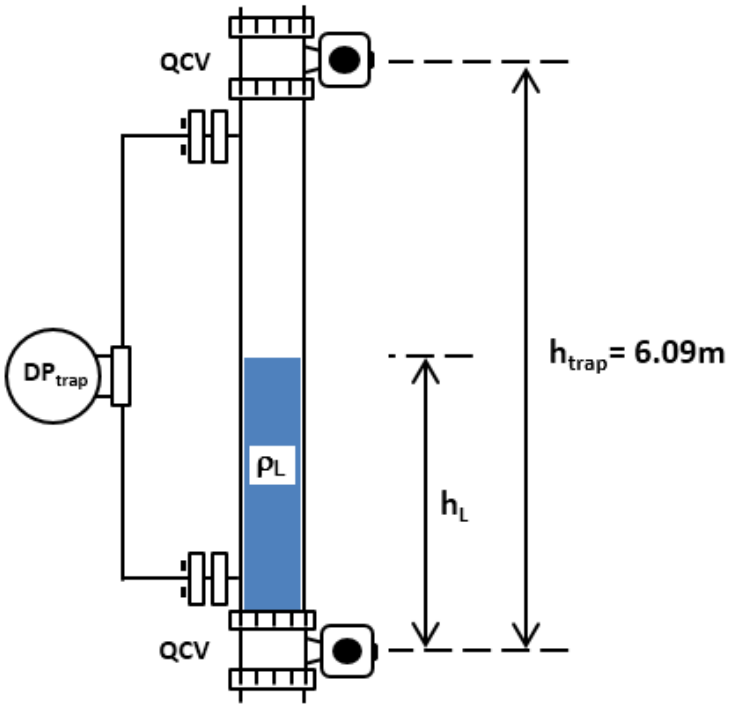

Figure 3.5 Schematics of the average liquid holdup measurement.

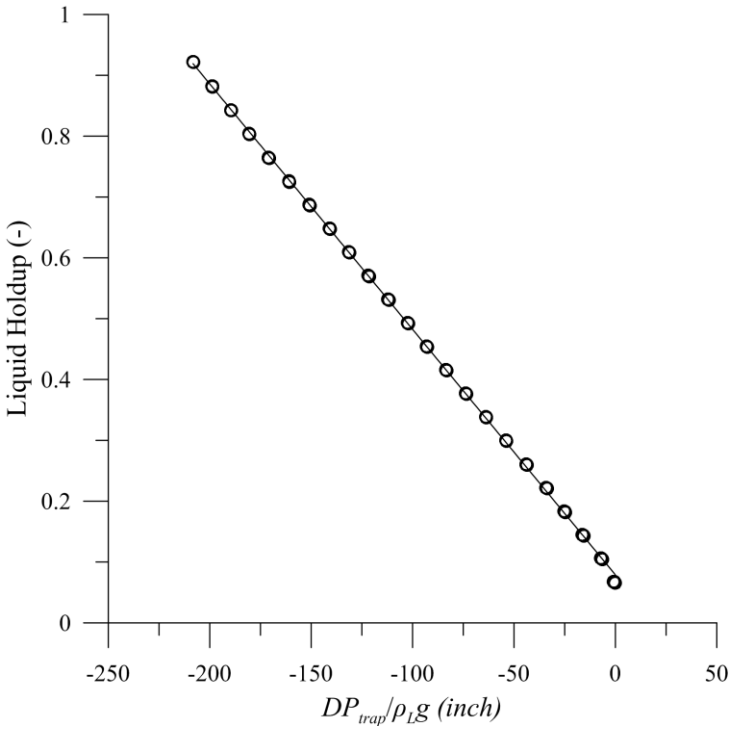

Figure 3.6 Average liquid holdup vs. $(DP_{trap}/\rho_L g)$.

3.3.3 Capacitance Sensors

In vertical downward flow with high viscosity oil, as dark-colored liquid film always exist along with the pipe wall, it is very difficult to identify flow patterns only with surveillance camera. Therefore, a pair of capacitance sensors are installed to identify flow patterns by analyzing liquid holdup Probability Distribution Function (PDF) of flow. Recorded capacitance sensor voltage signals converted into liquid holdup with the correlation from static calibration. Figure 3.7 and Figure 3.8 depict static calibration correlation curve for each capacitance sensor. Both of capacitance sensors are two-wire

type and have linear response as reported previously by other studies (Kora, 2010; Brito, 2012). Detailed explanations about characteristic of each flow pattern type will be treated in experimental results section.

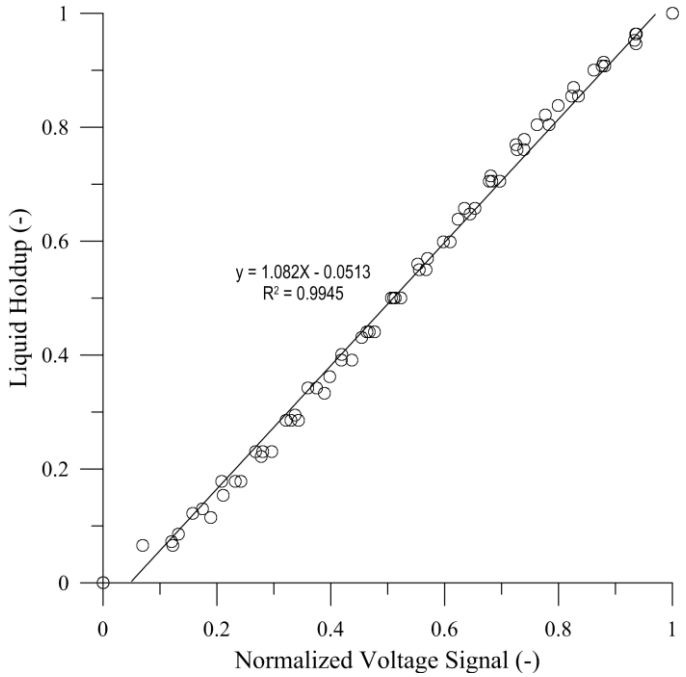

Figure 3.7 Static calibration correlation for Capacitance 1.

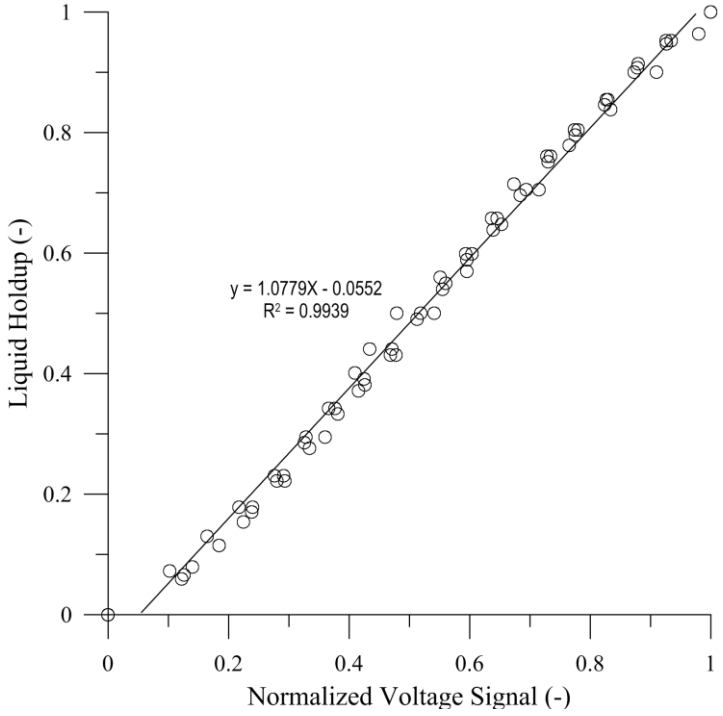

Figure 3.8 Static calibration correlation for Capacitance 2.

3.4 Experimental Procedure

An experimental procedure is for obtaining reliable experimental data; pressure drop, voltage signals from capacitance sensors and average liquid holdup. The procedure is given below.

1. Start air compressor.
2. Start data acquisition program, and monitor readings of all instruments.
3. Check all valves on test section to avoid operations problems.
4. Raise test section to vertical position
5. Check differential pressure transducer reading to examine DP zero correction is accurate.
6. Record empty pipe voltage reading for all capacitance sensors to obtained minimum voltage value. If for any capacitance sensor shows abnormally high values, lower the test section and adjust capacitance sensor readings to acceptable value.
7. Lower test section to horizontal position.
8. Check temperature of oil in main storage tank. Set-up heating system to adjust oil temperature should be done in previous day as it may take hours to reach required temperature.
9. Start oil pump, maintaining desired superficial oil velocity for testing.

10. Circulate single-phase oil until oil reaches back to oil tank.
11. Run single phase oil at two different v_{SL} values (0.2 m/s & 0.5 m/s) to check that all instruments display reasonable readings.
12. Check temperature transducers on test section for actual oil temperature in test section and adjust if necessary to desired temperature. The temperature should be kept constant during test for oil viscosity control.
13. Record voltage reading for single phase oil, to obtained maximum voltage value (horizontal position).
14. Raise test section to vertical position.
15. Close lower QCV and record voltage readings for single phase oil to obtained maximum voltage value in vertical position.
16. Open QCV and change QCV setting to capture entire trap section.
17. Open air valve and increase required superficial air velocity up to desired value.
18. Wait until the flow to be stabilized, monitoring temperature transducer and differential pressure transducer readings on test section.
19. Run low and high speed data acquisition system at a sampling frequency of 5 Hz for low speed data for 3 minutes (900 data points) and 1,000 Hz for high speed data for one minute (60,000 data points).
20. Run average liquid holdup measurement procedure:

a) Open bypass valve and close two QCVs simultaneously to trap fluid mixture

b) Wait for DP to be stabilized with the segregation of liquid and record it.

c) Calculate liquid holdup with average liquid holdup correlation.

d) Open two QCVs and then close bypass valve.

21. For each test point, repeat these steps (high/low speed data acquisition and average liquid holdup measurement) 3 times to confirm results.
22. Repeat there steps for different superficial air and oil velocities and viscosities which are listed in test matrix.
23. Shut down oil pump. Keep gas flowing to remove oil from the test section.
24. Lower test section to horizontal position.
25. Stop air flow.
26. Log out from data acquisition systems.
27. Shut down air compressor.
28. Set up heating system in oil tank for next day desired oil temperature.
29. Make backup copies of all the acquired data.

3.5 **Uncertainty analysis**

Since the true value can never be measured exactly, every measurement generates error, the difference between the true and measured values. Measurement uncertainty analysis is a numerical method for quantifying the potential error that exists in all data (Dieck, 2007). We can estimate the 95% confidence interval of the measurement that includes the true value.

Errors can be divided into 3 groups; random (precision), systematic (bias) and blunders (mistakes) errors. A random error is unpredictable fluctuation that is occurred among the measurements for the same test condition. Systematic error is the difference between a single true value and the average of measured values. Systematic error is a constant for all experiments. Blunders errors are occurred by improper performance of experimenter and assumed to be removed with good engineering practice.

Random Uncertainty: Random errors are values that affect test data in a random fashion from one reading to the next. Random uncertainty sources that cause scatter in the test results (Dieck, 2007). Experimental measurements are used to estimate random uncertainty. Random uncertainty is calculated by using the Student‘s t distribution. In these calculations, the random uncertainty is assumed to be normally distributed; therefore, the result is a symmetrical random uncertainty. Calculations related to uncertainty come from statistical methods. Scatter in samples is calculated by using the sample standard deviation definition (S_X),

$$S_X = \sqrt{\frac{\sum_{i=1}^{N}(X_i - \bar{X})^2}{N-1}} \quad (3\text{-}11)$$

where:

N = number of data points

X_i = the ith data point

$\bar{X}$ = the average of data points

(N-1) = the degrees of freedom for the data points

In order to find the error percentage in the average, the standard deviation of the average ($S_{\bar{X}}$) is estimated by:

$$S_{\bar{X}} = \frac{S_X}{\sqrt{N}}. \quad (3\text{-}12)$$

$S_{\bar{X}}$ is known as the random uncertainty with a confidence level of 68%. To determine the 95% confidence interval of a measurement, the student-t distribution t95 can be used. Therefore, the random uncertainty of measurement X is given by the uncertainty interval, $X = \bar{X} \pm t_{95} S_{\bar{X}}$. If several estimates of standard deviation are available, a better estimate of standard deviation is obtained by combining the individual estimates of the same standard deviation through a pooling process. The equation used to pool S_X is:

$$S_{X,pooled} = \left[\frac{\sum_{i=1}^{N} v_i \left(S_{X,i}\right)^2}{\sum_{i=1}^{N} v_i}\right]^{1/2} \quad (3\text{-}13)$$

where:

$S_{X,pooled}$ = the pooled standard deviation

N = number of standard deviation pooled

$S_{X,i}$= the ith standard deviation

v_i= the ith degrees of freedom

Systematic Uncertainty: Systematic error is constant for all experiments using a particular instrument and often provided by the manufacture. Systematic errors affect every measurement of a variable the same amount. The systematic uncertainty comes from various error sources. Each source of the elemental systematic uncertainty, b_i, needs to be combined by using the following equation,

$$b_R = \left[\sum_{i=1}^{N} (b_i)^2\right]^{1/2} \tag{3-14}$$

where b_R is the combined systematic uncertainty component of the uncertainty analysis. The systematic standard uncertainty is assumed to have infinite degrees of freedom. As such it represents 68% confidence interval. If systematic uncertainty is given as 95% confidence interval, the student-t would be 2 and we would divide our estimate of systematic uncertainty by 2.0 to use it in combined uncertainty equation. The systematic uncertainties of the measured parameters are listed in Table 3.1.

Table 3.1: Systematic Uncertainty of experimental instruments

Measured Parameters	**Instruments**		**Model**	**Systematic Uncertainty**
Gas Flow Rate	Micro Motion TM	MM3	83F08-DXW2/O	±0.1%
		MM4	83F08-DXW2/O	
Liquid Flow Rate	Micro Motion TM	MM1	RFT9739	±0.1%
Liquid Density	Micro Motion TM	MM1	RFT9739	±0.5 Kg/m3
Temperature	Rosemount Temperature Transducer	TT14	3144PD1A1E5B4 M5	±0.25^{o}C
Pressure	Rosemount Pressure Transducer	PT12	3051S2TA2A2E1 1A1AE5M5B4	±0.15% of Span
Differential Pressure	Rosemount Differential Pressure Transducer	DP15	3051S2CD2A2B1 2A1AB4E5M5	±0.15% of Span

Chapter 4 Experimental Results

This chapter covers the results of experimental works and their comparisons with experimental data for low viscosity vertical downward flow. Measured raw data were analyzed on the purpose of flow pattern identification, pressure drop measurement, and average liquid holdup measurement. Four temperature conditions, 70℉, 80℉, 100℉, and 120℉, are considered as test conditions. By equation (3-7), corresponding oil viscosities are estimated as 586 mPa·s, 401 mPa·s, 213 mPa·s, and 127 mPa·s, respectively. The superficial liquid and gas velocities vary with temperature conditions, having range of 0.05 to 0.7 m/s and 0.2 to 8 m/s, respectively. To estimate the uncertainty of average liquid holdup, each flow conditions has at least 3 measurements.

4.1 Flow Pattern

Considering the traditional flow pattern classification, all conditions can be categorized as annular flow. To describe more detailed physical phenomena, however, the Probability Distribution Function (PDF) are conducted from capacitance sensor signals and flow patterns were divided into three types: Falling Film (FF), Wavy Annular (WA) and Liquid Slip (LS). Videos for each flow condition were also utilized to help flow pattern distinction. Figure 4.1 shows typical PDF distributions and relating schematics for each flow pattern type which are observed in this study. Figure 4.2 depicts captured screenshot of video for each flow pattern.

Falling Film flow pattern occurs under low gas and liquid flow rate conditions. This flow pattern is frequently observed in previous researches (Oshinowo & Charles, 1974; Usui, 1989). Due to its low flow rates of each fluid, it shows low liquid entrainment into the gas core and small wave amplitude on liquid film (figure 4.2 (a)). PDF of Falling Film flow pattern are intensively distributed at relatively low value due to its thin film thickness and small wave amplitude (figure 4.1 (a)).

As liquid rate increases, liquid film starts getting thicker. Owing to combined effect of gravity and interfacial shear stress by gas flow, significant portion of liquid film near the liquid-gas interface starts to slip over the liquid film. This flow pattern is defined as Liquid Slip flow. A similar flow pattern was observed by Zadrazil et al. (2014a) for air-water downward flow at high liquid Reynolds numbers. As a result, a large and steady liquid entrainment is observed in the gas core region (figure 4.2 (c)). PDF of liquid slip flow pattern shows a long-tailed distribution towards high liquid holdup section, because of its large entrainment of liquid (figure 4.1 (c)).

With high gas rate, larger drag force acts on liquid film. It causes the erratic roll over waves with large amplitudes on liquid film surface as observed in figure 4.2 (b). Because the waves on liquid surface behave like roughness, high interfacial shear stress occurs between phases resulting in high pressure drop similar to an annular flow in vertical upward. PDF of wavy annular flow pattern shows wider distribution than Falling Film flow pattern, because waves occurs more frequently.

Figure 4.3 through 4.6 depicts the observed flow patterns for

different oil viscosities. As liquid viscosity decreases, liquid slip flow pattern is observed at higher v_{SG} and lower v_{SL} conditions. It means liquid slip are easy to slip at lower viscosity.

Each flow patterns can be distinguished using statistical parameter of PDF: skewness and kurtosis. PDF of Falling Film flow have relatively high kurtosis comparing other flow patterns because it has narrow and intensive distribution. For Wavy Annular flow, kurtosis is smaller than Falling Film flow due to the large role wave while Falling Film flow has small kurtosis owing to the large liquid droplet. Wavy Annular flow and Liquid Slip flow can be divided by skewness. Due to the small fraction of liquid entrainment, skewness of Wavy Annular flow is smaller than that of Liquid Slip flow. As Liquid Slip flow has irregular large liquid entrainment, PDF has a shape of long tail.

Figure 4.7 to 4.10 depict relationship between kurtosis and skewness depending on flow pattern for different oil viscosities. In same flow pattern group, kurtosis and have a positive correlation. When liquid viscosity increases, liquid tends to flow with small roll wave and small liquid entrainment. Consequently, both of skewness and kurtosis become small in Wavy Annular flow and Liquid Slip flow.

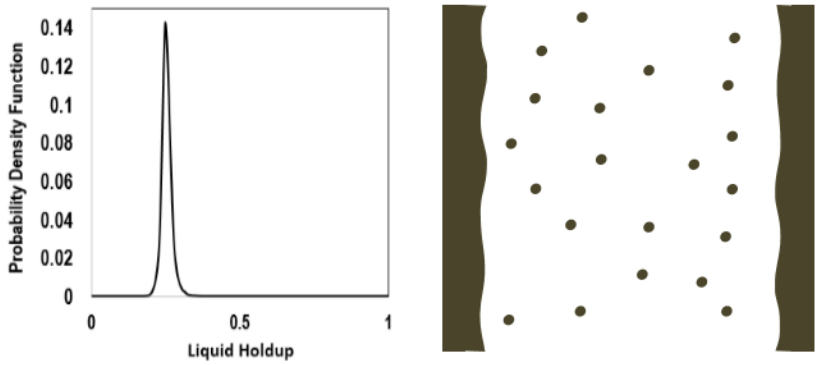

(a) type 1: Falling Film (FF)

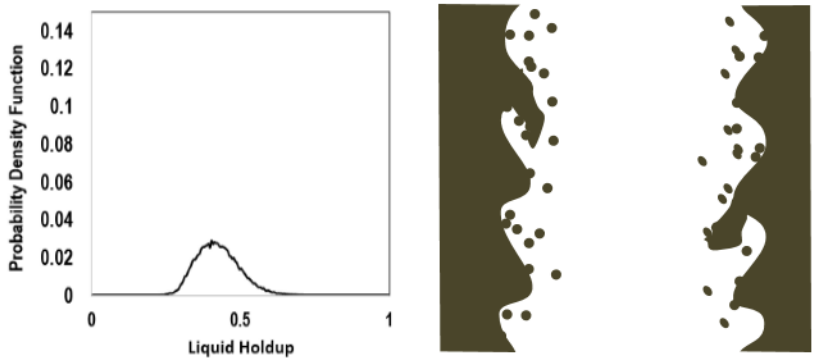

(b) type 2: Wavy Annular (WA)

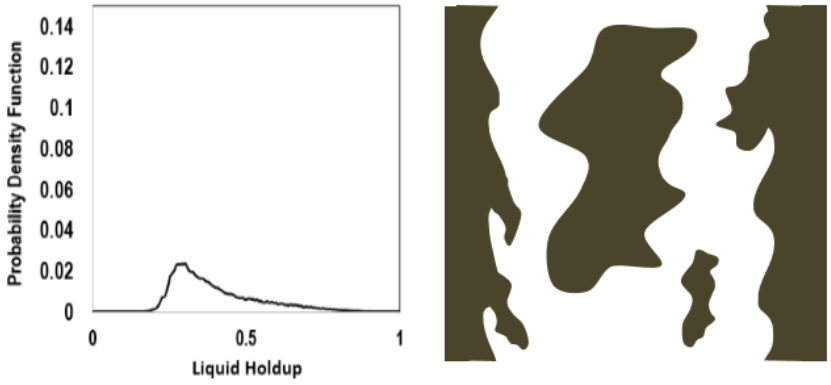

(c) type 3: Liquid Slip (LS)

Figure 4.1 Probabilistic Density Function (PDF) and schematics for each flow pattern type.

(a) Falling Film

v_{SL} = 0.06 m/s

v_{SG} = 0.64 m/s

(b) Wavy Annular

v_{SL} = 0.11 m/s

v_{SG} = 6.16 m/s

(c) Liquid Slip

v_{SL} = 0.7 m/s

v_{SG} = 0.7 m/s

Figure 4.2 Captured video screenshots for each flow pattern

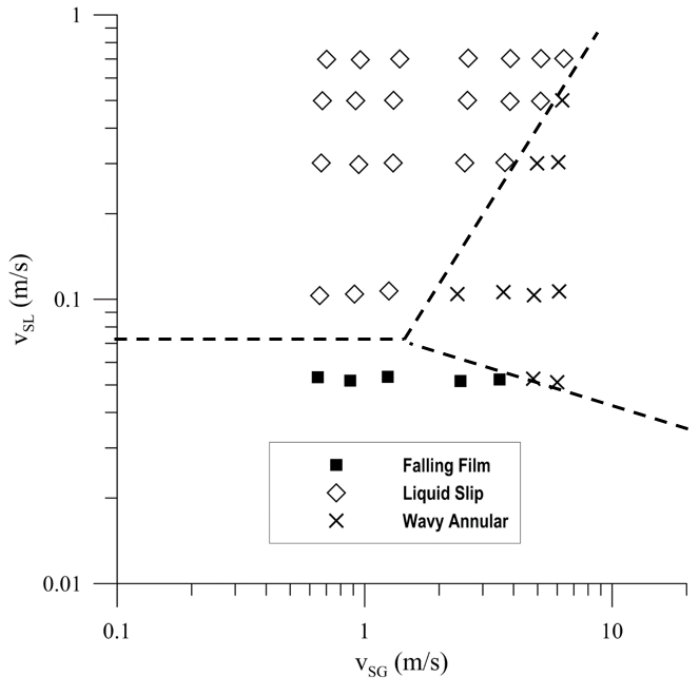

Figure 4.3 Observed flow pattern for μ_{oil} = 127 mPa·s

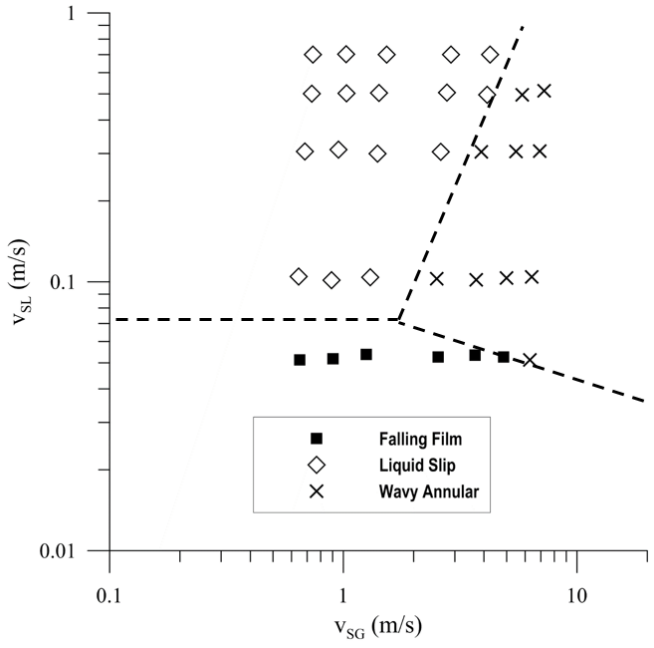

Figure 4.4 Observed flow pattern for μ_{oil} = 213 mPa·s

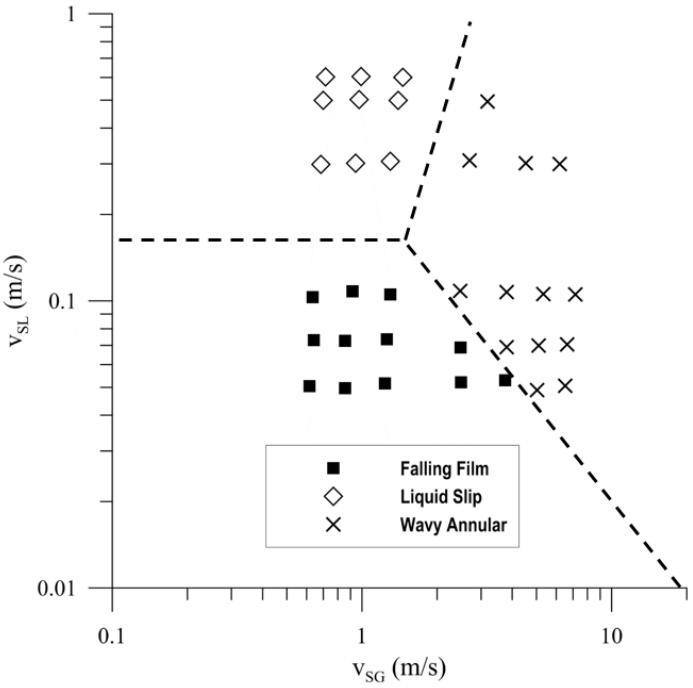

Figure 4.5 Observed flow pattern for μ_{oil} = 401 mPa·s

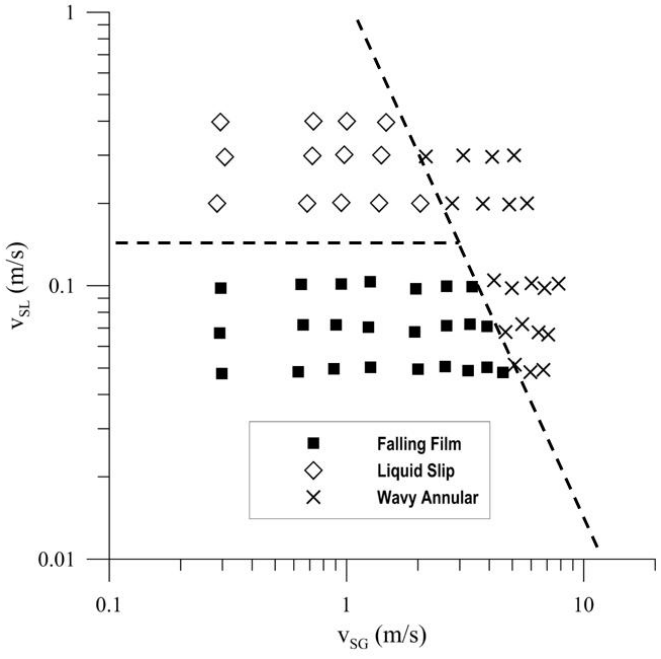

Figure 4.6 Observed flow pattern for μ_{oil} = 586 mPa·s

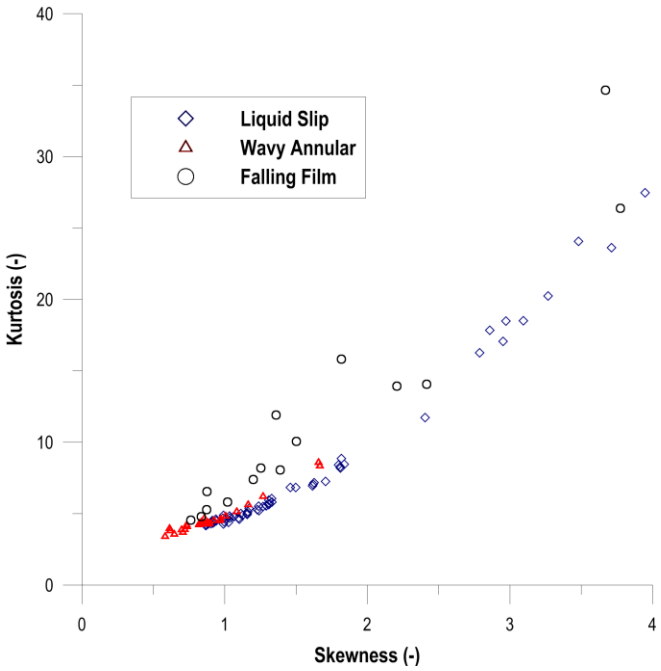

Figure 4.7 Skewness vs. kurtosis for μ_{oil} = 127 mPa·s

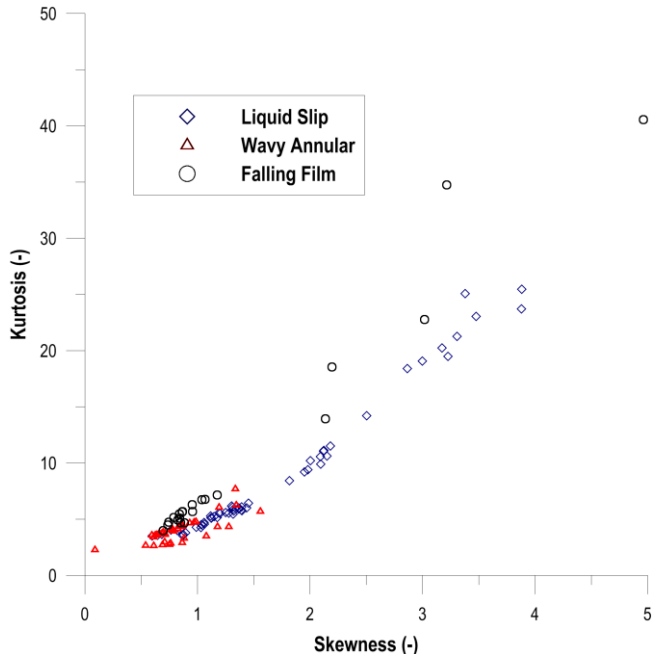

Figure 4.8 Skewness vs. kurtosis for μ_{oil} = 213 mPa·s

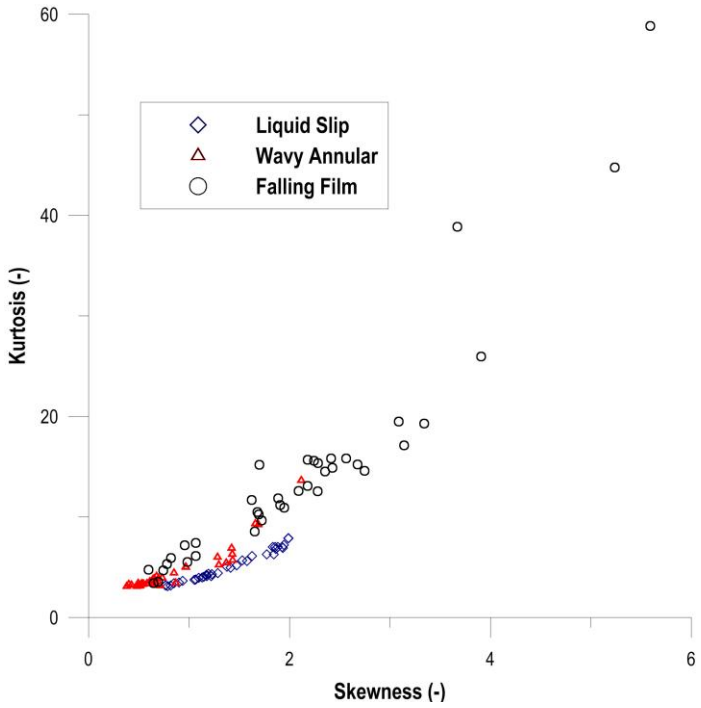

Figure 4.9 Skewness vs. kurtosis for μ_{oil} = 401 mPa·s

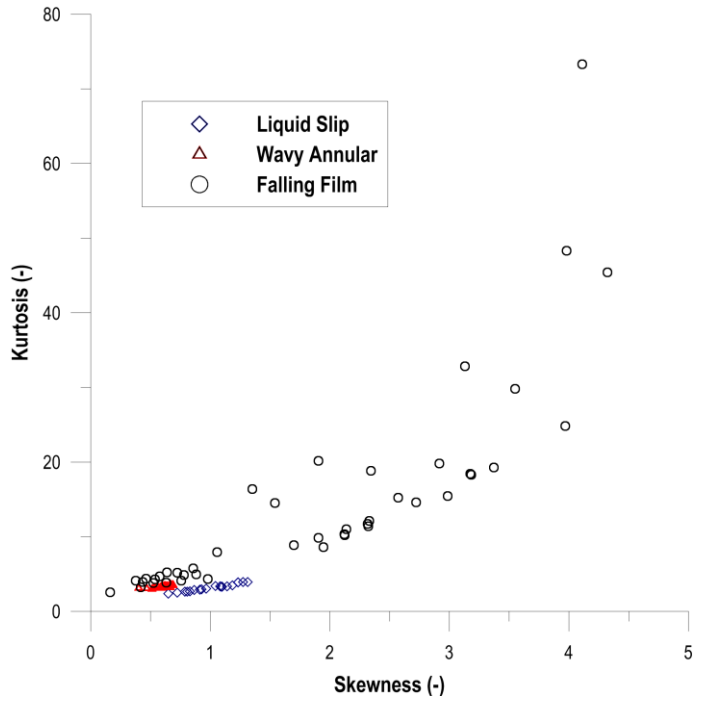

Figure 4.10 Skewness vs. kurtosis for μ_{oil} = 586 mPa·s

4.2 Pressure Gradient

Figures 4.11 to 4.14 show the measured pressure gradient vs. superficial gas velocity depending on oil viscosities. Pressure gradient significantly changes with the transition of flow pattern type. When Falling Film flow pattern occurs, as the liquid flows due to the gravity instead of pressure differences, pressure gradient is almost zero. For Liquid Slip flows, negative pressure gradient is observed for low gas rate conditions because of its high liquid flow rate. With the increase of gas rate, flow pattern changes to Wavy Annular flow. Pressure gradient increases sharply due to the high friction force. For wavy annular flow, pressure gradient increases linearly with increase of superficial gas velocity and its slope increases with higher v_{SL}.

Figures 4.15 compares pressure gradient for v_{SL}=0.3 m/s. Two features can be concluded from the figures. As liquid viscosity decreases, inflection point of pressure gradient positions at higher v_{SG} for same v_{SL}. This feature corresponds with which discussed in previous section; for lower liquid viscosity, annular wavy flow pattern occurs at higher gas rate condition. And slope of pressure gradient becomes larger for high liquid viscosity flow.

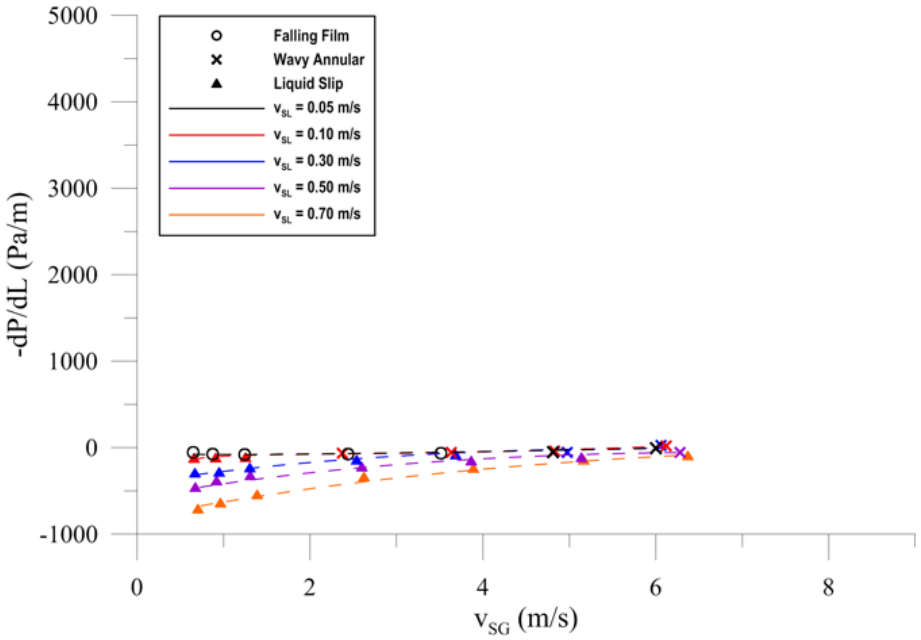

Figure 4.11 Pressure gradient vs. superficial gas velocity

for μ_{oil} = 127 mPa·s

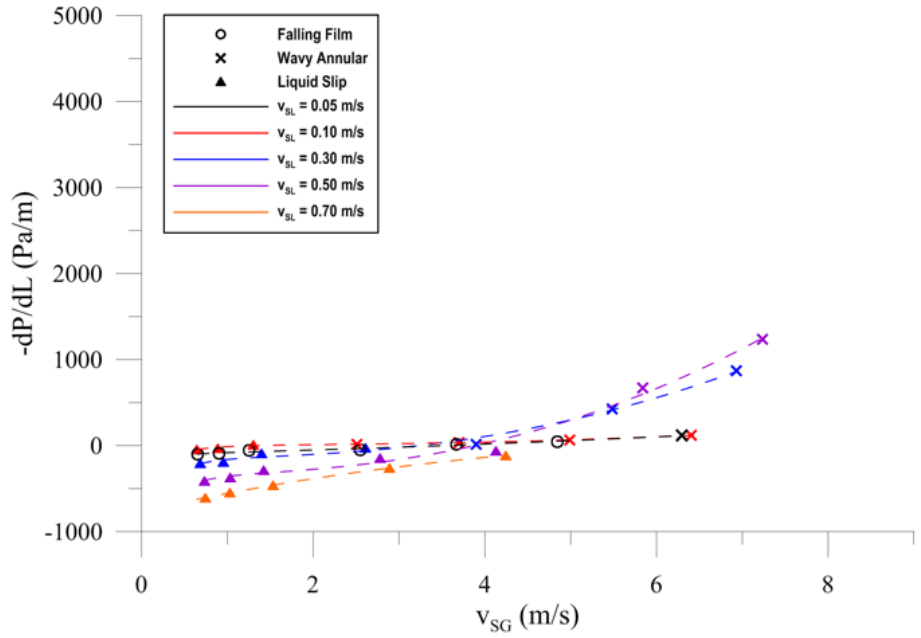

Figure 4.12 Pressure gradient vs. superficial gas velocity

for μ_{oil} = 213 mPa·s

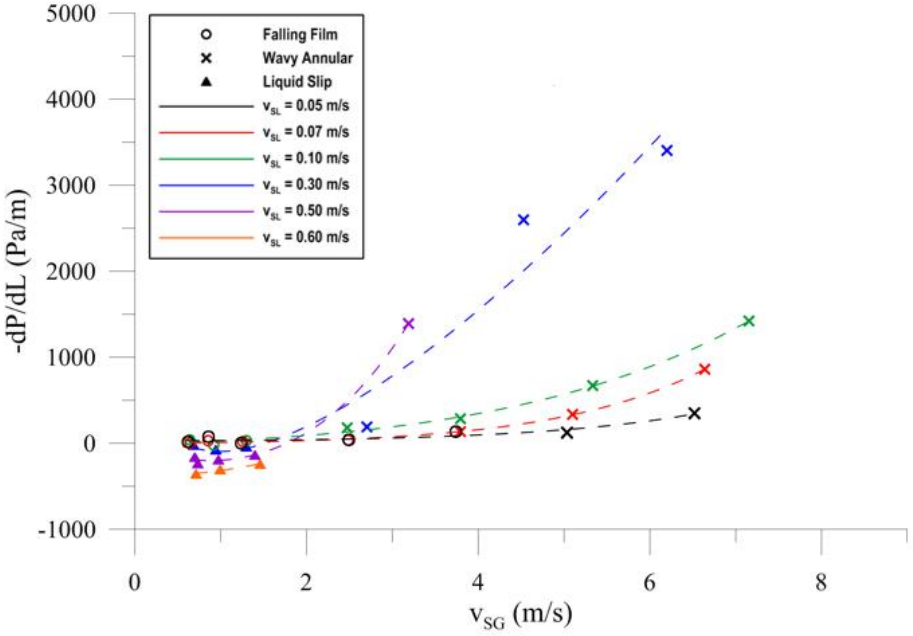

Figure 4.13 Pressure gradient vs. superficial gas velocity for μ_{oil} = 401 mPa·s

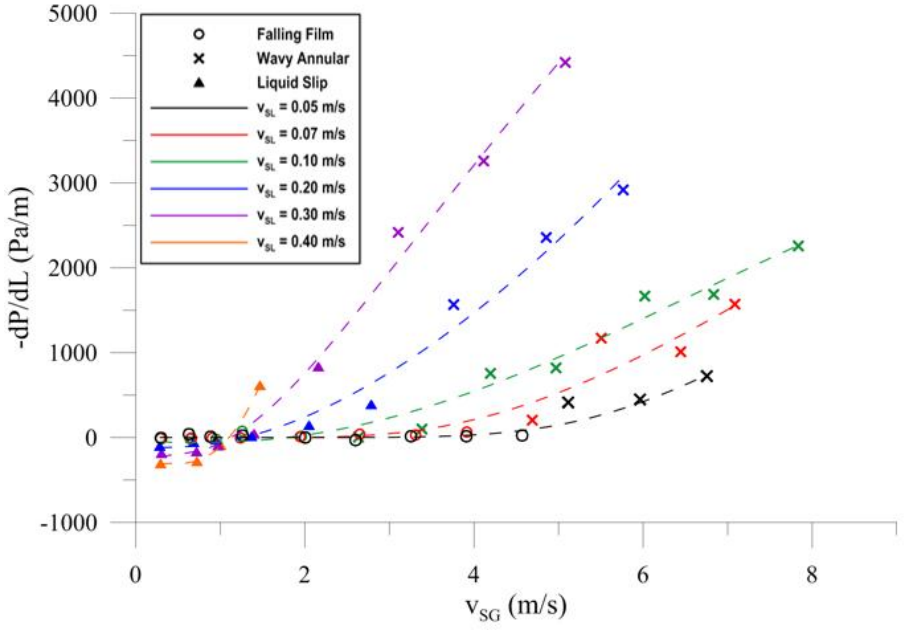

Figure 4.14 Pressure gradient vs. superficial gas velocity for μ_{oil} = 586 mPa·s

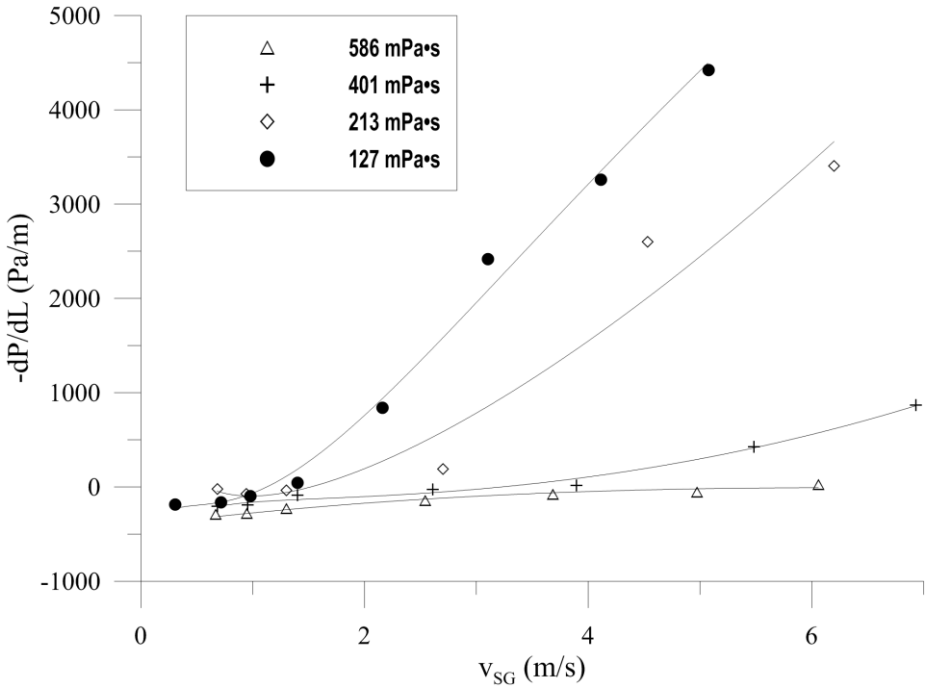

Figure 4.15 Comparison of pressure gradient for v_{SL}=0.3 m/s.

4.3 Average Liquid Holdup

Figures 4.16 to 4.19 show the average liquid holdup vs. superficial gas velocity depending on oil viscosities. Between Falling Film and Wavy Annular flow patterns, average liquid holdup shows no significant differences. For both flow patterns, most liquids flow in the liquid film region. On the other hand, average liquid holdup suddenly increases as the flow pattern changes from Liquid Slip to Wavy Annular for high viscosity condition. As flow pattern changes from liquid slip to wavy annular, gas tends to flow through center of the pipe pushing liquid droplet towards wall direction. Liquid droplets flow much faster than liquid film, and the deposition of liquid droplets to film region with flow pattern transition results in a decrease of average liquid velocity and an increase of average liquid holdup (Figure 4.20). However, liquid film can flow much faster in low viscosity condition, resulting large and clear role waves on liquid film surface. Consequently, as gas superficial velocity increases, liquid holdup decreases.

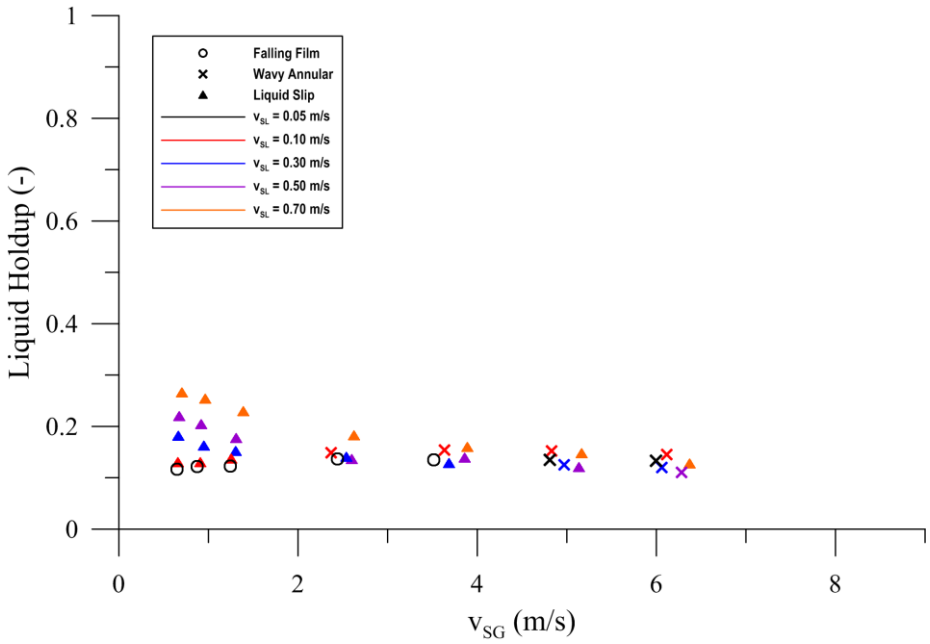

Figure 4.16 Liquid holdup vs. superficial gas velocity for μ_{oil} = 127 mPa·s

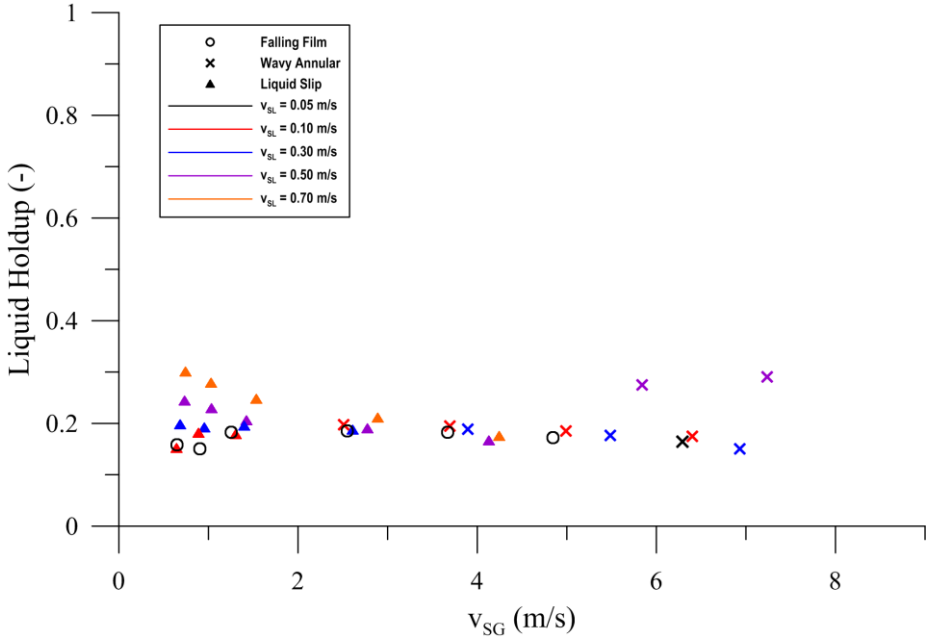

Figure 4.17 Liquid holdup vs. superficial gas velocity for μ_{oil} = 213 mPa·s

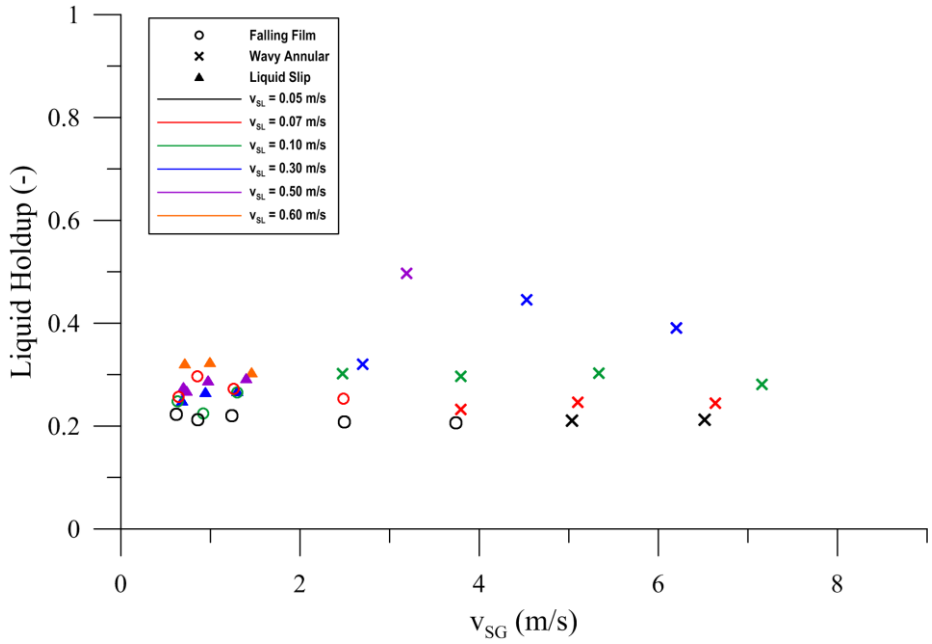

Figure 4.18 Liquid holdup vs. superficial gas velocity for μ_{oil} = 401 mPa·s

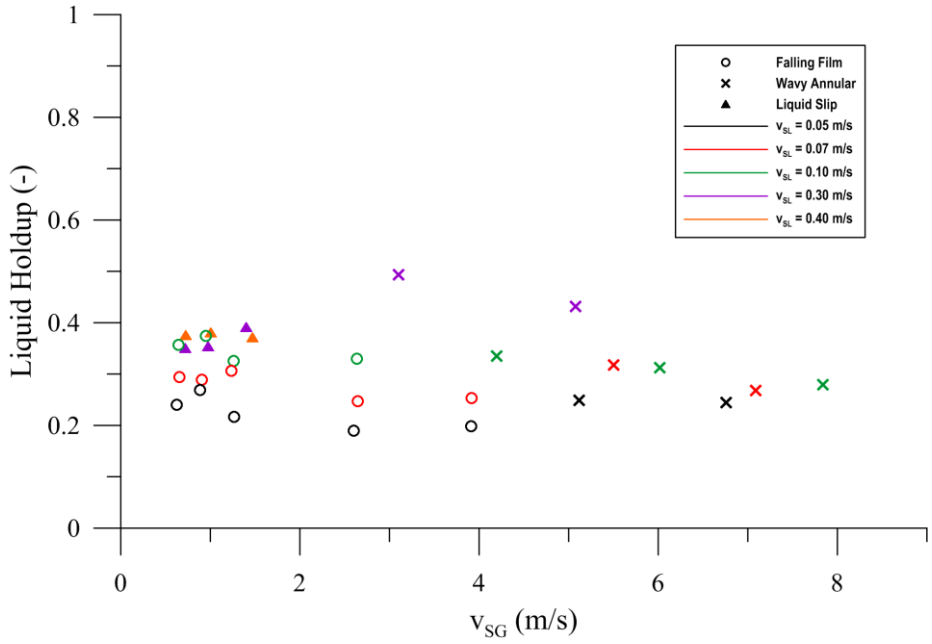

Figure 4.19 Liquid holdup vs. superficial gas velocity for μ_{oil} = 586 mPa·s

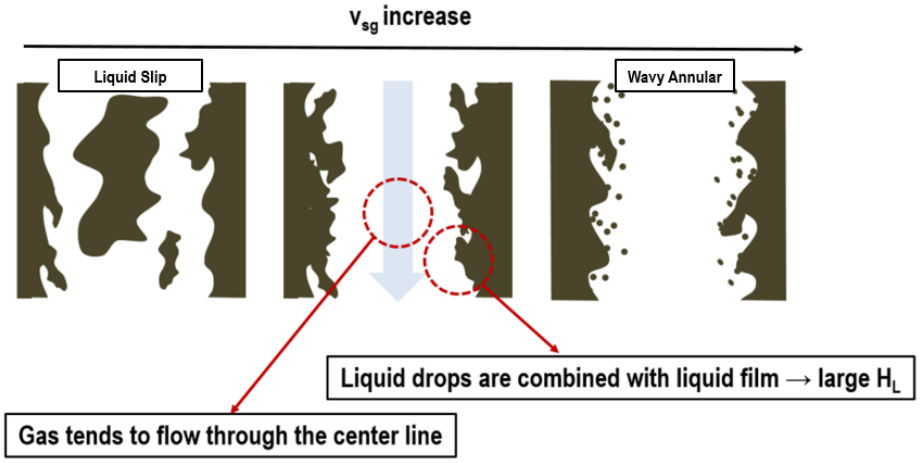

Figure 4.20 Schematic of sudden increase of liquid holdup between Liquid Slip and Wavy Annular flow patterns

Chapter 5 Discussions

5.1 Model Comparison

This section presents the evaluation of existing mechanistic models against the acquired two-phase flow data. The comparison is subdivided into sections of flow pattern, average liquid holdup, and pressure gradient.

5.1.1 Flow Pattern

Two models were considered for flow pattern prediction: Barnea et al. (1987), and TUFFP Unified (2011) model. Figure 5.1 through Figure 5.4 show the comparison between the observed flow patterns high oil viscosities and the predicted flow patterns map models of Barnea (1987), and TUFFP (2011) version 2011.

For most of the experimental conditions, the Barnea (1987) model and the TUFFP Unified (2011) model predict flow patterns as intermittent flow. For low viscosity condition, some of the point are included in annular flow in Barnea's (1987) model.

Transition criteria of annular flow and intermittent flow in Barnea's model is highly affected by slug liquid holdup. As the model was developed based on water-gas condition, it assumes slug liquid holdup as 0.7, while slug liquid holdup of high viscosity oil was reported as higher than 0.95. TUFFP unified model calculates transition criteria of annular flow and intermittent

flow based on slug flow parameters. As the film length goes infinite, slug flow changes to annular flow or stratified flow.

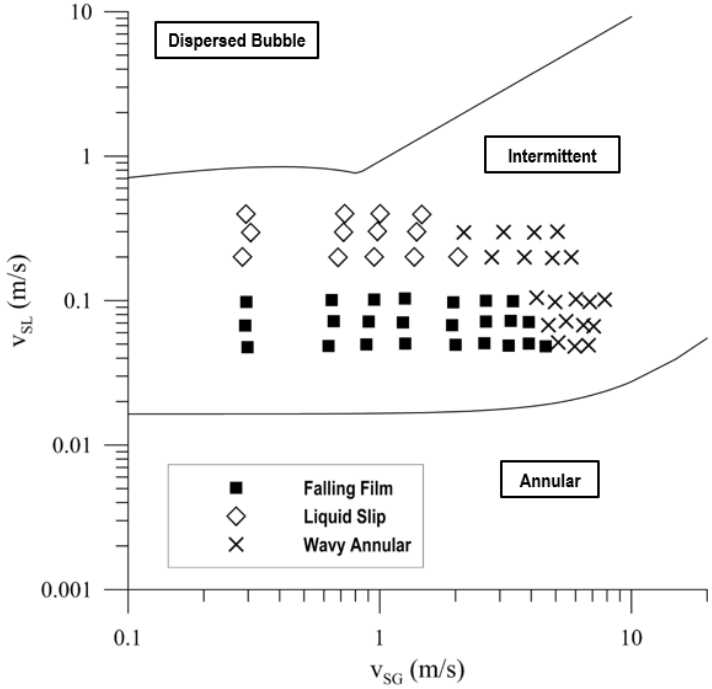

(a) Barnea's model (1987)

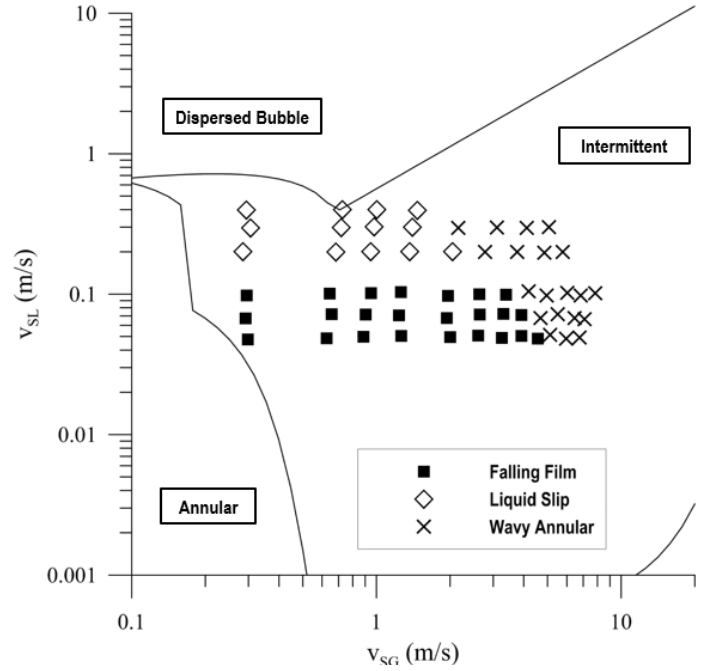

(b) TUFFP Unified (2011) model

Figure 5.1 Flow pattern map compared with observed flow patterns for μ_{oil} = 586 mPa·s

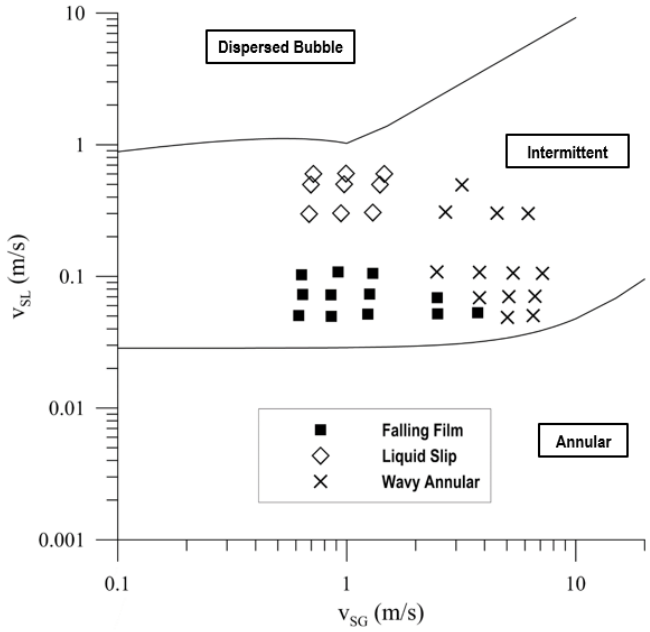

(a) Barnea's model (1987)

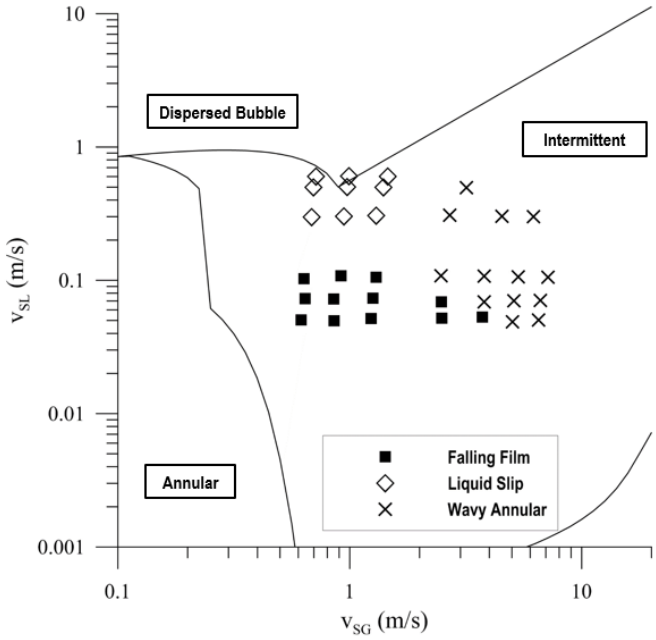

(b) TUFFP Unified (2011) model

Figure 5.2 Flow pattern map compared with observed flow patterns for μ_{oil} = 401 mPa·s

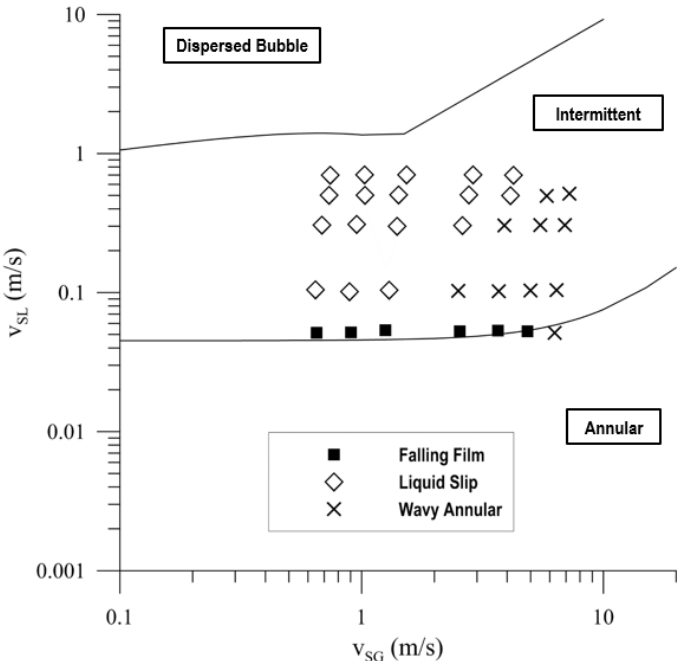

(a) Barnea's model (1987)

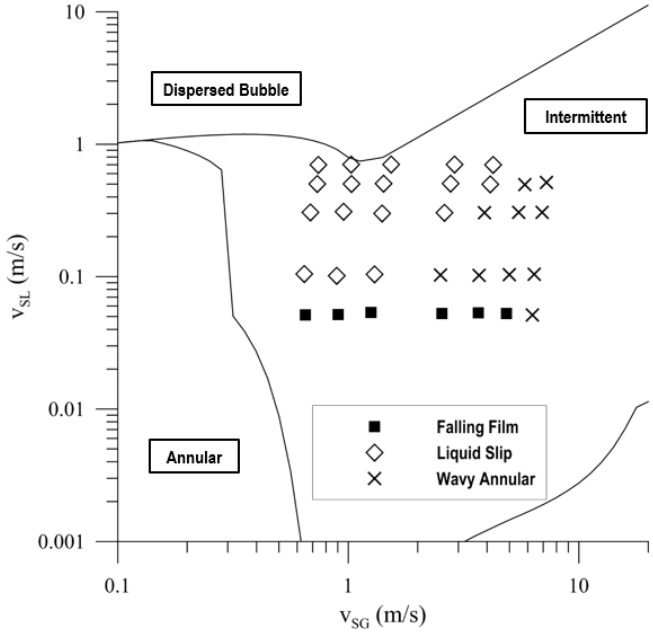

(b) TUFFP Unified (2011) model

Figure 5.3 Flow pattern map compared with observed flow patterns for μ_{oil} = 213 mPa·s

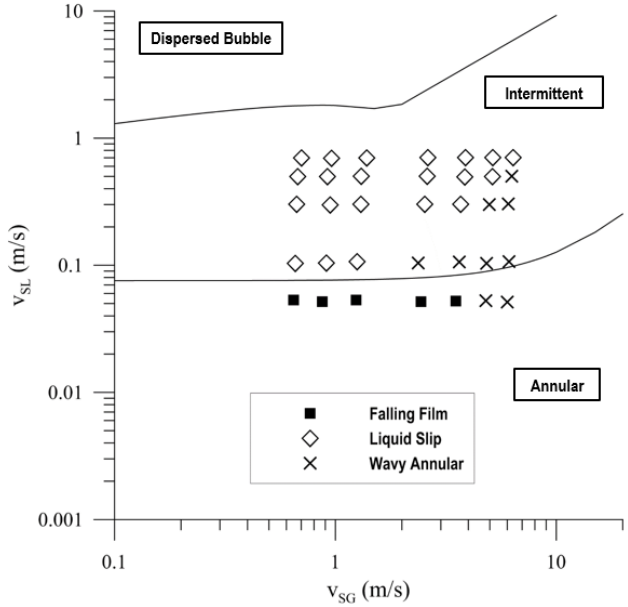

(a) Barnea's model (1987)

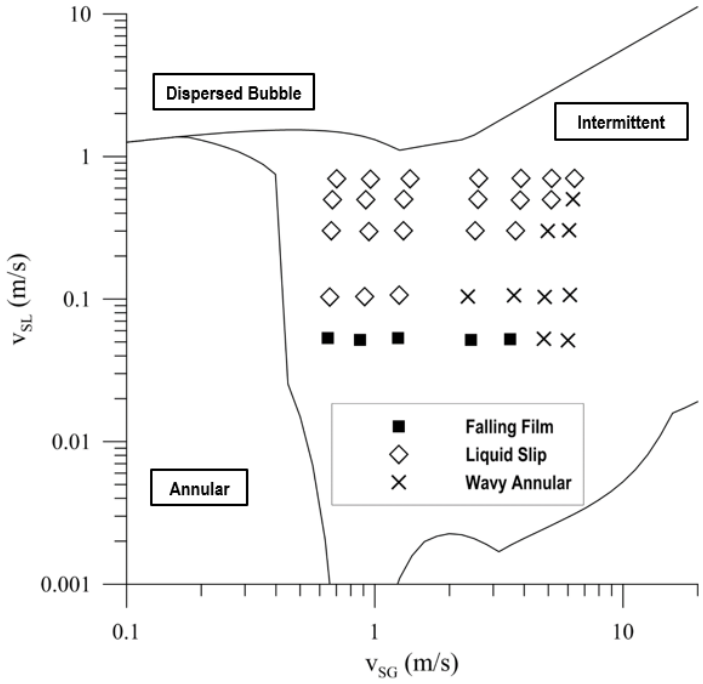

(b) TUFFP Unified (2011) model

Figure 5.4 Flow pattern map compared with observed flow patterns for μ_{oil} = 127 mPa·s

5.1.2 Pressure Gradient

Three models are compared against the experimental data for pressure gradient; TUFFP Unified (2011), OLGA version 7.2.3 steady-state model (OLGAS), and the annular model suggested by Alves et al. (1991). The correlations of Al-Sarkhi et al. (2011) and Wallis (1969) are used for liquid droplet entrainment fraction and interfacial friction factor, respectively. Figure 5.5 through Figure 5.8 show the comparison between the measured pressure gradient and the pressure gradient prediction of TUFFP (2011), OLGAS, and Alves's model.

When μ_{oil} = 586 mPa·s, Alves's annular model shows better prediction performance than others, especially for wavy annular flow. For other viscosity conditions, OLGA model shows better prediction performance than others, except it underestimates pressure gradients at μ_{oil} = 586 mPa·s. TUFFP model shows a tendency of overestimation over all viscosity conditions especially when the flow pattern is Falling Film or Liquid Slip. Alves model cannot predict negative pressure gradient over the all viscosities regardless flow patterns. Models show a tendency of over-prediction for all ranges of viscosity. Over-prediction of pressure gradients becomes severe for lower oil viscosities.

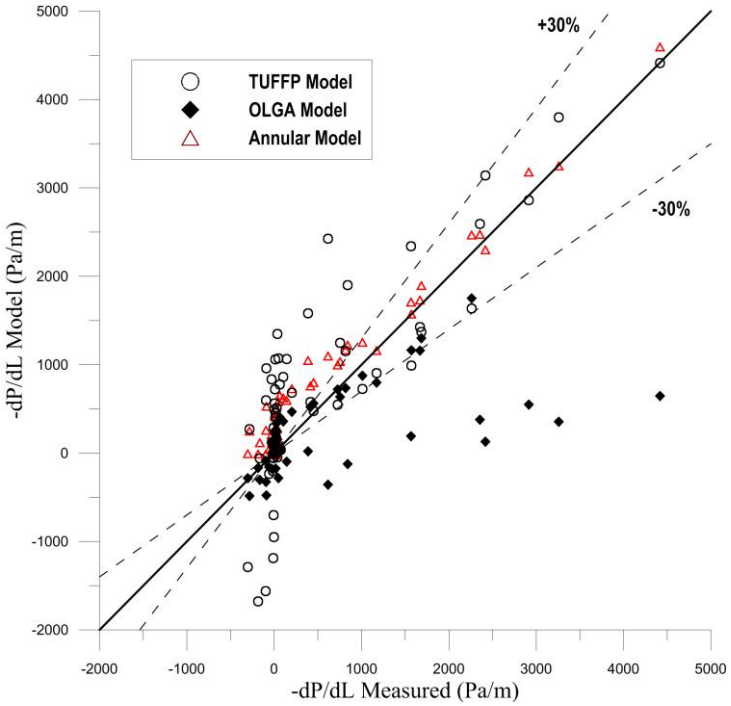

(a) Model prediction of pressure gradient

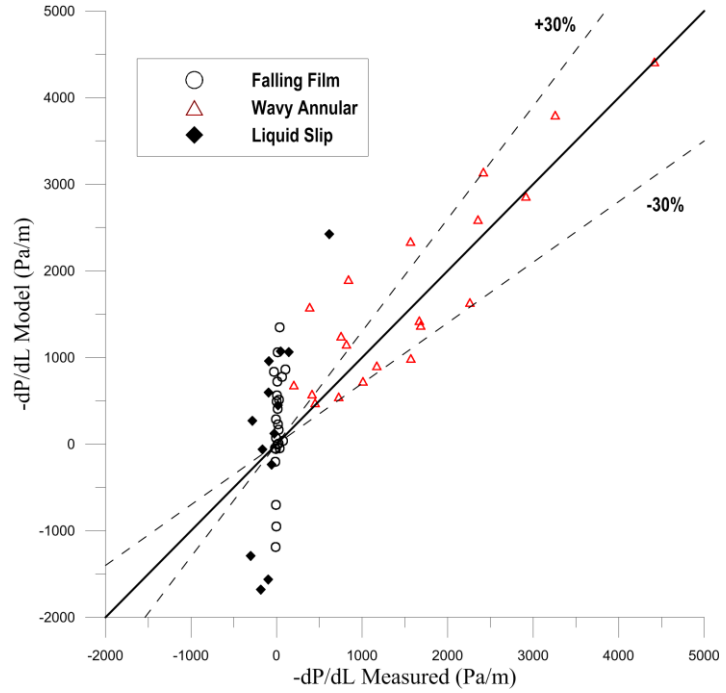

(b) TUFFP Unified (2011) model prediction marked with flow pattern

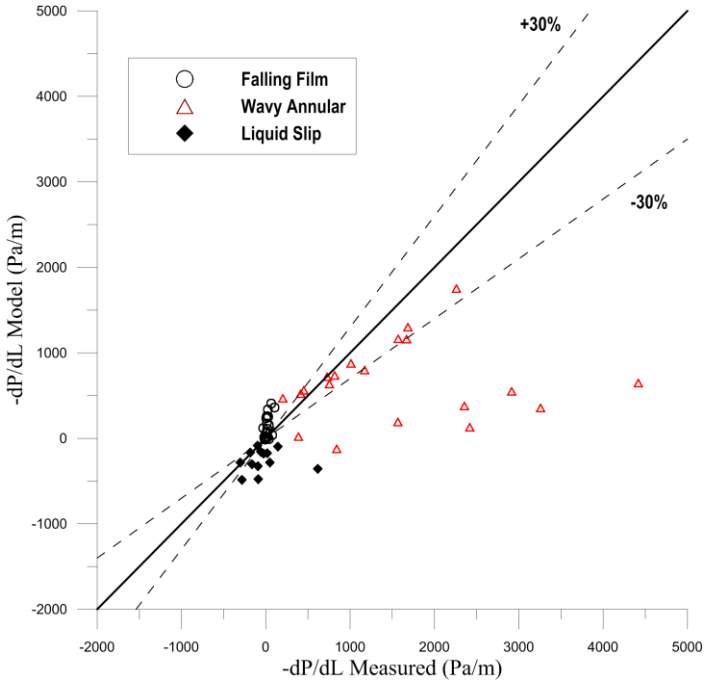

(c) OLGA model prediction marked with flow pattern

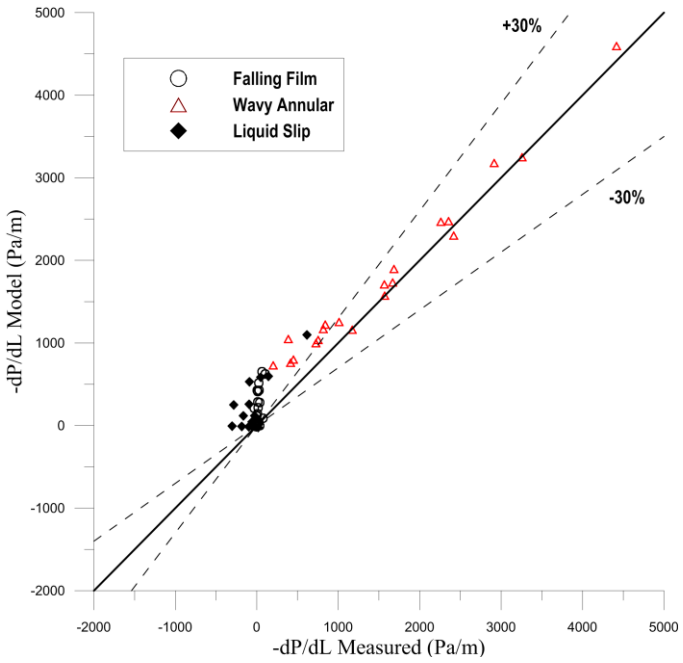

(d) Alves et al. (1991) model prediction marked with flow pattern

Figure 5.5 Pressure gradient prediction compared with measured data for μ_{oil} = 586 mPa·s

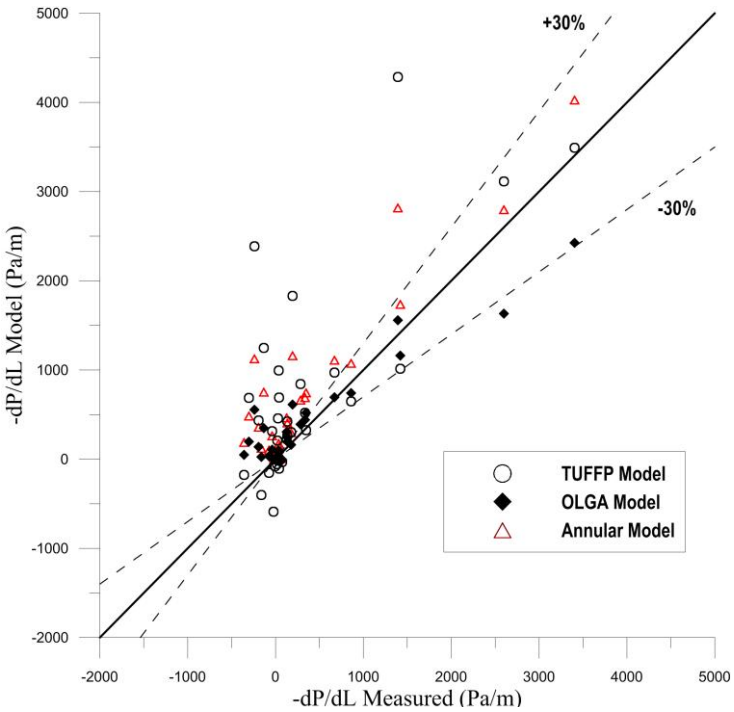

(a) Model prediction of pressure gradient

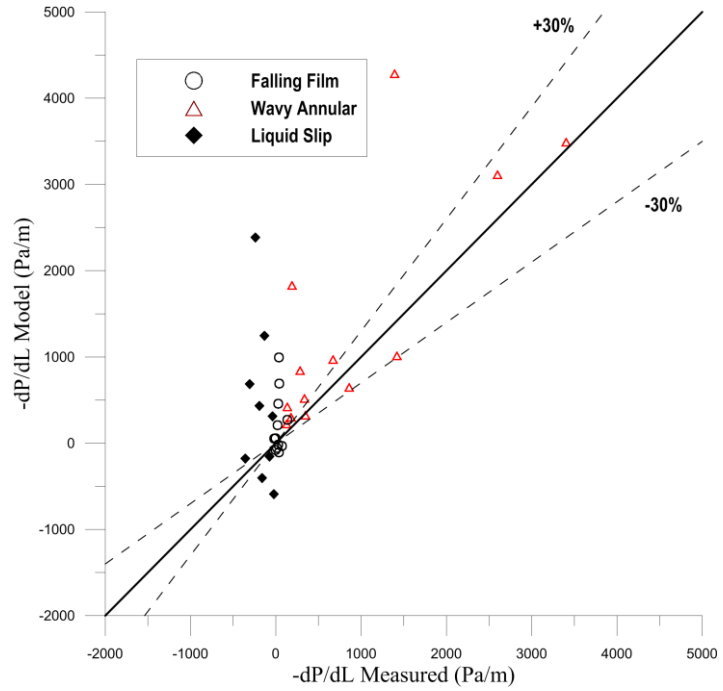

(b) TUFFP Unified (2011) model prediction marked with flow pattern

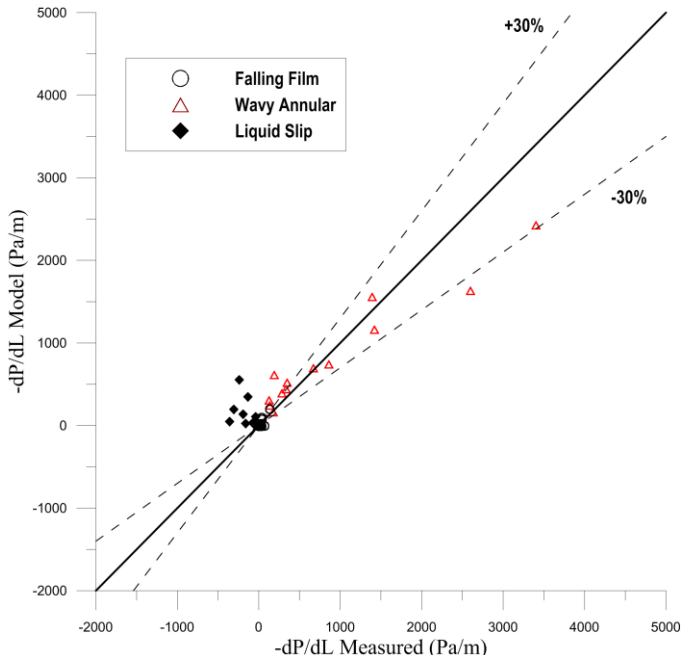

(c) OLGA model prediction marked with flow pattern

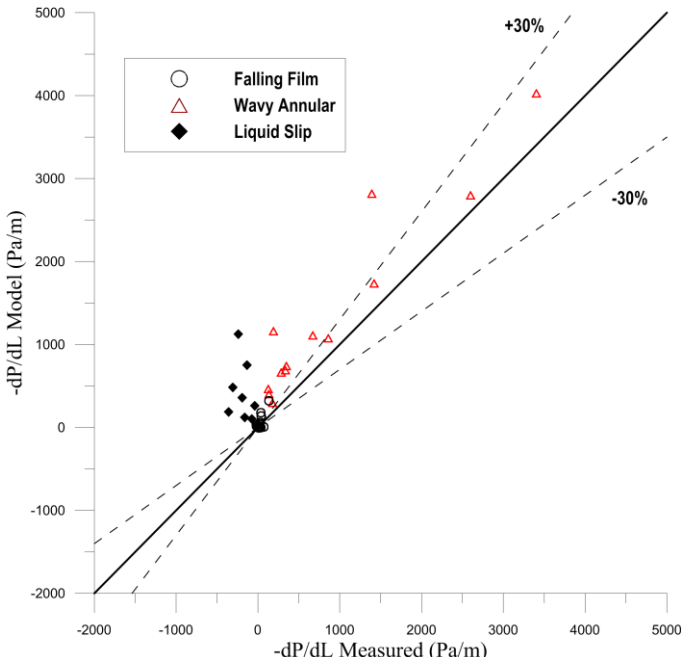

(d) Alves et al. (1991) model prediction marked with flow pattern

Figure 5.6 Pressure gradient prediction compared with measured data for μ_{oil} = 401 mPa·s

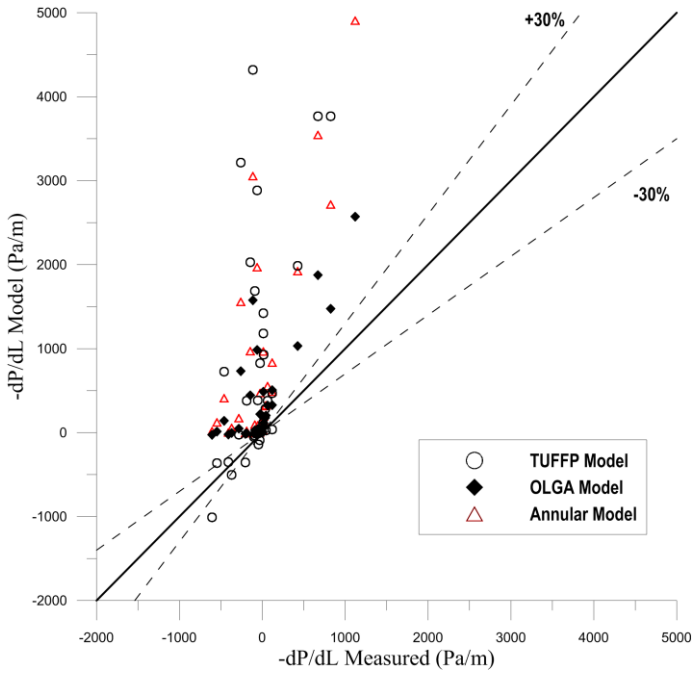

(a) Model prediction of pressure gradient

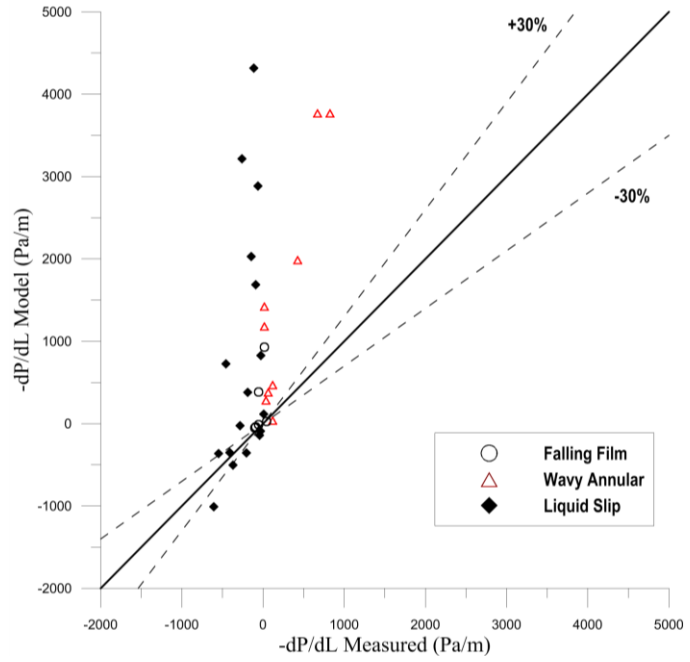

(b) TUFFP Unified (2011) model prediction marked with flow pattern

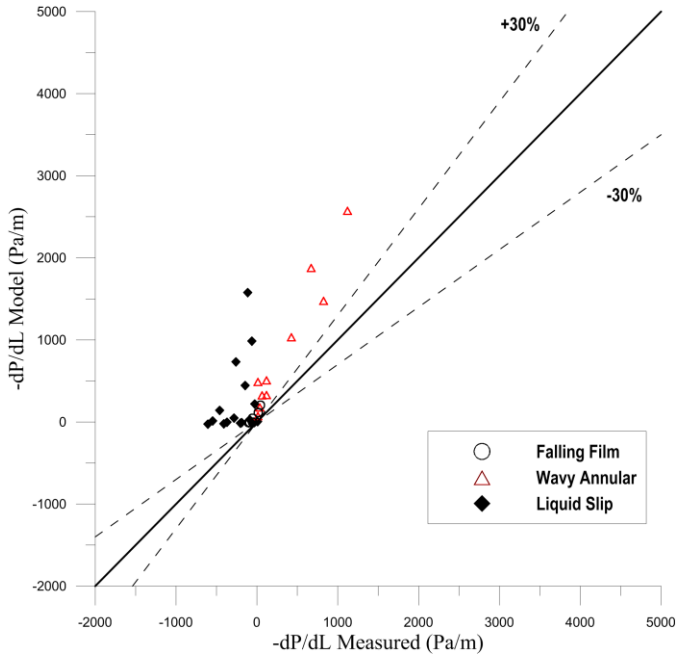

(c) OLGA model prediction marked with flow pattern

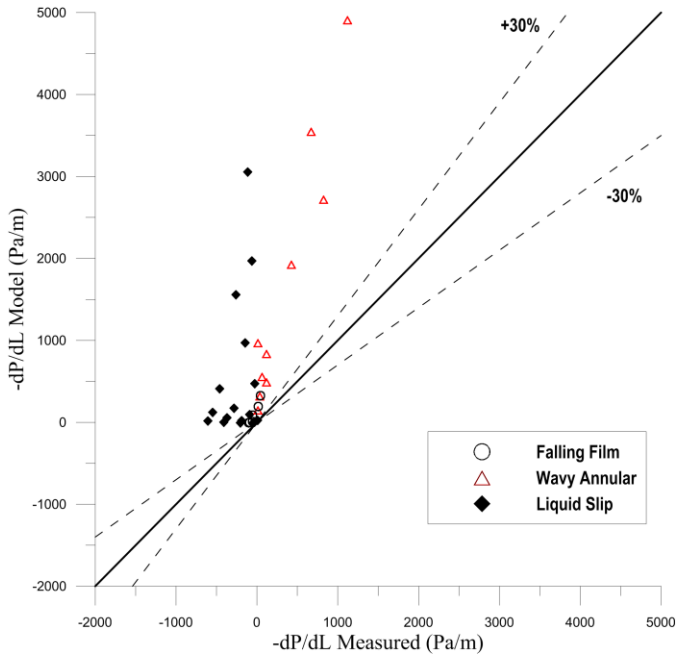

(d) Alves et al. (1991) model prediction marked with flow pattern

Figure 5.7 Pressure gradient prediction compared with measured data for μ_{oil} = 213 mPa·s

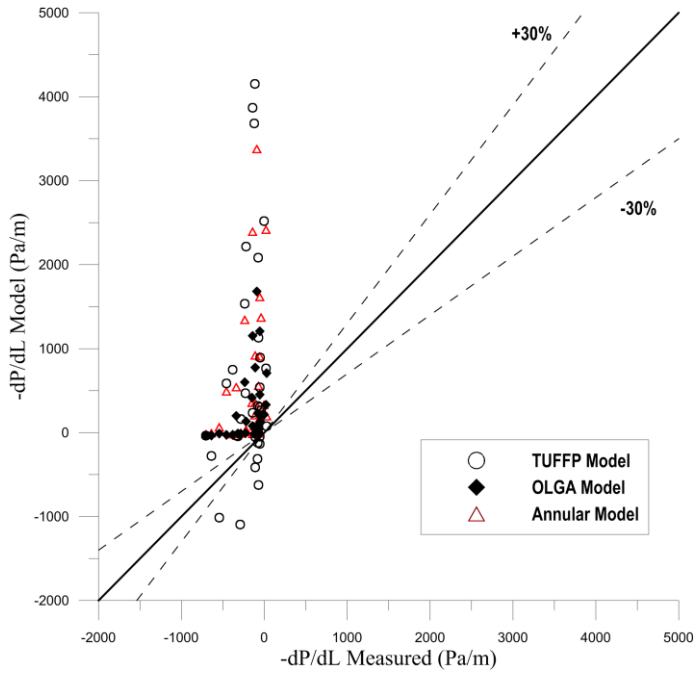

(a) Model prediction of pressure gradient

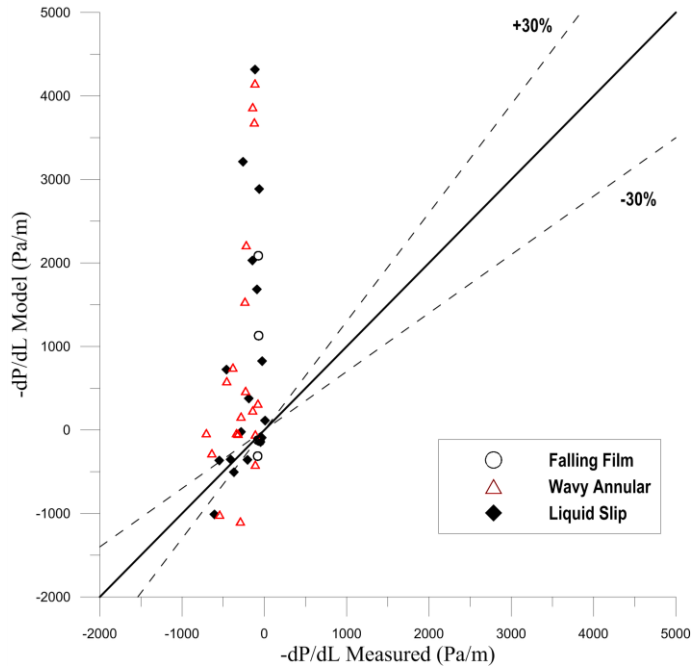

(b) TUFFP Unified (2011) model prediction marked with flow pattern

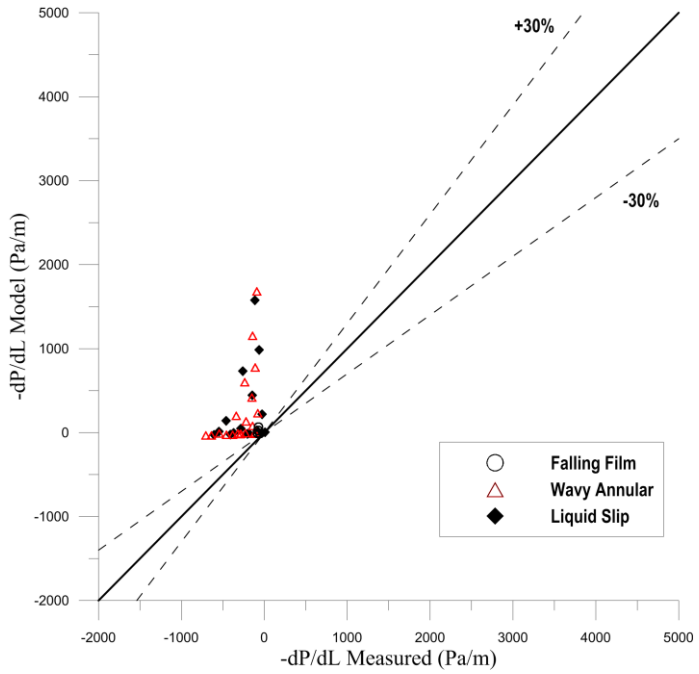

(c) OLGA model prediction marked with flow pattern

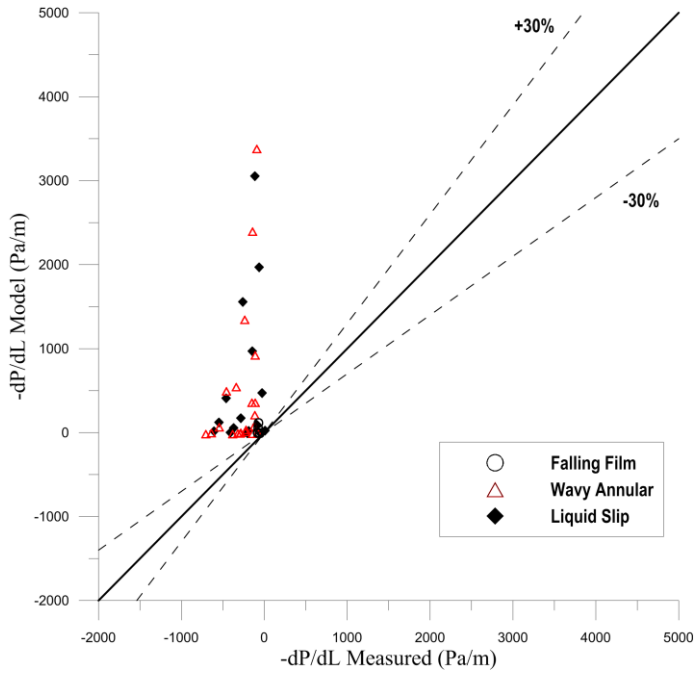

(d) Alves et al. (1991) model prediction marked with flow pattern

Figure 5.8 Pressure gradient prediction compared with measured data for μ_{oil} = 127 mPa·s

5.1.3 Average Liquid Holdup

Three models are compared against the experimental data for average liquid holdup; TUFFP Unified (2011), OLGA version 7.2.3 steady-state model (OLGAS), and the annular model suggested by Alves et al. (1991). The correlations of Al-Sarkhi et al. (2011) and Wallis (1969) are used for liquid droplet entrainment fraction and interfacial friction factor, respectively. Figure 5.9 through Figure 5.12 show the comparison between the measured average liquid holdup and the average liquid holdup prediction of TUFFP (2011), OLGAS, and Alves's model.

Liquid holdups are overestimated, especially for the liquid slip flow pattern. As Al-Sarkhi's (2011) liquid entrainment model was developed based on upward flow of low viscosity liquid, it underestimates the amount of liquid entrainment into the gas core. Actual average liquid holdup is much lower for liquid slip flow because liquid drops in the gas core flow very fast. As liquid viscosity decreases, roll waves on the liquid film surface transport liquid faster for all flow patterns, resulting in lower liquid holdup values without heavy liquid droplet entrainment.

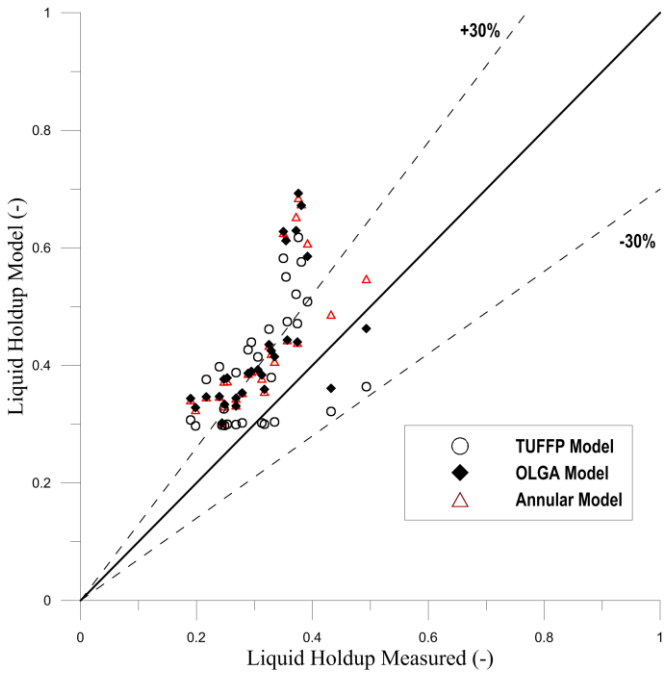

(a) Model prediction of average liquid holdup

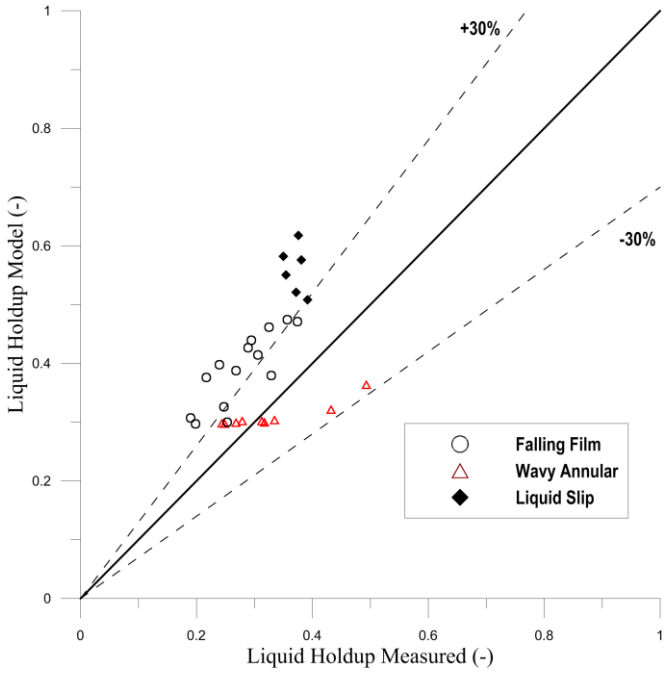

(b) TUFFP Unified (2011) model prediction marked with flow pattern

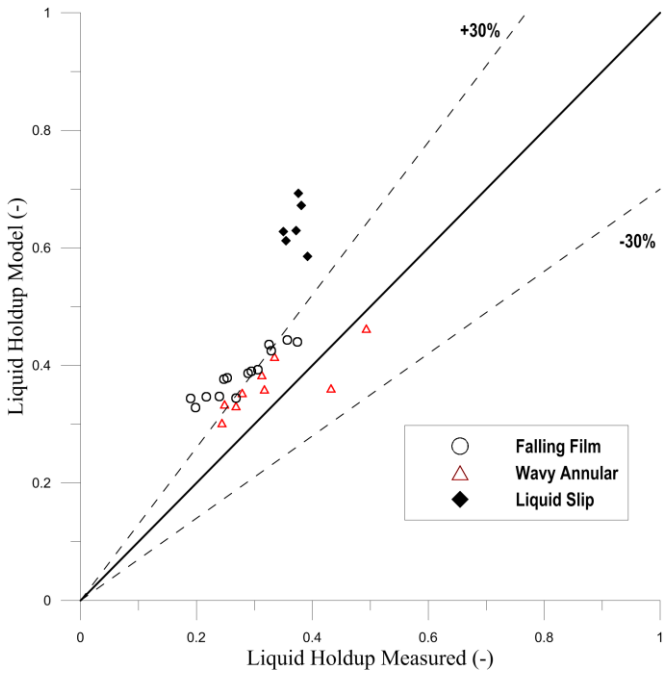

(c) OLGA model prediction marked with flow pattern

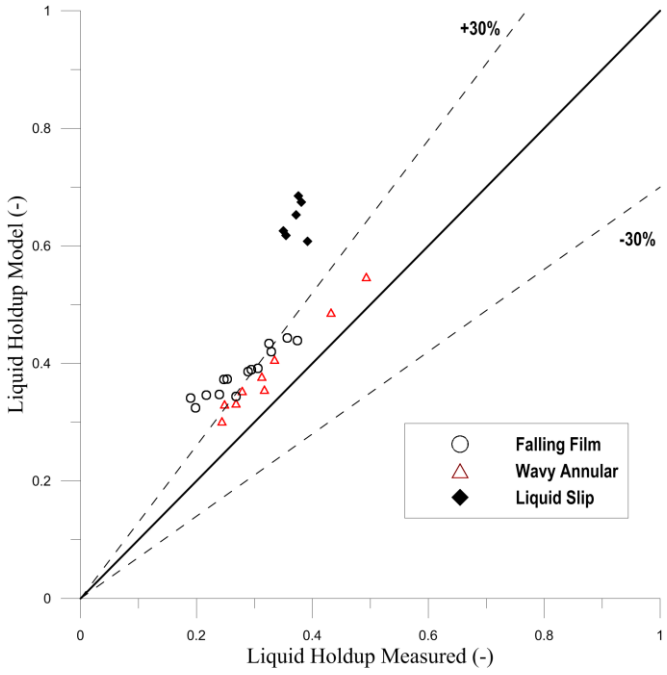

(d) Alves et al. (1991) model prediction marked with flow pattern

Figure 5.9 Average liquid holdup prediction compared with measured data for μ_{oil} = 586 mPa·s

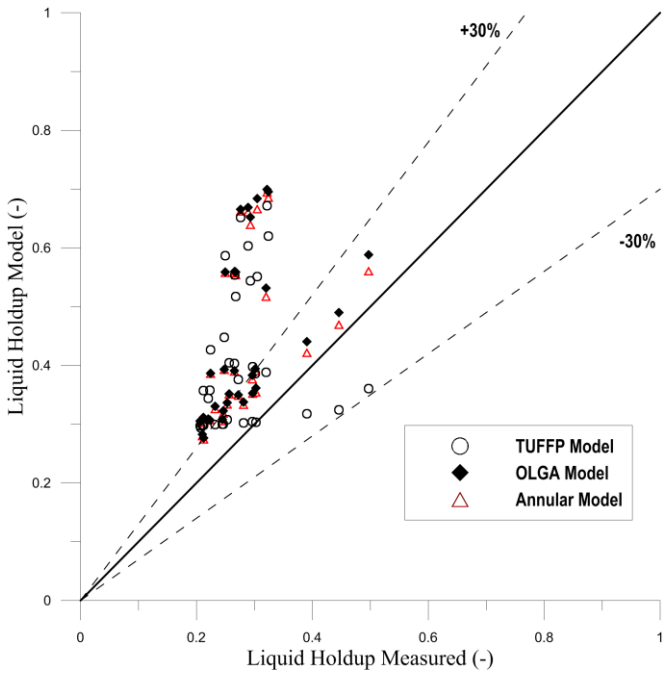

(a) Model prediction of average liquid holdup

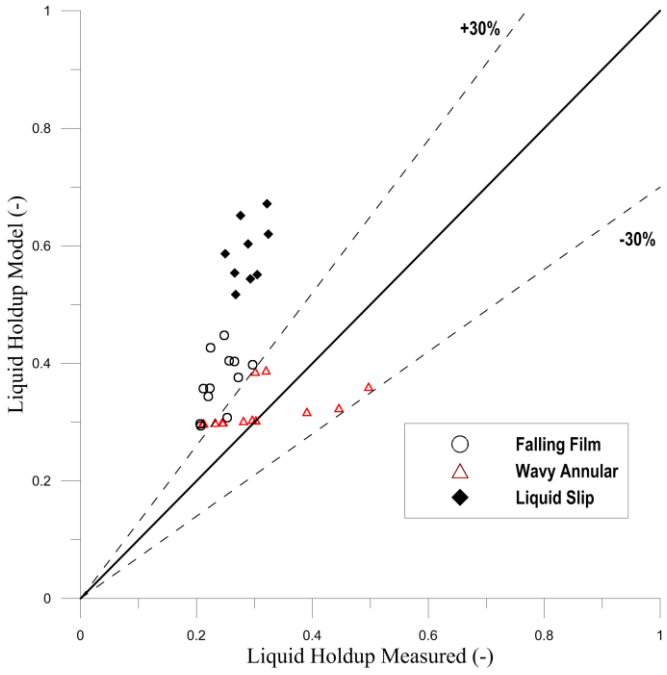

(b) TUFFP Unified (2011) model prediction marked with flow pattern

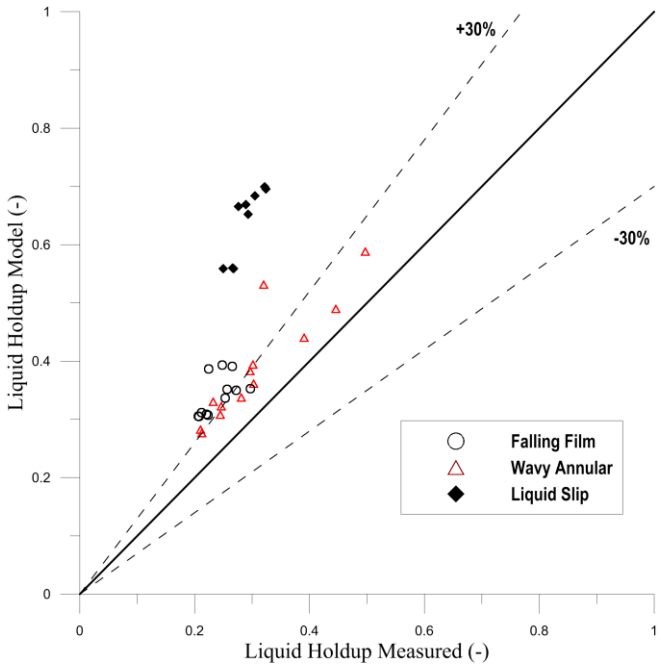

(c) OLGA model prediction marked with flow pattern

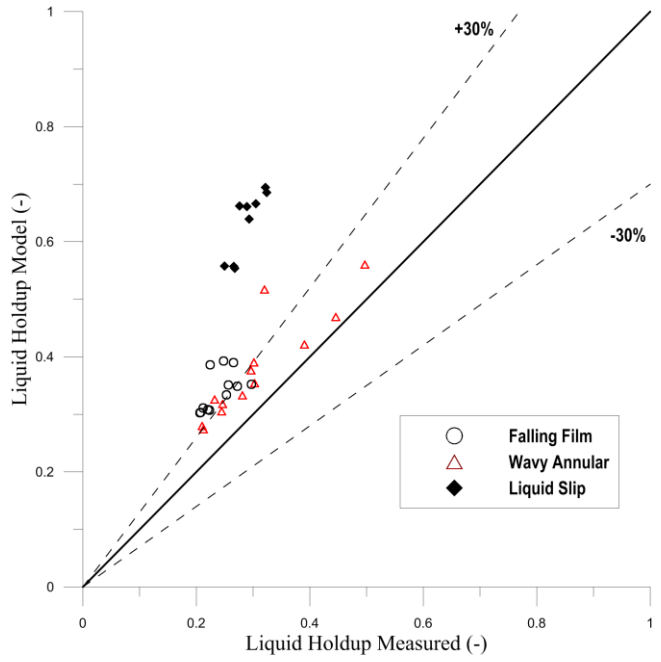

(d) Alves et al. (1991) model prediction marked with flow pattern

Figure 5.10 Average liquid holdup prediction compared with measured data for μ_{oil} = 401 mPa·s

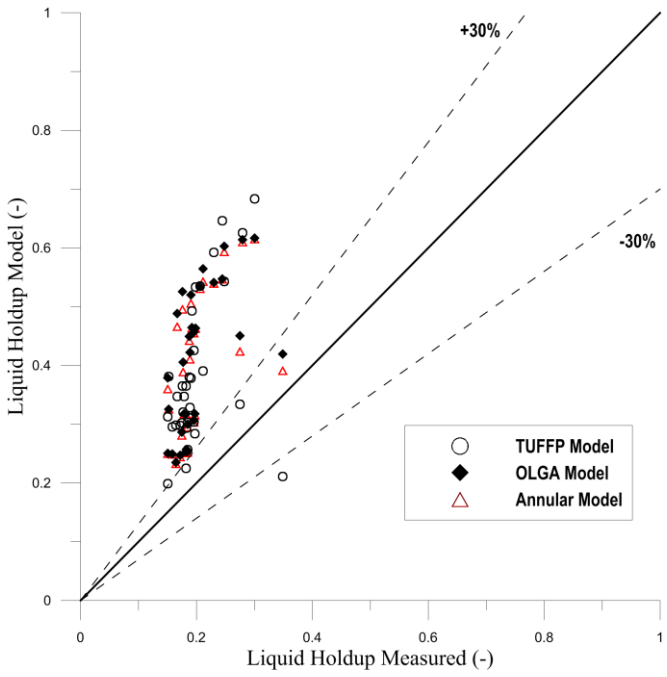

(a) Model prediction of average liquid holdup

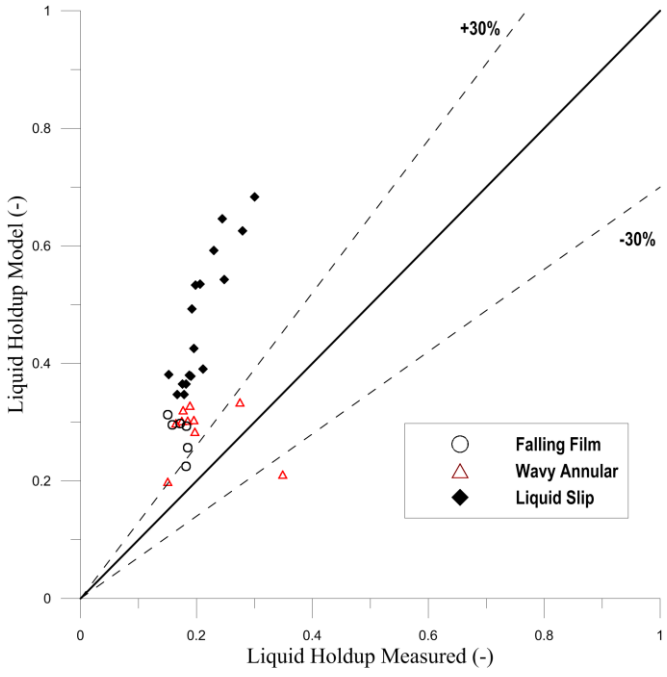

(b) TUFFP Unified (2011) model prediction marked with flow pattern

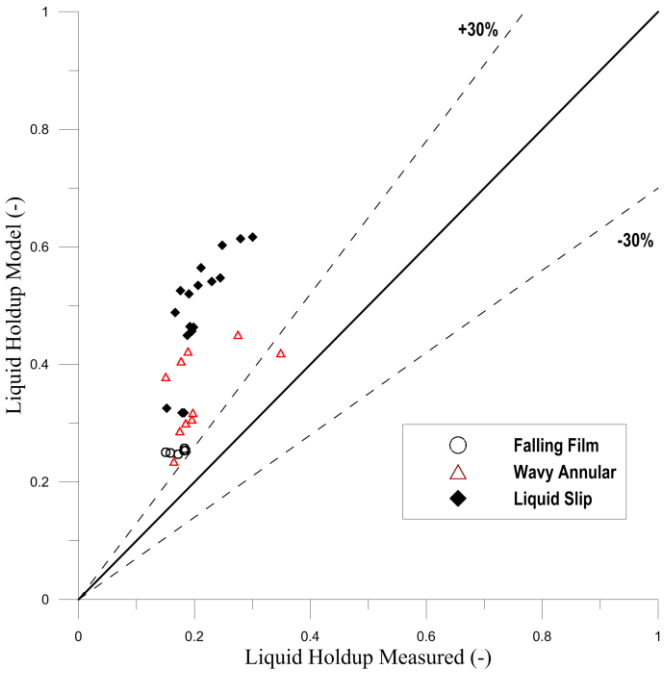

(c) OLGA model prediction marked with flow pattern

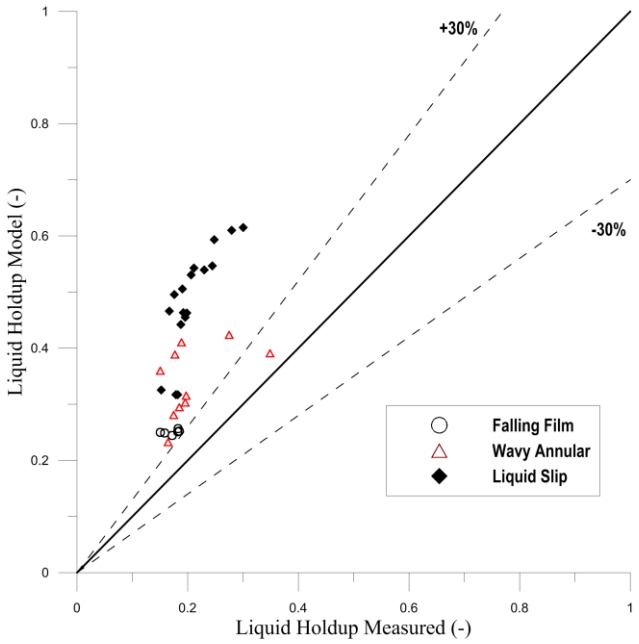

(d) Alves et al. (1991) model prediction marked with flow pattern

Figure 5.11 Average liquid holdup prediction compared with measured data for μ_{oil} = 213 mPa·s

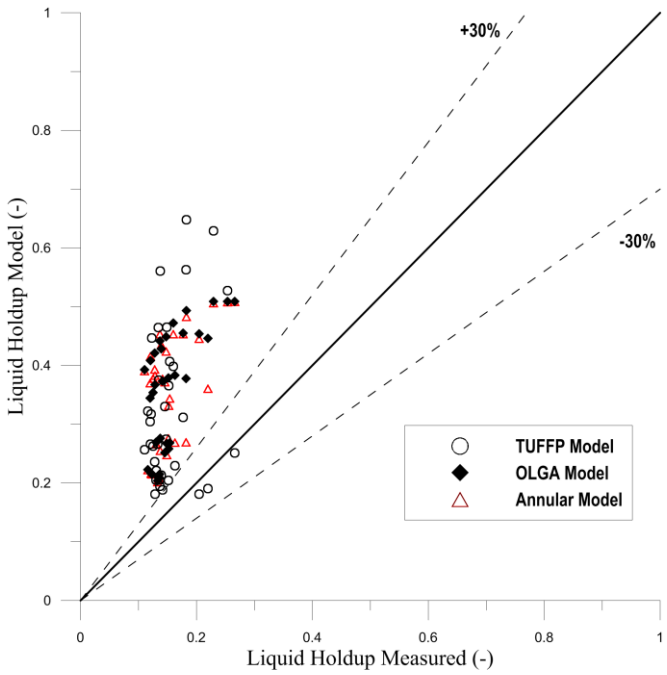

(a) Model prediction of average liquid holdup

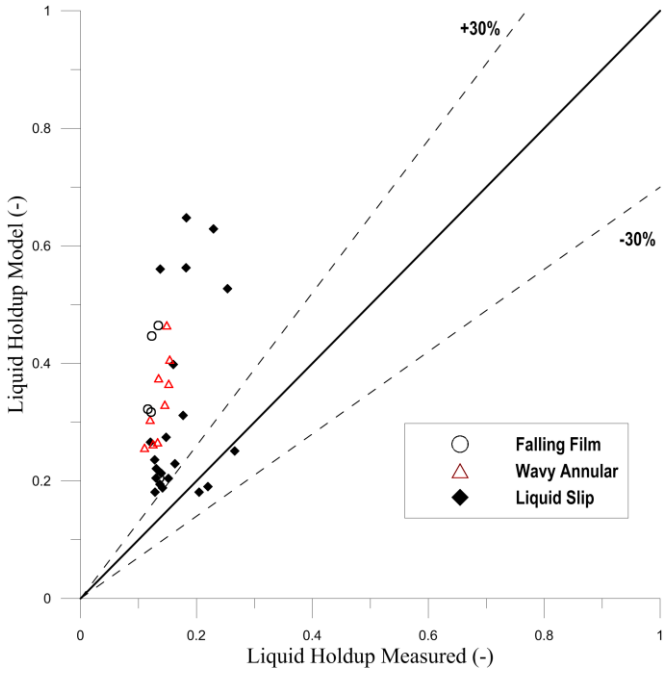

(b) TUFFP Unified (2011) model prediction marked with flow pattern

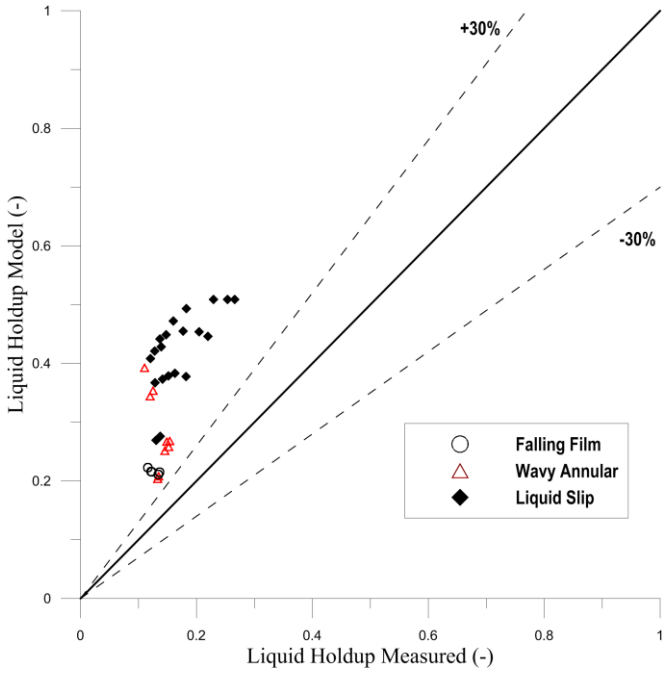

(c) OLGA model prediction marked with flow pattern

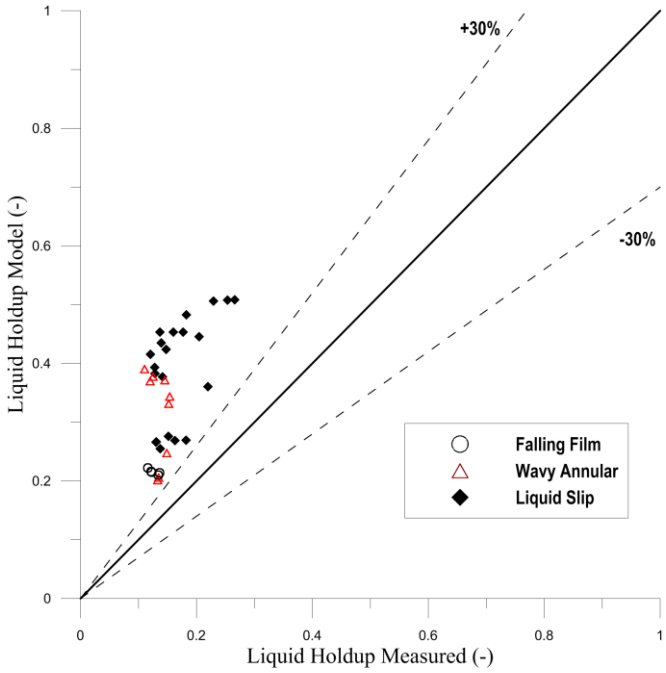

(d) Alves et al. (1991) model prediction marked with flow pattern

Figure 5.12 Average liquid holdup prediction compared with measured data for μ_{oil} = 127 mPa·s

5.2 Effect of Liquid Viscosity on Vertical Downward Flow

Mukherjee (1979) performed experimental study of inclined two-phase flow with low viscosity liquids including vertical downward flow. Kerosene and lube oil was used with the viscosity range of 1.0 ~ 2.5 mPa·s. Inner diameter of pipeline was 1.5 inch. Mukherjee's (1979) experimental data for low viscosity vertical downward flow are presented to discuss the effect of liquid viscosity on vertical downward flow.

The observed four flow patterns for vertical downward flow are, namely, stratified, annular mist, slug, and bubble flow. In his study, stratified (27 experimental points) and annular mist flow patterns (38 experimental points) correspond to Falling Film/liquid slip and wavy annular flow patterns, respectively. Stratified flow converted to annular mist flow as the superficial gas velocity increased (Figure 5.13).

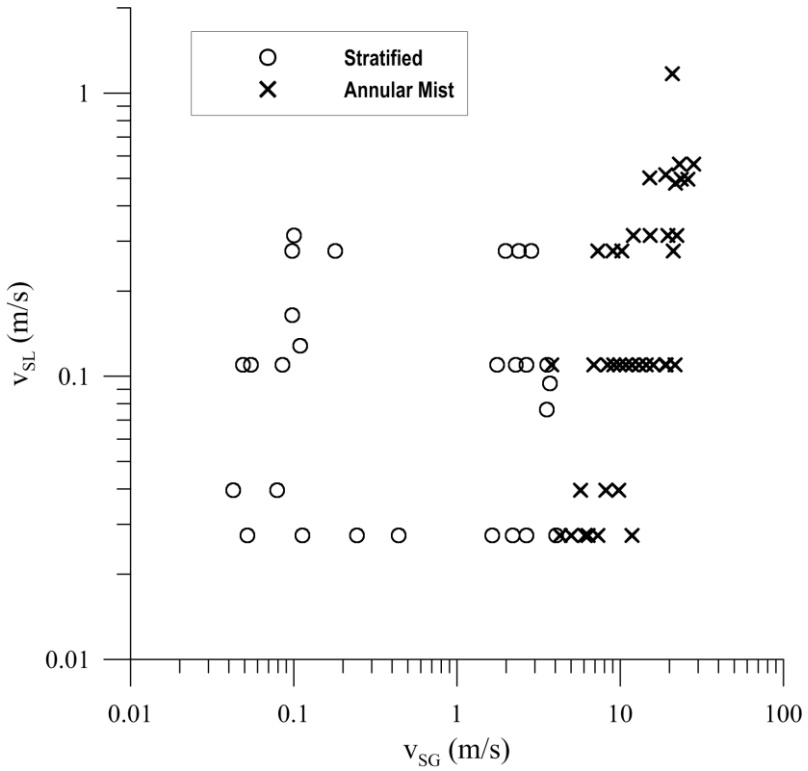

Figure 5.13 Observed flow pattern for vertical downward flow observed by Mukherjee (1979)

Figures 5.14 presents pressure gradient vs. superficial gas velocity from Mukherjee's study. Same as high viscosity case, pressure gradient sharply increase as the flow pattern changes from 'Stratified flow" to 'Annular Mist flow' with increase of gas velocity. As the flow pattern changes at higher v_{SG} comparing high viscosity case, the increase of pressure gradient occurs at higher v_{SG}.

Average liquid holdup is getting lower as superficial gas velocity increases. Rapid increase of liquid holdup was not observed as flow pattern changes from 'Stratified flow" to 'Annular Mist flow' due to low liquid viscosity (Figure 5.15).

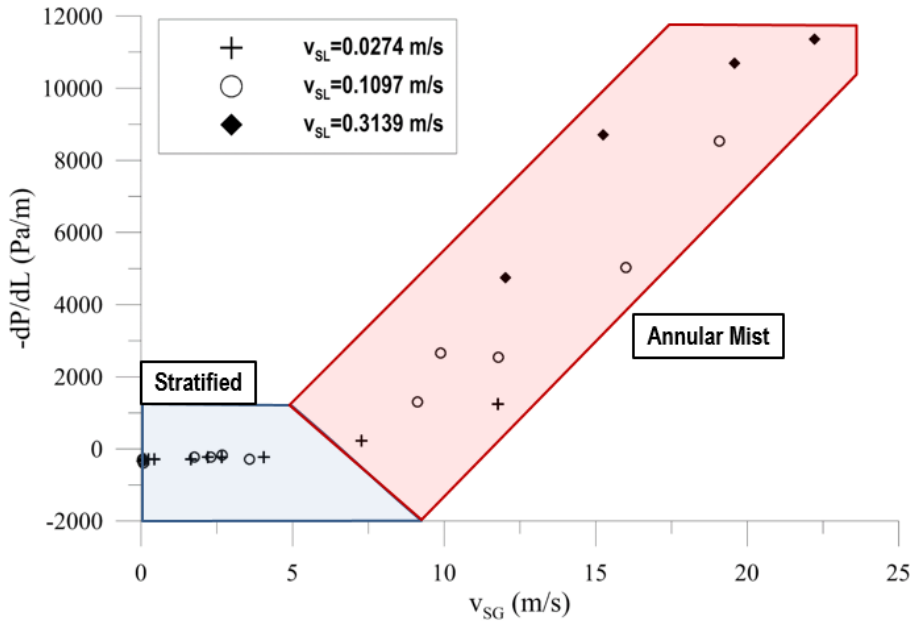

(a) μ_{oil} > 1.5 mPa·s

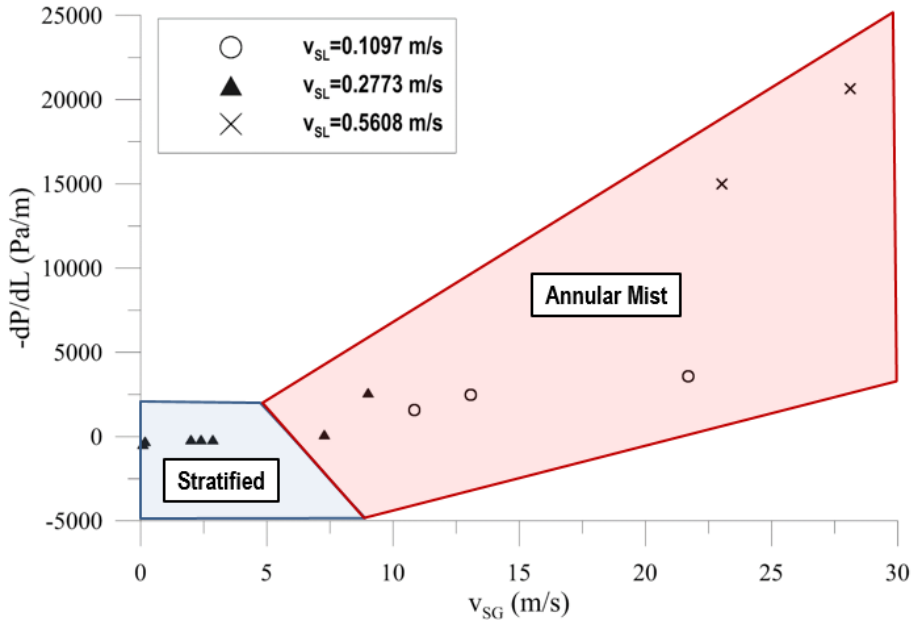

(b) μ_{oil} < 1.5 mPa·s

Figure 5.14 Pressure gradient vs. superficial gas velocity in Mukherjee's study

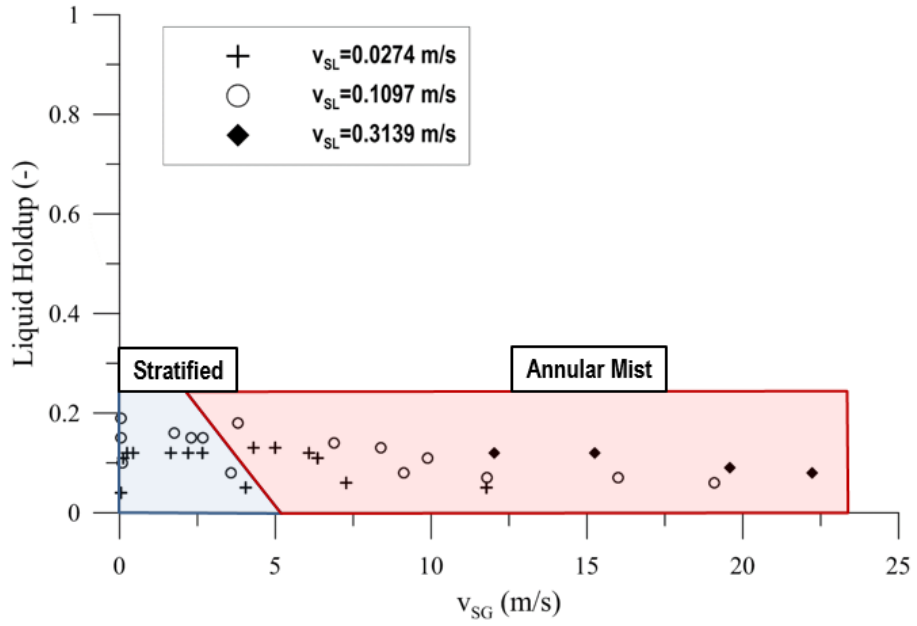

(a) μ_{oil} > 1.5 mPa·s

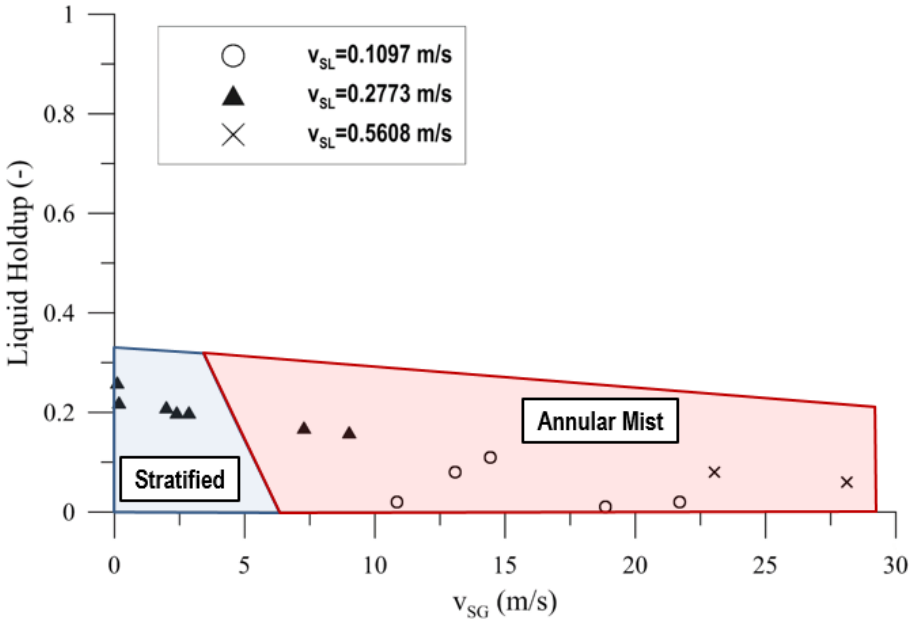

(b) μ_{oil} < 1.5 mPa·s

Figure 5.15 Liquid holdup vs. superficial gas velocity in Mukherjee's study

5.3 Closure Relationships for Annular Model

Two types of closure relationships are necessary in annular model; interfacial shear correlation and liquid entrainment fraction correlation. In section 5.1, Wallis (1969) and Al-sharkhi (2012)'s correlations are used. However, the prediction performance of model comparison results was dissatisfactory. In this section, performance of various closure relationships are examined for vertical annular flows. Two additional data was considered, Alruhaimani (2015) and Mukherjee (1979), to discuss the effects of flow direction and viscosity.

5.3.1 Liquid Entrainment Fraction Correlations

Two correlations were considered for liquid entrainment fraction correlation; Ishii & Mishima (1989) model and Al-Sarkhi's (2012) model. Ishii & Mishima (1989) is one of the common correlation for prediction of liquid entrainment in annular flow. It is based on a modified weber number defined as

$$We' = \frac{\rho_G v_G^2 d_F}{\sigma}\left(\frac{\rho_L - \rho_G}{\rho_G}\right)^{1/3} \tag{5-1}$$

where d_F is the hydraulic diameter of liquid film. Entrainment fraction can be

calculated from

$$f_E = \tanh\left[7.25 \times 10^{-7}(We')^{1.25} Re_F^{0.25}\right] \tag{5-2}$$

where Re_F is the liquid film Reynolds number.

Al-Sarkhi's (2012) model is modified from the model of Sawant et al. (2008). Entrainment fraction can be calculated as below:

$$f_E = f_{E,max}[1 - exp(-We_{SG}/We_{SG}^*)]$$

$$We_{SG} = \frac{\rho_G v_{SG}^2 D}{\sigma}\left(\frac{\rho_L - \rho_G}{\rho_G}\right)^{\frac{1}{4}},\ \alpha = 0.000231\ Re_{SL}^{-0.358} \tag{5-3}$$

$$We_{SG}^* = \left(\frac{f_{E,max}}{\alpha}\right)^{0.925},\ f_{E,max} = \left[1 - exp\left(-\left(\frac{Re_{SL}}{1400}\right)\right)^{0.6}\right]$$

5.3.2 Interfacial shear correlations

Three correlations were considered for liquid entrainment fraction correlation; Al-Sarkhi (2013), Whallet & Hewitt (1978), and Henstock & Hanratty (1976). Interfacial shear correlations can be expressed as equation (5-4)

$$I = \frac{f_I}{f_{SC}} \tag{5-4}$$

and each model calculates f_I. Liquid entrainment fraction correlations which are considered here are as below:

Al-Sarkhi (2013):

$$I = 1 + C\frac{\delta_L}{d} \tag{5-5}$$

C=750 (annular flow), 1270 (wavy annular), 21000 (slug and churn)

Whallet & Hewitt (1978):

$$I = 1 + 24\left(\frac{\rho_L}{\rho_G}\right)^{1/3}\left(\frac{\delta_L}{d}\right) \tag{5-6}$$

Henstock & Hanratty (1976):

$$I = 1 + 1{,}400F\left\{1 - exp\left[-\frac{(1 + 1{,}400F)^{1.5}}{13.2FG}\right]\right\} \tag{5-7}$$

$$F = \frac{(0.42Re_F^{1.25} + 2.8 \times 10^{-4}Re_F^{2.25})^{0.4}}{Re_{SG}^{0.9}}\frac{\mu_L}{\mu_G}\left(\frac{\rho_G}{\rho_L}\right)^{0.5}$$

$$G = \frac{\rho_L dg}{\rho_G v_{SG}^2 f_{SG}}$$

Al-Sarkhi's (2013) model is modified from the model of Wallis(1969). If C=300, it becomes Wallis's (1969) correlation.

5.3.3 Comparison with vertical upward annular flow experiment

For Alruhaimani's (2015) experimental data, vertical upward annular flow for

high viscosity oil, liquid holdup and pressure gradient prediction performances are presented in Figure 5.16 and Figure 5.17. As the liquid entrainment fraction is less than 1% due to the high viscosity, type of liquid entrainment correlations are not critical for average liquid holdup prediction. However type of interfacial shear correlation has an effect as it determines pressure gradient of fluid. Al-Sarkhi's correlation and Henstock & Hanratty's correlation show acceptable prediction performance.

However for vertical downward flow, liquid holdup is overestimated especially for Liquid Slip flow pattern. As we visually observed in the experiment, liquid entrainment fraction is much higher comparing vertical upward cases. Consequently, annular model shows disappointing prediction performances of pressure gradient and average liquid holdup.

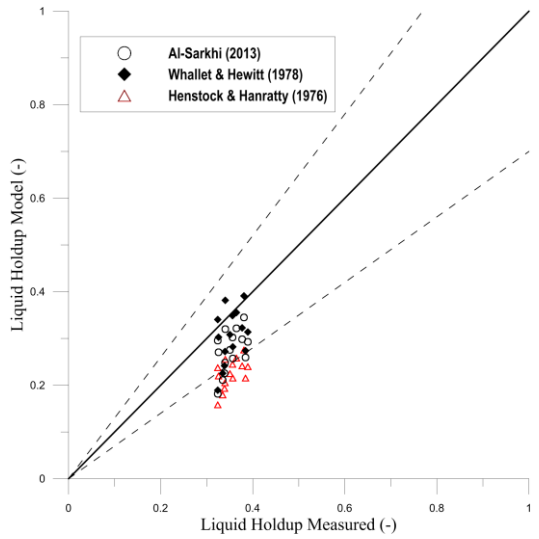

(a) Ishii & Mishima (1989)

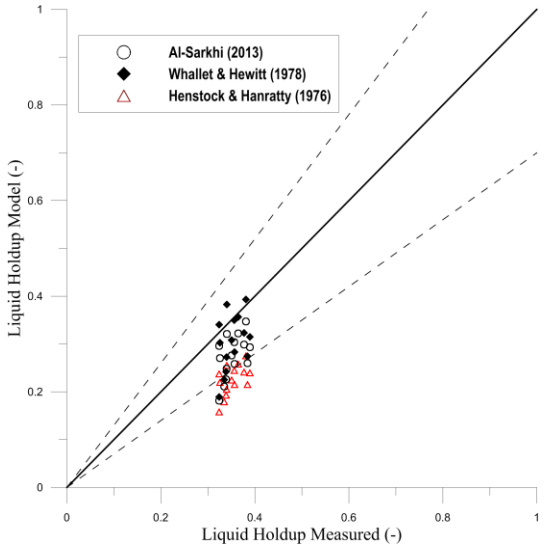

(b) Al-Sarkhi's (2011)

Figure 5.16 Average liquid holdup prediction for Alruhaimani's (2015) vertical upward annular flow

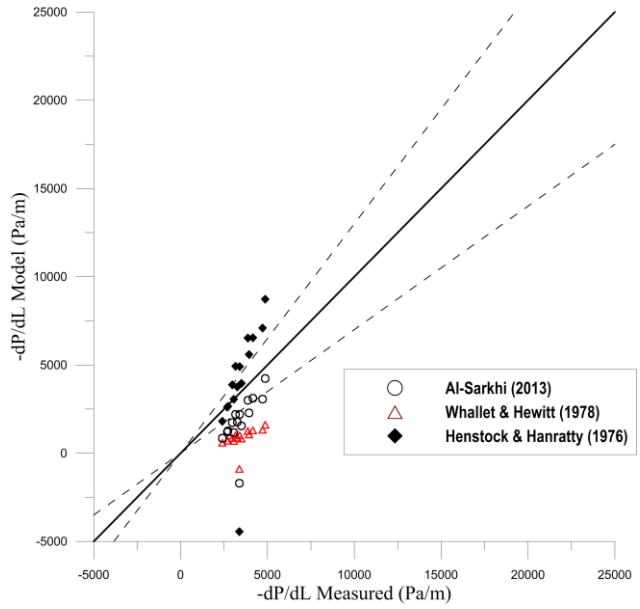

(a) Ishii & Mishima (1989)

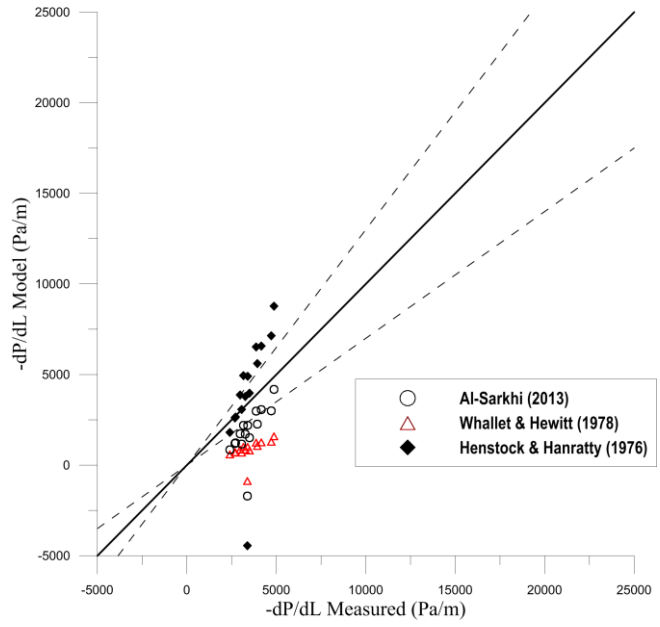

(b) Al-Sarkhi's (2011)

Figure 5.17 Pressure gradient prediction for Alruhaimani's (2015) vertical upward annular flow

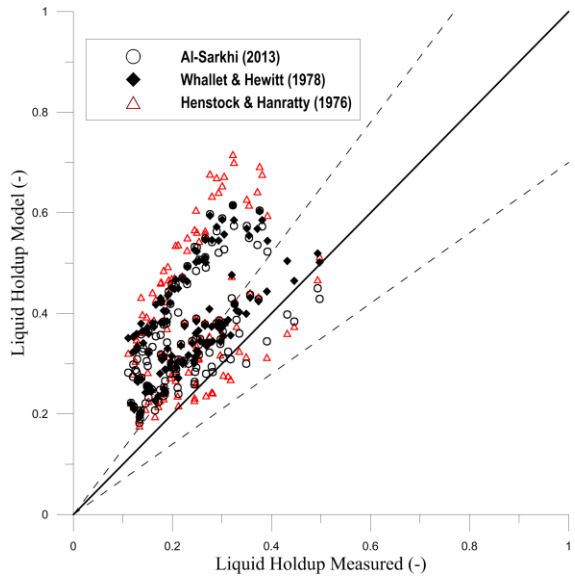

(a) Ishii & Mishima (1989)

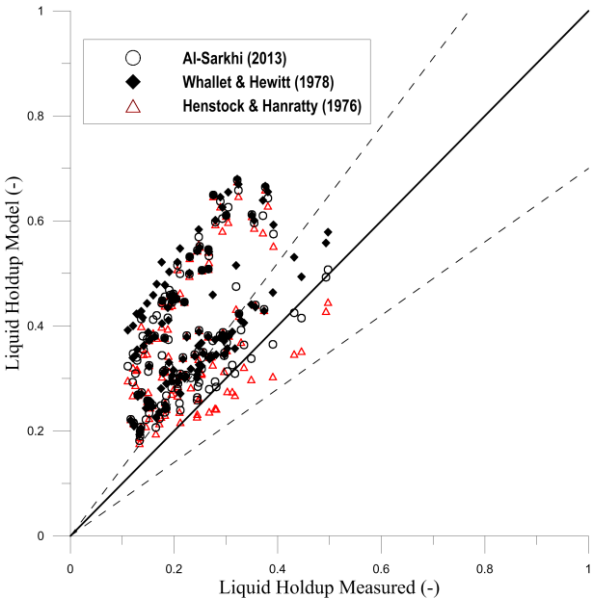

(b) Al-Sarkhi's (2011)

Figure 5.18 Average liquid holdup prediction for vertical downward annular flow

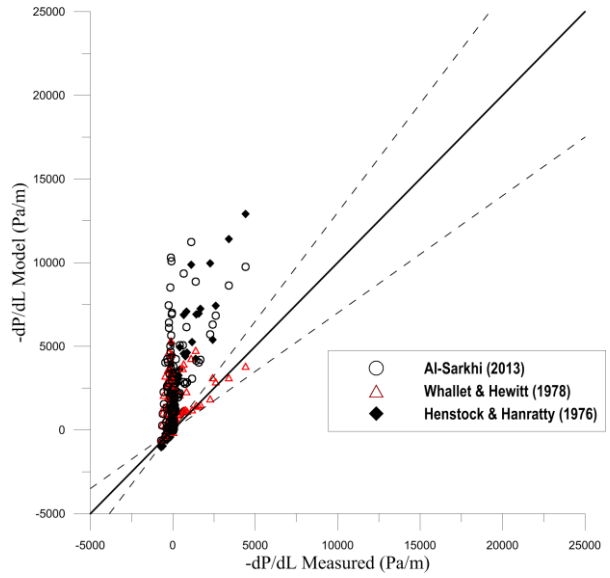

(a) Ishii & Mishima (1989)

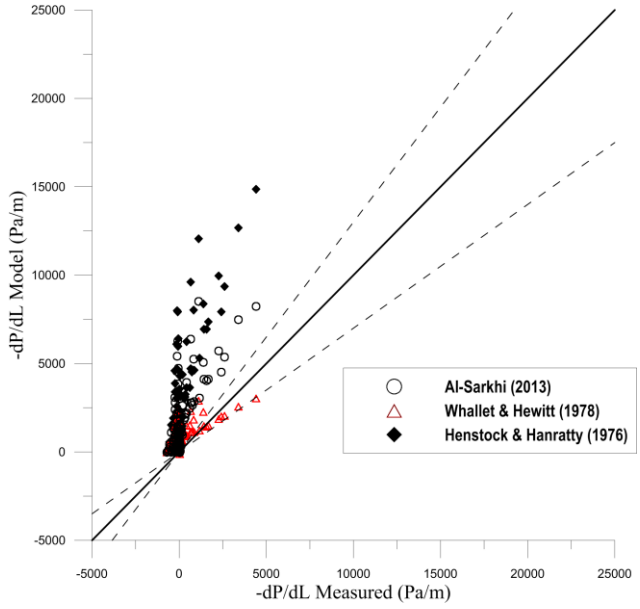

(b) Al-Sarkhi's (2011)

Figure 5.19 Pressure gradient prediction for vertical downward annular flow

Chapter 6 Conclusions and Future Works

6.1 Conclusions

Based on the experimental investigation and model evaluation conducted in this study, the following conclusions are reached:

(1) This study confirmed three different flow regime based on the Probability Distribution Function (PDF) from capacitance sensor signals: Falling Film (FF), Wavy Annular (WA) and Liquid Slip (LS). Flow patterns can be distinguished by skewness and kurtosis of PDF. Considering the traditional flow pattern classification, all conditions can be categorized as annular flow.

(2) When both of gas and liquid have low flow rate, Falling Film flows are observed with the pressure gradients near zero. Liquid Slip flows have negative pressure gradients and are observed in low gas and high liquid flow rate conditions. When gas flow rate increases, flow pattern changes to Wavy Annular flow and pressure gradient sharply increases due to the high shear forces.

(3) Between Falling Film and Wavy Annular flow patterns, average liquid holdup shows no significant differences. Average liquid

holdup suddenly increases as the flow pattern changes from Liquid Slip to wavy annular for high viscosities above 127 mPa·s.

(4) As the liquid viscosity increases, Liquid Slip flow patterns are observed in narrower range. Transition from Wavy Annular to Liquid Slip occurs at lower gas velocity. For higher oil viscosity condition, pressure gradient increases more sharply. And liquid droplet becomes hard to be entrained into the gas core, resulting higher average liquid holdup after flow pattern is changed from Liquid Slip to Wavy Annular.

(5) With high viscosity liquids, existing mechanistic model for annular flow shows poor performance for downward flow while vertical upward flow shows acceptable prediction performance. It comes from miscalculation of liquid droplet entrainment fraction. For vertical downward flow, different type of liquid entrainment correlation should be suggested, as the entrainment mechanism is quite different from upward annular flow.

6.2 Future Works

(1) Predicting thickness of liquid film is highly important as it could affect in determining the portion of liquid entrained into the gas core. There are some studies (Zhang et al, 2000; Mendoza, 2011) which investigate the characteristic of liquid film in vertical or deviated downward flow. The modified closure relationship for liquid film can be suggested.

(2) As aforementioned, closure relationship should about liquid entrainment can lead mispredicting of average liquid holdup. Also the measurement of liquid droplet velocity might lead to prediction of liquid holdup portion occupied by entrained liquid droplet.

(3) Using Computational Fluid Dynamics (CFD) software to simulate high viscosity liquid-gas two-phase flow in vertical pipes is highly recommended to study the effect of high viscosity on two-phase flow behavior.

References

Akhiyarov, D.T., Zhang, H.-Q., and Sarica, C. 2010. High-Viscosity Oil-gas Flow in Vertical Pipe. *Presented at Offshore Technology Conference*, Houston, TX, 3-6 May.

Al-Sarkhi, A., Sarica, C., and Qureshi, B. 2012. Modeling of Droplet Entrainment in Co-current Annular Two-phase Flow: A New Approach. *International Journal of Multiphase Flow* **39** (1): 21-28. http://dx.doi.org/10.1016/j.ijmultiphaseflow.2011.10.008

Alves, I.N., Cartano, E.F., Minami, K., and Shoham, O. 1991. Modeling Annular Flow Behavior for Gas Wells. *SPE Production Engineering* **6** (4): 435-440. SPE-20384-PA. http://dx.doi.org/10.2118/20384-PA

Barnea, D., Shoham, O., and Taitel, Y. 1982. Flow Pattern Transition for Vertical Downward Two Phase Flow. *Chemical Engineering Science* **37** (5): 741-744. http://dx.doi.org/10.1016/0009-2509(82)85034-3

Barnea, D. 1987. A Unified Model for Predicting Flow-pattern Transitions for the Whole Range of Pipe Inclinations. *International Journal of Multiphase Flow* **13** (1): 1-12. http://dx.doi.org/10.1016/0301-9322(87)90002-4

Bhagwat, S.M. and Ghajar, A.J. 2011. Flow Patterns and Void Fraction in Downward Two Phase Flow. *Paper presented at ASME Early Career Technical Conference*, Fayetteville, AR, 31 March-2 April.

Bhagwat, S. M. and Ghajar, A. J. 2012. Similarities and Differences in the Flow Patterns and Void Fraction in Vertical Upward and Downward Two Phase Flow. *Experimental Thermal and Fluid Science* **39**: 213-227. http://dx.doi.org/10.1016/j.expthermflusci.2012.01.026

Brito, R. 2012. *Effect of Medium Oil Viscosity on Two-phase Oil-gas Flow Behavior in Horizontal Pipes*. MS Thesis, University of Tulsa, Tulsa, OK.

Colmenares, J., Ortega, P., Padrino, J., and Trallero, J.L. 2001. Slug Flow Model for the Prediction of Pressure Drop for High Viscosity Oils in a Horizontal Pipeline. *Paper SPE 71111 presented at SPE International Thermal Operations and Heavy Oil Symposium*, Margarita Island, Venezuela, 12-14 March. http://dx.doi.org/10.2118/71111-MS

Dieck, R. 2007. *Measurement Uncertainty – Methods and Applications*, fourth edition. NC, USA: ISA.

Farsetti, S., Farisè, S., and Poesio, P. 2014. Experimental Investigation of

High Viscosity Oil–air Intermittent Flow. *Experimental Thermal and Fluid Science* **57**: 285-292. http://dx.doi.org/10.1016/j.expthermflusci.2013.12.004

Furukawa, T. and Fukano, T. 2001. Effects of Liquids Viscosity on Flow Pattern in Vertical Upward Gas-liquid Two-phase Flow. *International Journal of Multiphase Flow* **27**: 1109-1126. http://dx.doi.org/10.1016/S0301-9322(00)00066-5

Godbole, P.V., Tang, C.C., Ghajar, A.J. 2011. Comparison of Void Fraction Correlations for Different Flow Patterns in Upward Vertical Two Phase Flow. *Heat Transfer Engineering* **32** (10): 843–860. http://dx.doi.org/10.1080/01457632.2011.548285

Gokcal, B. 2008. *An Experimental and Theoretical Investigation of Slug Flow for High Oil Viscosity in Horizontal Pipes*. PhD Dissertation, University of Tulsa.

Gomez, L.E., Shoham, O., Schmidt, Z., Chokshi, R., Brown, A., and Northug, T. 2000. Unified mechanistic Model for Steady-State Two-Phase Flow: Horizontal to Vertical Upward Flow. *SPE Journal* **5** (3): 339-350. SPE-65705-PA. http://dx.doi.org/10.2118/65705-PA

Hibiki, T., Goda, H., Kim, S., Ishii, M., and Uhle, J. 2004. Structure of

Vertical Downward Bubbly Flow. *International Journal of Heat and Mass Transfer* **47** (8): 1847-1862. http://dx.doi.org/10.1016/j.ijheatmasstransfer.2003.10.027

Ishii, M. and Mishima, K. 1989. Droplet Entrainment Correlation in Annular Two-Phase Flow. *International Journal of Heat and Mass Transfer* **32** (10): 1835. http://dx.doi.org/10.1016/0017-9310(89)90155-5

Ishii, M., Paranjape, S. S., Kim, S., and Sun, X. 2004. Interfacial Structures and Interfacial Area Transport in Downward Two-phase Bubbly Flow. *International Journal of Multiphase Flow* **30** (7): 779-801. http://dx.doi.org/10.1016/j.ijmultiphaseflow.2004.04.009

Jeyachandra, B. 2011. *Effect of Pipe Inclination on Flow Characteristics of High Viscosity Oil-gas Two-phase Flow.* M.S. Thesis, University of Tulsa, Tulsa, OK.

Kim, S., Paranjape, S. S., Ishii, M., and Kelly, J. 2003. Interfacial Structures and Regime Transition in Co-current Downward Bubbly Flow. In ASME/JSME 2003 4th Joint Fluids Summer Engineering Conference, *American Society of Mechanical Engineers*, Honolulu, Hawaii, 6-10 July. http://dx.doi.org/10.1115/FEDSM2003-45541

Kora, C. 2010. *Effect of High Oil Viscosity on Slug Liquid Holdup in*

Horizontal Pipes. MS Thesis, University of Tulsa, Tulsa, OK.

Mukherjee, H. 1979. *An Experimental Study of Inclined Two-phase Flow.* PhD Dissertation, University of Tulsa, Tulsa, OK.

Mukherjee, H. and Brill, J.P. 1985. Empirical Equations to Predict Flow Patterns in Two-phase Inclined Flow. *International Journal of Multiphase Flow* **11** (3): 299-315. http://dx.doi.org/10.1016/0301-9322(85)90060-6

Nädler, M., and Mewes, D. 1995. Effects of the Liquid Viscosity on the Phase Distributions in Horizontal Gas-liquid Slug Flow. *International Journal of Multiphase Flow* **21** (2): 253-266. http://dx.doi.org/10.1016/0301-9322(94)00067-T

Nuland, S., Malvik, I., Valle, A., and Hende, P. 1997. Gas Fractions in Slugs in Dense-gas Two-phase Flow from Horizontal to 60 Degrees of Inclination. *Proceedings of the ASME Fluids Eng. Div. Summer Meeting*, 22-26 June.

Oshinowo, T. and Charles, M. E. 1974(a). Vertical Two-phase Flow: Part I. Flow Pattern Correlations. *The Canadian Journal of Chemical engineering* **52** (1): 25-35. http://dx.doi.org/10.1002/cjce.5450520105

Oshinowo, T. and Charles, M. E. 1974(b). Vertical Two-phase Flow: Part II. Holdup and Pressure Drop. *The Canadian Journal of Chemical Engineering* **52** (4): 438-448. http://dx.doi.org/10.1002/cjce.5450520402

Picard, A. Davis, R. S. Glaser, M. and Fujii, K. 2008. Revised Formula for the Density of Moist Air (CIPM-2007). *Metrologia* **45**: 149-155. http://dx.doi.org/10.1088/0026-1394/45/2/004

Ros, N.C.J. 1961. Simultaneous Flow of Gas and Liquid as Encountered in Well Tubing. *Journal of Petroleum Technology* **13** (10): 1037-1049. SPE-18-PA. http://dx.doi.org/10.2118/18-PA

Rosa, E.S. and Netto, J.R.F. 2004. Viscosity Effect and Flow Development in Horizontal Slug Flows. Paper 306 presented at 5th International Conference on Multiphase Flow, Yokohama, Japan, 30 May-4 June.

Taitel, Y., and Barnea, D. 1990. Two-phase Slug Flow. *Advances in Heat Transfer* **20**: 83-132.

Troniewski, L. and Spisak W. 1987. Flow Patterns in Two-phase Downflow of Gas and Very Viscous Liquid. *International Journal of Multiphase Flow* **13** (2): 257-260. http://dx.doi.org/10.1016/0301-9322(87)90033-4

Usui, K. and Sato, K. 1989. Vertically Downward Two-phase Flow, (I). *Journal of Nuclear Science and Technology* **26**(7): 670-680. http://dx.doi.org/10.1080/18811248.1989.9734366

Usui, K. 1989. Vertically Downward Two-phase Flow, (II). *Journal of Nuclear Science and Technology*, **26**(11): 1013-1022. http://dx.doi.org/10.1080/18811248.1989.9734422

Wang, S., Zhang, H.-Q., Sarica, C., and Pereyra, E. 2014. A Mechanistic Slug-liquid-holdup Model for Different Oil Viscosities and Pipe-inclination Angles. *SPE Production & Operations* **29** (4): 329–336. SPE-171563-PA. http://dx.doi.org/10.2118/171563-PA

Wallis, G.B. 1969. *One-dimensional Two-phase Flow.* NY, USA: McGraw-Hill Book Co. Inc.

Yamazaki, Y. and Yamaguchi, K. 1979. Characteristics of Cocurrent Two-Phase Downflow in Tubes: Flow Pattern, Void Fraction and Pressure Drop. *Journal of Nuclear Science and Technology* **16**(4): 245-255. http://dx.doi.org/10.1080/18811248.1979.9730898

Zadrazil, I., Matar, O. K., and Markides, C. N. 2014(a). An Experimental Characterization of Downwards Gas–liquid Annular Flow by Laser-induced Fluorescence: Flow Regimes and Film

Statistics. *International Journal of Multiphase Flow* **60**: 87-102. http://dx.doi.org/10.1016/j.ijmultiphaseflow.2013.11.008

Zadrazil, I. and Markides, C. N. 2014(b). An Experimental Characterization of Liquid Films in Downwards Co-current Gas–liquid Annular Flow by Particle Image and Tracking Velocimetry. *International Journal of Multiphase Flow* **67**: 42-53. http://dx.doi.org/10.1016/j.ijmultiphaseflow.2014.08.007

Zhang, H.-Q., Wang, Q., Sarica, C., and Brill, J.P. 2003(a). Unified Model for Gas Liquid Pipe Flow via Slug Dynamics – Part 1: Model Development. *J. Energy Res, Tech*. **125** (4): 266-273. http://dx.doi.org/10.1115/1.1615246

Zhang, H.-Q., Wang, Q., Sarica, C., and Brill, J.P. 2003(b). Unified Model for Gas Liquid Pipe Flow via Slug Dynamics - Part 2: Model Validation. *J. Energy Res, Tech*. **125** (4): 274-283. http://dx.doi.org/10.1115/1.1615618

요약 (국문초록)

이 연구는 수직 하방관에서 고점성도 오일-가스 2상 유동의 특징을 실험적으로 분석한다. 해상 중질유 처리시설의 해저 배관망에서 일어나는 해당 유동의 압력 구배, 평균 액체 점유율 등의 예측은 생산 시설 설계 및 용량 결정 과정에서 대단히 중요하다.

이전의 실험들은 대부분 저, 중점성도 유체에 대한 평가이므로 고점성도 오일의 경우 유동 특성 및 인자 예측의 정확도에 대한 검증이 필요하다. 따라서 본 연구에서는 수직 2인치 관과 고점성도 오일을 이용하여 오일 점성도에 따른 유동 패턴, 압력 구배, 평균 액체 점유율 등의 변화 양상을 실험하였다. 서로 다른 4가지 오일 점성도(586 mPa·s, 337 mPa·s, 213 mPa·s, 127 mPa·s)와 지정된 범위 내의 공탑 액체 속도(0.05 m/s ~ 0.7 m/s), 공탑 기체 속도(0.3 m/s ~ 8.0 m/s)를 사용하였다.

실험을 통해 세 종류의 유동 패턴(Falling Film, Wavy Annular, Liquid Slip)을 관찰하였으며 각각의 유동패턴이 갖는 압력구배 및 평균 액체 점유율 등의 특징과 이에 대한 점성도의 영향을 분석하였다. 나아가 본 연구에서는 측정된 결과와 기존의 2상 유동 예측 모델들을 통해 예측한 결과를 정량적으로 비교하였다. 기존 모델들은 대부분의 유동 조건에 대해 슬러그 유동 패턴을 예측하고,

낮은 점성도 오일 조건에서 평균 액체 점유율을 크게 과대평가하는 경향을 확인하였다.

기존 모델들의 적용성을 평가하기 위해 본 연구에서는 저점성도 수직 하방 환상유동 및 고점성도 수직 상방 환상유동 실험 데이터와의 비교를 통해 환상유동의 유동 예측 모델에 사용되는 관계식의 예측성능을 평가하였다. 연구 결과 기존 환상유동 모델에 사용되는 관계식들은 고점성도 유체의 수직 상방유동에 대해 만족할만한 결과를 보여주나 수직 하방 유동에 대해서는 가스 코어 내의 액체 침투율을 과소평가하는 결과를 보여주었다. 이 연구는 해상 중질유 필드의 원유 처리시설 설계 자료로 활용될 수 있는 기술로 기대된다.

주요어: 2상유동, 수직하방유동, 고점성도, 관내유동, 유동패턴, 압력구배, 평균액체점유율

학 번: 2010-30260

공학박사 학위논문

Characteristics of High Viscous Oil-Gas Flow in Downward Vertical Pipes

수직 하방 관내 고점성 오일-가스 2상 유동 특징 연구

2016년 2월

서울대학교 대학원

에너지시스템공학부

정 성 훈

Characteristics of High Viscous Oil-Gas Flow in Downward Vertical Pipes

지도교수 강 주 명

이 논문을 공학박사 학위논문으로 제출함

2015년 12월

서울대학교 대학원

에너지시스템공학부

정 성 훈

정성훈의 공학박사 학위논문을 인준함

2016년 1월

위 원 장 _____ (인)

부위원장 _____ (인)

위 원 _____ (인)

위 원 _____ (인)

위 원 _____ (인)

Abstract

Characteristics of High Viscous Oil-Gas Flow in Downward Vertical Pipes

Sunghoon Chung

Department of Energy Systems Engineering

The Graduate School

Seoul National University

There is a recent interest on the production of medium to heavy oils in offshore environments. The use of multiphase pumps located in platforms has been proposed to ensure the transport of the fluids to the shoreline facilities. After the platform, the multiphase flow stream is redirected to the sea floor using a down comer. Thus, the understanding of the viscosity effect in downward vertical flow becomes critical for the system design.

An experimental study on the viscosity effect has been carried out using a 2-in. ID multiphase flow facility. The viscosity of the oil ranged from 127 to 586 mPa·s. The superficial gas and liquid velocities varied from 0.3 to 7 m/s and 0.05 to 0.7 m/s, respectively. Flow pattern, pressure gradient and liquid holdup data were acquired and compared with previous

air-water experiments.

Three different flow patterns have been identified based on visual observations and capacitance sensor readings. Flow pattern, superficial velocities and viscosity effects on pressure gradient and liquid holdup are presented. Comparisons with available mechanistic models and simulators are reported. Existing mechanistic models dominantly predicts flow pattern as slug flow, and over-predicts average liquid holdup especially low liquid viscosity condition.

To ensure applicability of existing annular flow model, experimental data of upward flow for high viscosity oil. As a result, closure relationship is affordable for vertical upward flow due to its low liquid entrainment fraction, while it shows disappointing prediction performance in vertical downward flow.

Keywords : two-phase flow, vertical downward flow, high viscosity, pipe flow, flow pattern, pressure gradient, average liquid holdup

Student Number : 2010-30260

Table of Contents

List of Tables

List of Figures

Chapter 1 Introduction

The petroleum production system consists of vertical and horizontal pipe networks and thereby the accurate analysis of multiphase flow, e.g. oil, water, and gas, have been essential to accomplish the optimality in production and transportation. A large number of experimental and modeling studies on multiphase flow have been carried out owing to its importance in industrial applications.

1.1 Multiphase Flow of Heavy Oil in Vertical Downward Pipes

Flow characteristic of multiphase flow is highly affected by the pipe inclination due to the effect of gravity. Pipe inclination determines the direction of gravity. The difference of densities among the phases causes the buoyant force, resulting the slippage between gas and liquid. Thus flow characteristics of vertical downward flow are quite different from those of vertical upward flow due to the difference of gravity direction. Flow patterns appearing in vertical pipes are shown in Figure 1.1.

In vertical upward flow, the gravity obstructs the flow of fluids and buoyant force helps the gas to flow faster. Accordingly, it has a tendency of high liquid holdup and pressure drop comparing horizontal condition. A dominant flow pattern is slug flow. In downward flow, however, as the

orientation of gravity is towards mean flow direction, heavier phase (i.e. liquid phase) becomes easy to flow resulting relatively lower liquid holdup. As potential energy of fluids can compensate frictional energy loss and could have small or negative pressure drop.

There is a recent interest on the production of medium to heavy oils in offshore environments (Table 1.1). The heavy oil is defined to have the range from 100 to 10,000 mPa·s. In offshore field, the use of multiphase pumps located in platforms has been proposed to ensure the transport of the fluids to the shoreline facilities or FPSO (Floating production storage and offloading) units. After the platform, the multiphase flow stream is redirected to the sea floor using a down comer. In heavy oil field, to overcome the limited oil mobility, the multiphase flow of oil-gas mixture are considered as an option for transportation.

As the water depths of offshore heavy oil fields vary from hundreds to thousands of feet, the understanding of the viscosity effect in downward vertical flow becomes critical for the system design. Unlike any light oil, any multiphase transportation and production system controlling high viscous and dense liquid requires facilities with high specifications that overcomes high frictional pressure drop, which is frequently challenging in offshore field owing to the spatial limitations of platform. Hence the recent concern of heavy oil and multiphase flow increases the necessity to evaluate two factors, i.e. the pressure drop and the liquid holdup, accurately (Wang et al., 2014). In spite of its importance in heavy oil production, however, commonly used laboratory liquids in most of studies on vertical downward two-phase flow

have viscosities less than 20 mPa·s.

The quantitative analysis related to liquid viscosity in pipes have been limited at experimental observations and the development of a mechanistic model that shows poor accuracy with experimental results (Gokcal, 2008; Kora, 2010). As the liquid viscosity increases, slug liquid hold up, translational velocity, and slug frequency are changed.

Table 1.1 List of offshore heavy oil fields

Field	**Status**	**Depth (ft)**	**Operator**	**Country**	**Viscosity (mPa·s)**
Captain	Producing	350	Chevron	UK	50-150
Mariner	Under Dev.	363	Statoil	UK	67 & 508
Bentley	Under Dev.	373	Xcite Energy	UK	1,500
Kraken	Under Dev.	386	EnQuest PLC	UK	78-161
Bressay	Discovered	337	Statoil	UK	540
Pazflor	Producing	2,369-3,399	Total	Angola	3,000 (dead oil)
Jubarte	Producing – Under Dev.	4,505	Petrobras	Brazil	3,000 (dead oil)

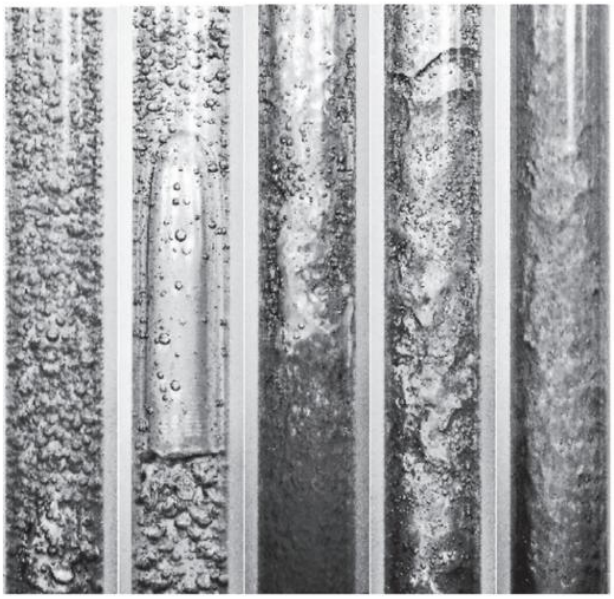

(a) Vertical upward flow (Godbole et al., 2011)

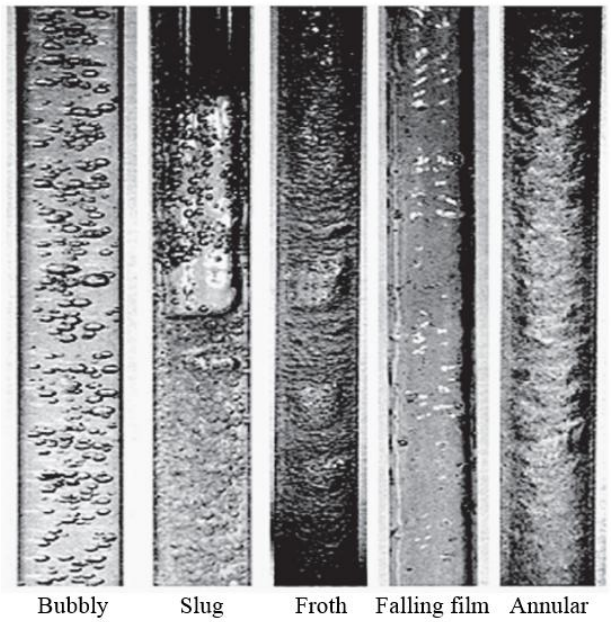

(b) Vertical downward flow (Bhagwat and Ghajar, 2011)

Figure 1.1 Flow patterns in vertical two phase flow

1.2 Motivation

In petroleum industries, relatively few investigations in vertical downward two-phase flow have been reported. Downward flow has been traditionally encountered in relatively short length of pipes in offshore production operations while vertical upward flow can be easily encountered in production wells and risers. Most of the studies on vertical downward flow are based on chemical and nuclear engineering scheme with air-water two-phase conditions and small pipe diameter. The major concern of these studies is to predict gas void fraction instead pressure drop of the pipe. But in petroleum industry, pressure gradient should be considered as one of main parameter.

The motivation of this research divides into two necessities: to examine the prediction performance of existing mechanistic model and to analyze the influenced factors to determine both of pressure drop and liquid holdup integrating experimental and numerical studies, quantitatively.

Some mechanistic models have been developed for various flow inclination of angle (Barnea, 1987; Zhang, et al, 2003; Gokcal, 2008; Kora, 2010). These models show dissatisfied matching for two-phase flow containing high viscous liquid but they fail to find the causes and remain quantitative investigations based on experimental results with high viscous oil and gas flow. However, as can be seen in previous studies by the University of Tulsa (Gokcal, 2008; Kora, 2010), existing mechanistic models show dissatisfied performance for two-phase flow with high viscosity liquids. Similarly, prediction performance for vertical downward flow with high

viscosity liquid is still unclear. As Troniewski and Spisak (1987) reported, however, high liquid viscosity has a possibility to result different flow characteristics.

1.3 Objectives of Study

The main objective of this project is to perform experimental and modeling study for two-phase downward flow in vertical pipes with high-viscosity-oil. A 50.8-mm-ID (2-in.) and 22.72-m-long horizontal test section was used in this experimental study. The experiments were conducted with various oil viscosities, namely, 586 mPa·s, 401 mPa·s, 213 mPa·s, and 127 mPa·s, corresponding to oil temperatures of 70 °F, 80 °F, 100 °F, and 120 °F. The selected oil viscosities cover medium to high oil viscosities.

The effect of high viscosity oil on two-phase behavior was investigated. The targeted flow parameters are flow pattern, pressure drop and average liquid holdup. Specific features were analyzed from experimental measurements. And the performance of existing correlations and models for different parameters as flow patterns, pressure gradient, and average liquid holdup are evaluated against acquired experimental data. Finally, existing closure relationship are quantitatively examined on its applicability on various flow conditions.

1.4 Structure of the Dissertation

This study is divided into 6 chapters as described below and some other related information is provided in appendices:

Chapter 1 provides an introduction to the dissertation, defining the problems, objectives of the study and structure of the dissertation.

Chapter 2 contains a review of published work on vertical downward flow and effect of liquid viscosity on two-phase flow.

Chapter 3 gives the description of details on test fluids, test matrix, a description of the experimental facility, instrumentation, data acquisition and processing, and an uncertainty analysis.

Chapter 4 contains the results from the experiment and findings.

Chapter 5 provides the discussion on model comparison and applicability of existing correlations.

Chapter 6 pieces together all the key conclusions from this study. And, recommendations for further work are also provided.

Chapter 2 Literature Review

2.1 Gas-Liquid Two-phase Vertical Downward Flow

Many empirical correlations and mechanistic models have been developed for two-phase downward flow in vertical pipes. The empirical correlations are developed by obtaining mathematical relations between known parameters and design variables, such as pressure gradient and liquid holdup, based on experimental data. Empirical correlations are often limited by the range of data used in the development of the correlation.

The mechanistic models are based on fundamental principles (conservation of mass, momentum and energy). These models require the prediction of the flow pattern to model multiphase flow in pipes. Consequently, for the predicted flow pattern, a hydrodynamic model can be used to predict both of pressure gradient and liquid holdup. If a mechanistic model can predict the flow behavior in all the flow patterns at a given inclination angle, it is called a comprehensive mechanistic model. On the other hand, when a mechanistic model can predict the flow behavior in all flow patterns and for all inclination angles is referred to as a unified model.

In this section, a summary of well-known two-phase vertical downward flow empirical correlations is reviewed first. Then a review of the unified models for two-phase flow is presented.

2.1.1 Comprehensive correlations

For vertical downward concurrent flow, most of the studies are based on chemical and nuclear engineering scheme with air-water two-phase conditions and small pipe diameter. As the major concern of these studies is to predict gas void fraction accurately, most of them did not consider the calculation of pressure gradient.

Oshinowo and Charles (1974) experimentally investigated flow pattern correlation, liquid holdup and pressure drop in vertical downward flow. They suggested empirical correlations for flow pattern transition and claimed that Lockhart-Martinelli scheme met with limited success while the scheme was satisfactory in correlating frictional pressure drop and holdup in upward flow.

Yamazaki and Yamaguchi (1979) experimentally studied transition of flow pattern in vertical downward flow. They also suggested empirical correlations for void fraction and pressure drop prediction.

Barnea et al. (1982) and Usui (1989) identified transition criteria of flow patterns for two-phase downward flow. Barnea et al. divided downward flow with three patterns; annular, slug and dispersed bubble while Usui subdivided annular flow into annular flow and falling film flow.

Mukherjee and Brill (1985) investigated empirical equations to predict flow patterns transition for different inclination angles including horizontal and vertical flow. They claimed that flow regime map for downward flow conformed more to the Mandhane et al. (1974) while the

transition of upflow were similar to those proposed by Duns and Ros (1963).

Barnea (1987) combined different mechanistic models proposed for horizontal, near horizontal, upward vertical, downward vertical, upward inclined, and downward inclined to propose a unified model for predicting flow pattern transitions for the whole range of pipe inclinations. In addition to pipe geometry, the model considers fluid properties and flow conditions.

Usui and Sato (1988) investigated correlation to predict the average void fraction for each flow regime including falling film and annular drop flow.

A set of studies investigating the prediction of void fraction in vertical downward flow are based on similar drift flux concept; Goda et al (2003), Hibiki et al. (2004), Ishii et al. (2004), and Sun et al. (2004).

Kim et al. (2003) experimentally investigated flow pattern correlation. It was found that the flow regimes in the co-current downward flow strongly depend on the channel size.

Bhagwat and Ghajar (2012) compared characteristics of Vertical Upward and Downward Flow. They tested the performance of the Void Fraction Correlations and proposed top five performing correlations.

2.1.2 Unified Models

Gomez et al. (2000a) proposed a unified steady-state two-phase flow mechanistic model for the prediction of flow pattern, liquid holdup and pressure drop that is applicable to the range of inclination angles from

horizontal to vertical. The model adapts Barnea et al. (1987) unified model for flow pattern prediction. For slug flow, Gomez et al. used Taitel and Barnea (1990) slug flow model with a new developed slug liquid holdup closure relationship. For annular flow, Gomez et al. extended Alves et al. (1991) model to the entire range of inclination angles.

Zhang et al. (2003a and 2003b) developed a unified hydrodynamic model (TUFFP unified model) to predict flow pattern transitions, pressure gradient, and liquid holdup for all inclination angles from -90° to 90°. The model is based on the dynamics of slug flow and is applicable to all pipe geometries and fluid properties. The momentum equations for slug flow were used to predict flow pattern transitions from intermittent flow to other flow patterns. In this model, the defined flow patterns are bubble, intermittent, and stratified/annular flows. This classification is based on hydrodynamic characteristics of each flow pattern. Model prediction was compared with experimental data that included different pipe diameters, flow patterns, inclination angles, fluid physical properties, and gas-liquid flow rates. The comparisons showed agreement for both flow pattern and hydrodynamic behavior predictions.

2.2 Effect of Liquid Viscosity on Two-Phase Flow

Ros (1961) conducted a dimensional analysis study and eliminated irrelevant dimensionless groups characterizing pipe inclination angle, wall contact angle, gas viscosity, and wall roughness. The retained dimensionless groups characterize liquid viscosity, pipe diameter, velocity ratio, liquid velocity and gas-liquid density ratio. It was reported that at higher oil viscosities (51.5, 290 and 337 mPa·s) the increase in pressure gradient is not only due to an increase in friction factor but also due to the higher slippage between gas and liquid, especially at low liquid flow rates.

Nadler and Mewes (1995) conducted experiments with viscosity range of 1.0 to 37.0 mPa·s, and investigated the effect of liquid viscosity on slug flow for horizontal pipes keeping other fluid physical properties constant. Their experimental results indicated that when viscosity of liquid increased, the average liquid holdup increased.

Nuland (1999) experimentally studied the effect of liquid viscosity on slug liquid holdup. Experiments were conducted with liquid viscosity of 50 mPa·s to 400 mPa·s in horizontal pipes. Nuland (1999) concluded that the effect of viscosity on slug liquid holdup is weak in comparison to the effect of flow rates.

Furukuwa & Fukano (2001) experimentally studied the effect of liquid viscosity on flow patterns in upward vertical gas-liquid two-phase flow. Water and two different concentrations of aqueous glycerol solutions with viscosities up to 15 mPa·s were used in a 19.2 mm ID vertical pipe. They

concluded that flow pattern transitions are dependent on liquid viscosity.

Colmenares et al. (2001) studied pressure drop and flow pattern models for horizontal slug flow for viscous oils. Their experimental results suggested that the slug flow region in the flow pattern map enlarged when the oil viscosity increased. They also evaluated existing slug models, and concluded that the Taitel and Barnea (1990) model was the best candidate to be used for high viscosity oils. A modified model was developed by using experimental data for a liquid viscosity of 480 mPa·s. They concluded that slug frequency and liquid film height increased, and the slug length decreased as the liquid viscosity increased.

Shosho and Ryan (2001) conducted an experimental study with Newtonian and non-Newtonian fluids to investigate the effects of viscosity and tube size on drift velocity for vertical and inclined tubes. The drift velocity was correlated in terms of three dimensionless numbers; Froude, Eötvös, and Morton numbers. For non-Newtonian fluids with high Morton number, Froude number was affected by both viscous forces and tube size.

Shosho and Ryan (2003) experimentally studied the effects of a high liquid viscosity on two-phase flow in vertical pipe. Water and glycerin solutions were used as test liquids. The liquid viscosities were 1.0, 50, 200, and 550 mPa·s. Mostly, annular flow was observed in their study. They concluded that low viscosity correlations for entrained liquid fraction and interfacial friction factor were not suitable for the highly viscous liquids. A new correlation for the interfacial friction factor was developed based on collected high viscosity data.

Rosa et al. (2004) experimentally investigated the influence of liquid viscosity on gas-liquid slug flow in horizontal pipes. Air-water and air-glycerin (27 mPa·s) were used 32 as the two pairs of test fluids. Bubble shape, velocity and void fraction, bubble and slug lengths, slug frequency and coalescence rate were studied. They concluded that as liquid viscosity increased, the average slug length and coalescence rate decreased, while the bubble front velocity and slug frequency increased.

Gokcal (2005) performed an experimental investigated the effect of high viscosity oil (181 mPa·s - 587 mPa·s) on two-phase flow behavior in a 50.8 mm ID horizontal pipe. For flow pattern prediction, Gokcal concluded that, as liquid viscosity increases within his investigation range of viscosities, the data did not show a significant effect of the oil viscosity on the transition boundaries. On the other hand, considerable difference has been observed with respect to low viscosity oil data. The study also showed that the pressure gradient increased with the increase in liquid viscosity. This became more pronounced with increasing superficial oil and gas velocities. The comparison of the pressure drop experimental data against the TUFFP unified model predictions showed an unsatisfactory performance for high viscosity oil conditions. Gokcal et al. (2006) modified the closure relationships in the TUFFP unified model resulting in improved predictions of the experimental data for flow pattern transition, pressure gradient, and liquid holdup.

Schmidt et al. (2008) experimentally studied the phase and velocity distributions in vertically upward high-viscosity (up to 7000 mPa·s) two-phase flow. Void fraction measurements were made using a gamma-densitometer.

Pressure gradient was not reported in their experimental study. They concluded that existing void fraction correlations do not predict the average void fraction properly.

Akhiyarov et al. (2010) experimentally studied the effect of high oil viscosity on two-phase behavior in upward vertical flow. Oil viscosity of 120 - 510 mPa·s and Tulsa City Natural gas were used as the two-phase fluid system in a 52.5 mm ID pipe. Flow pattern, pressure gradient, and average liquid holdup were recorded. Comparing the obtained experimental data with model predictions showed poor performance of the models for high oil viscosity.

Jeyachandra (2011) experimentally studied the effect of high viscosity oil (181 mPa·s - 587 mPa·s) on two-phase flow behavior in a 50.8 mm ID slightly inclined ($\pm 2^{o}$) pipes. Flow pattern, pressure gradient, average liquid holdup, and slug characteristics were measured and analyzed. The obtained experimental results agreed with Gokcal (2005) observations. As oil viscosity increased, pressure gradient and slug frequency increased, slug length decreased, and no significant change in average liquid holdup or slug liquid holdup was observed within the viscosity range used in the experiments.

Brito (2012) experimentally studied the effect of medium oil viscosity (39 mPa·s - 166 mPa·s) on two-phase flow behavior in a 50.8 mm ID horizontal pipe. Flow pattern, pressure gradient, average liquid holdup, translational velocity, slug liquid holdup, film holdup, slug length, and slug frequency were measured and analyzed. The obtained experimental results were compared with Gokcal (2005). It was found that pressure gradient and

average liquid holdup increased with increasing oil viscosity.

Farsetti et al. (2014) experimentally investigated the flow of high viscosity oil (900 mPa·s) and gas in a 22.8 mm ID horizontal and slightly inclined (-10^{o} to $+15^{o}$) pipes. Pressure gradient, translational velocity, slug frequency, slug length, and average liquid holdup were measured using capacitance probes. They concluded that correlations 34 available in literature (validated for the low viscosity liquid case) cannot be extended to the high viscosity case.

Kim (2014) experimentally studied the the pipe diameter effects in high viscosity oil (181 mPa·s - 587 mPa·s) and gas two-phase condition with a 76.2 mm ID horizontal pipes. Flow pattern, pressure gradient, average liquid holdup and slug characteristics (translational velocity, slug frequency, slug length, slug liquid holdup and film liquid holdup) were measured using capacitance probes. They concluded that the slug liquid holdup and slug frequency increase, and the film liquid holdup and slug length decrease as the pipe diameter increases.

2.3 **Summary**

Only limited experimental studies of low viscosity oil-gas two-phase flow in vertical downward pipes are available in literature. And also most of them are focused on transition of flow pattern and prediction of volume fractions of each phase. Furthermore, studies of high viscosity oil-gas two-phase flow commonly claim that existing mechanistic models must be verified with

higher viscosity liquid-gas two-phase flow experimental data. If models show poor predictions with high viscosity data, the existing models need to be investigated quantitatively on its applicability.

Chapter 3 Experimental Facility

The experimental study was conducted on a TUFFP three phase flow facility. ND-50 mineral oil and compressed air were used as a liquid and a gas, respectively. The following sections present facility description, fluids properties and details of instruments.

3.1 Facility Description

The experimental work was conducted using the TUFFP 2-in. ID three-phase flow facility located at the University of Tulsa North Campus Research Complex. Figure 3.1 depicts the schematic of the facility loop. A coated steel oil storage tank with an internal baffle was used for oil and gas separation. The capacity of oil tank is 2,900 gallons. The tank is equipped with an electrical heater and a recirculation pump to increase and maintain oil temperature. Oil tank is connected to the progressive cavity pump Robbins-Myers R&M 1000 to circulate the oil. Maximum working pressure of pump is 290 psi. Thus, a pressure relief valve, which open at 100 psi, is connected at the pump discharge to control excessive pressure over test section. The oil density and mass flow rate is measured with a CMF100 coriolis flow meter from Micro Motion™ with RTF9739 transmitter. Maximum mass flow rate is 1,000 lb/min. Finally, pressure and temperature are measured to monitor the oil properties.

A dry rotary screw compressor supplies compressed air with a

capacity of 1,030 cubic feet at 100 psig. A pair of Endress-Hauser Promass 83F coriolis flow meter are installed to measure gas mass flow rate. Before the each coriolis meter, an automatic control valves are connected to control gas flow rate. These valves can be operated in parallel or individually. A feedback control, using the valve opening, is utilized to maintain gas flow rate constant. The phases flow through the mixing tee at the inlet section of test section. Liquid-gas mixture flows through upward section which consists of 22.72-m-long and 2-inch ID pipe. Bended 2-inch steel pipe links upward and downward flow sections. Downward section has three part; 15.85-m-long steel pipe, 3.59-m-long transparent polycarbonate pipe and 3.28-m-long steel pipe. End of downward flow section is connected to oil tank with flexible hose.

Figure 3.2 shows schematics of test section. Test section is mounted on a boom with a hoisting lift system and can be inclined at any angle between horizontal and vertical. Two capacitances were used to examine flow patterns. A Resistance Temperature Detector (RTD) temperature transducer and a pressure transducer are installed to measure temperature and pressure of fluids. A pair of Quick-Closing Valves (QCV) are used to measure the average liquid holdup combined with differential pressure transmitter. Differential pressure transmitter also provides pressure drop with flow. A surveillance camera was installed to collect video of flow for flow pattern identification. Length of trapping section and pressure drop measurement are 6.09 m (L/D = 120) and 5.36 m (L/D = 105), respectively.

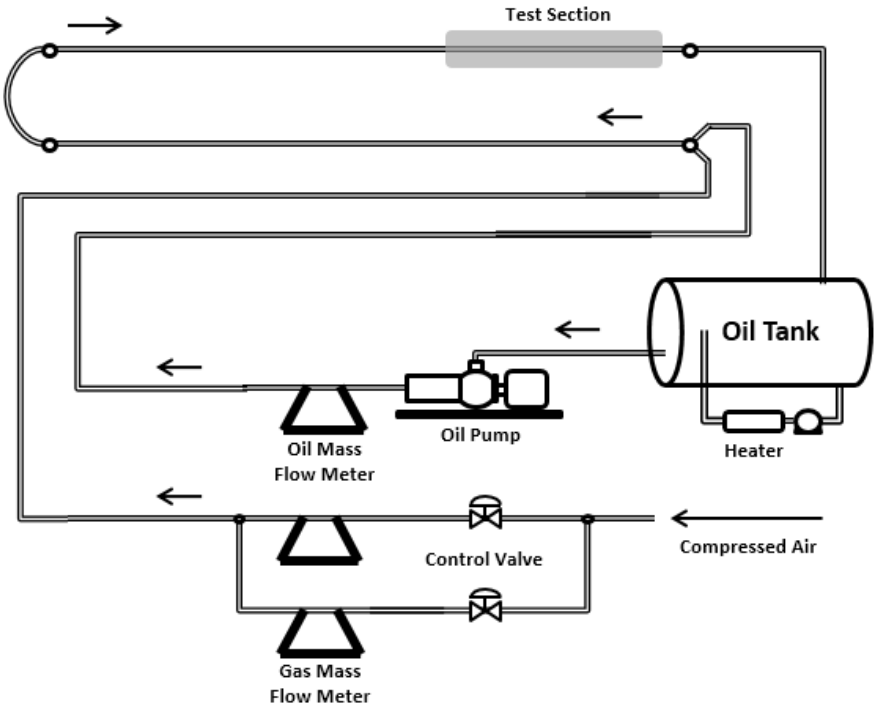

Figure 3.1 Facility Schematic.

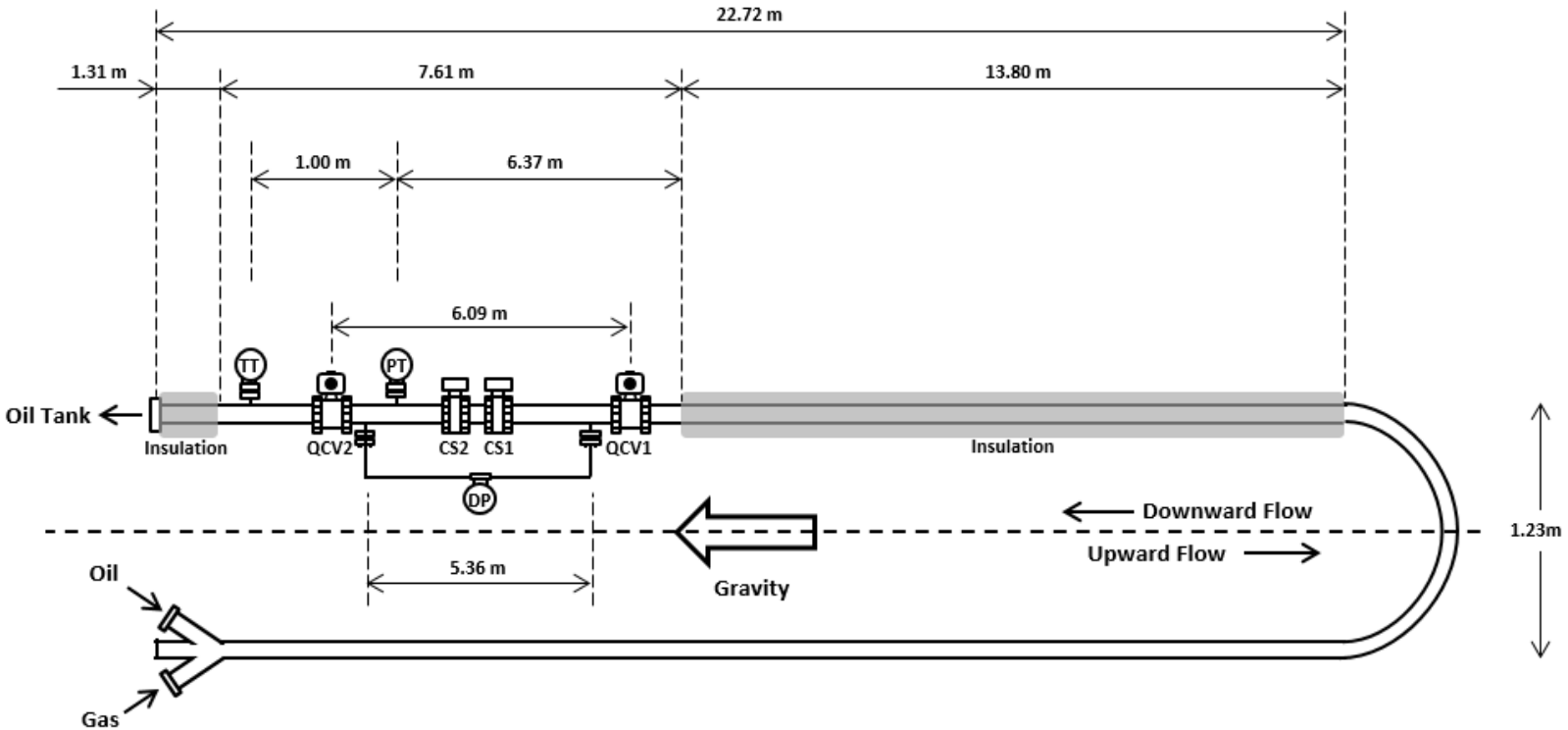

Figure 3.2 Schematic of Test Section.

3.2 Fluids

3.2.1 Air Properties

Compressed air was used as the gas phase. Since properties of gas are very sensitive to pressure and temperature because of high compressibility, they were calculated from known correlations. Air density was calculated using revised CIPM-2007 formula for moisture air (Picard et al., 2008) as follows:

$$\rho_{air} = 3.48349 \times 10^{-3} \frac{p}{ZT}(1 - 0.378X_v), \tag{3-1}$$

where p is the pressure in Pascal, T is the temperature in Kelvin, Z is the compressibility factor, and X_v is the mole fraction of water vapor. X_v is calculated from equation (3-2).

$$X_v = h\frac{p_{sv}}{p} f(p, T_t). \tag{3-2}$$

h is the relative humidity. It is assumed 0.6 in this study. $f(p, T_t)$ is the enhancement factor at the ambient pressure and temperature:

$$f(p, T_t) = 1.00062 + 0.0000000314p + 0.00000056T_t^2, \tag{3-3}$$

where T_t is the temperature in degree Celsius. p_{sv} in equation (3-2) is saturation vapor pressure in Pascal at ambient temperature. It is calculated by equation (3-4).

$$p_{sv} = Exp(1.2378 \times 10^{-5} T^2 - 0.01912T + 33.937 - 6343T^{-1}) \quad (3\text{-}4)$$

The correlation for compressibility factor (Z) and coefficients are as given:

$$Z = 1 - \frac{p}{T}\left[a_0 + a_1 T_t + a_2 T_t^2 + (b_0 + b_1 T_t) X_v + (c_0 + c_1 T_t) X_v^2\right]$$

$$+ \left(\frac{p}{T}\right)^2 (d + e X_v^2), \quad (3\text{-}5)$$

$a_0 = 1.58123 \times 10^{-6}$ K Pa^{-1}, $a_1 = -2.9331 \times 10^{-8}$ Pa^{-1},

$a_2 = 1.1043 \times 10^{-10}$ K^{-1}Pa^{-1}, $b_0 = 5.707 \times 10^{-6}$ K Pa^{-1},

$b_1 = -2.051 \times 10^{-8}$ Pa^{-1}, $c_0 = 1.9898 \times 10^{-4}$ K Pa^{-1},

$c_1 = -2.376 \times 10^{-6}$ Pa^{-1}, $d = 1.83 \times 10^{-11}$ K^2 Pa^{-2},

$e = -0.765 \times 10^{-8}$ K^2 Pa^{-2}.

The air viscosity was calculated with Sutherland's Law (1893). Air viscosity is the function of temperature as follows:

$$\mu = \mu_0 \frac{T_0 + C}{T + C} \left(\frac{T}{T_0}\right)^{3/2}. \quad (3\text{-}6)$$

In Sutherland's formula, μ_0, T_0 and C are the reference viscosity in mPa·s, the reference temperature in $^{\circ}K$ and Sutherland's constant for air, respectively.

For air, $\mu_0 = 1.827 \times 10^{-2}$ mPa · s, $T_0 = 291.15$ K and C = 120 $^{\circ}K$.

3.2.2 Oil Properties

Lubsoil ND-50 mineral oil was selected as the test oil due to the high viscosity and Newtonian behavior in the testing range. The viscosity of oil was measured 7 times using the rheometer, a RheoScope 1™. For each measurements, oil temperature was changed from 60 to 120 $^{\circ}F$. The obtained oil viscosity correlation is as given:

$$\mu_{oil} = 1.0134 \times 10^8 \, T^{-2.839} \quad (3\text{-}7)$$

where T is in $^{\circ}F$, and μ_{oil} is in mPa·s. Figure 3.3 depicts correlation curve

between oil viscosity and oil temperature.

As oil is assumed incompressible, oil density which was measured from coriolis flow meter can be used. Additional physical properties of ND-50 are as follows:

- API gravity: 28.5°.
- Density: 884.4 kg/m3 @ standard condition.
- Pour and flash point temperatures: -15 ℃ (5 ℉) and 265 ℃ (510 ℉), respectively.
- Surface tension: 35.75 dynes/cm at 19.8 ℃ (68 ℉) and atmospheric pressure.

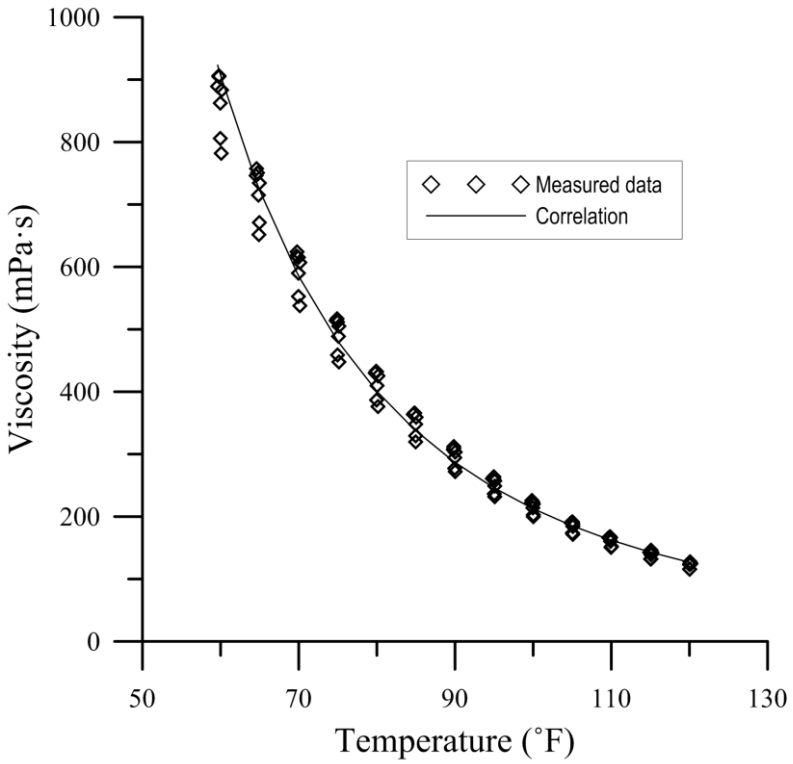

Figure 3.3 Viscosity vs. Temperature of oil.

3.3 Instrumentation

The following instrumentation was used to perform the identification of flow pattern, and the measurement of pressure gradient and liquid holdup.

3.3.1 Basic Instrumentation

Temperature data was collected by calibrated resistance temperature detector (RTD) temperature transducers. They were installed oil metering section, gas metering section and test section, being calibrated to have $\pm 0.25\,℃$ of uncertainty. To measure pressure of test section, a Rosemount gauge pressure transducer was mounted between the Quick Closing Valves. Uncertainty of pressure transducer is $\pm 0.15\%$.

Rosemount differential pressure transducer was installed to measure pressure drop in flowing condition and liquid holdup in trapped condition. It has a systematic uncertainty of ±0.055%. The impulse line of differential pressure system, divided into two sections connected by pressure transducer, is designed for real-time measure of the pressure differences between two different points. It is filled with silicon oil to catch the small change in pressure drop of the flow. As the test section is raised up to vertical position, however, the hydrostatic pressure of silicon oil occurs significant pressure difference, zero-DP, even the pipe is empty. To obtain the pressure differences between two points accurately, measured zero-DP in vertical position was

subtracted from the measured pressure drop readings.

CMF100 coriolis flow meter from Micro Motion™ with RTF9739 transmitter was used to measure oil mass flow rate and oil density. The known uncertainties of density and mass flow rate measurement are ±0.5kg/m^3 and ±0.1%, respectively. For measurement of gas mass flow rate, two Endress-Hauser Promass 83F coriolis flow meters are used. They are reported to have uncertainty of ±0.1% of their readings.

3.3.2 Quick Closing Valve System

A pair of Quick Closing Valves are installed to measure an average liquid holdup with a differential pressure transducer. The measured pressure difference varies with liquid level of trap section due to hydrostatic pressure of liquid column. To obtain liquid holdup-pressure difference correlation, a special type of calibration was conducted. First, trap section was filled with water, and the pressure difference in trap condition (DP_{trap}) was recorded repeatedly after draining predetermined volume of water. Figure 3.4 shows the correlation between total drained volume and DP_{trap}.

While this calibration was conducted with water as liquid phase, the correlation should be modified with liquid density. When we drained predetermined volume of water, *DP* changes as follows:

$$\Delta DP_{trap} = \rho_L g \Delta h_L = \rho_L g \Delta H_L h_{trap} \text{ and}$$
$$\Delta H_L = 1 - (\Delta V_{drain}/V_{QCV}) = \Delta h_L / h_{trap} \quad (3\text{-}8)$$

where ρ_L, h_L, H_L, h_{trap}, V_{drain} and V_{QCV} are density of liquid, height of liquid column, liquid holdup, total length of trap section, volume of drained water and volume between QVCs, respectively (Figure 3.5). From equation (3-8), we can obtain

$$H_L \, \alpha \, (DP_{trap}/\rho_L g) \quad (3\text{-}9)$$

regardless the liquid density. Figure 3.6 depicts the correlations between liquid holdup and $DP_{trap}/\rho_L g$. Following equations can be used to calculate liquid holdup from the DP_{trap} reading:

$$H_L = -0.0041 \, (DP_{trap}/\rho_L g) + 0.0694. \quad (3\text{-}10)$$

As DP_{trap} changes when from 945 ml to 12,058 ml and V_{QCV} is 12,952 ml from the measurement, equation (3-10) can be applied for the range between 0.069 and 0.926.

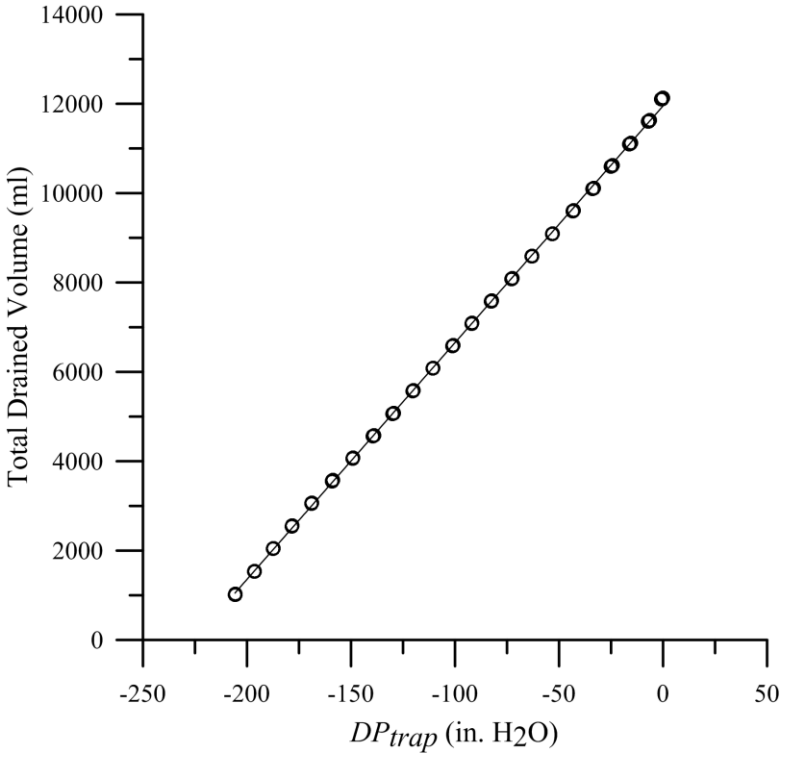

Figure 3.4 Total drained water volume vs. DP_{trap}.

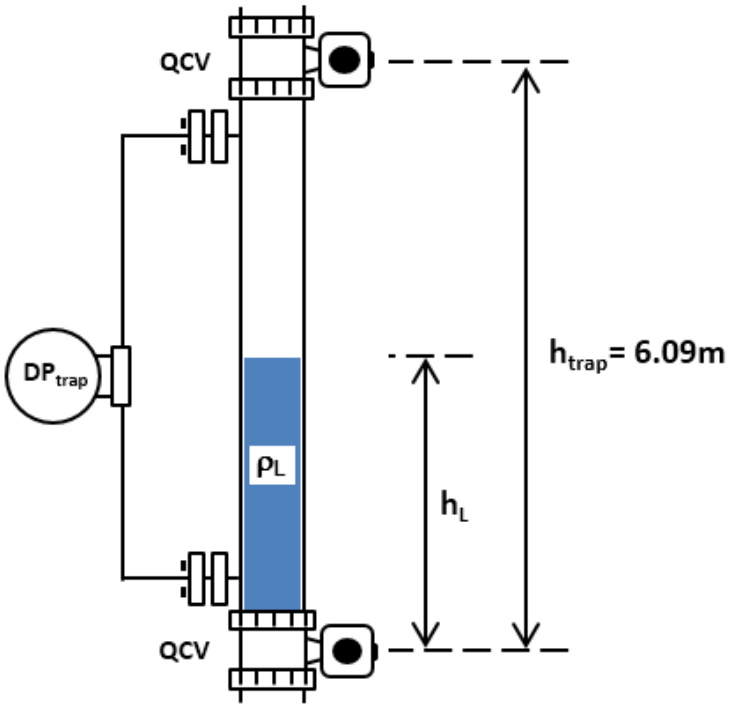

Figure 3.5 Schematics of the average liquid holdup measurement.

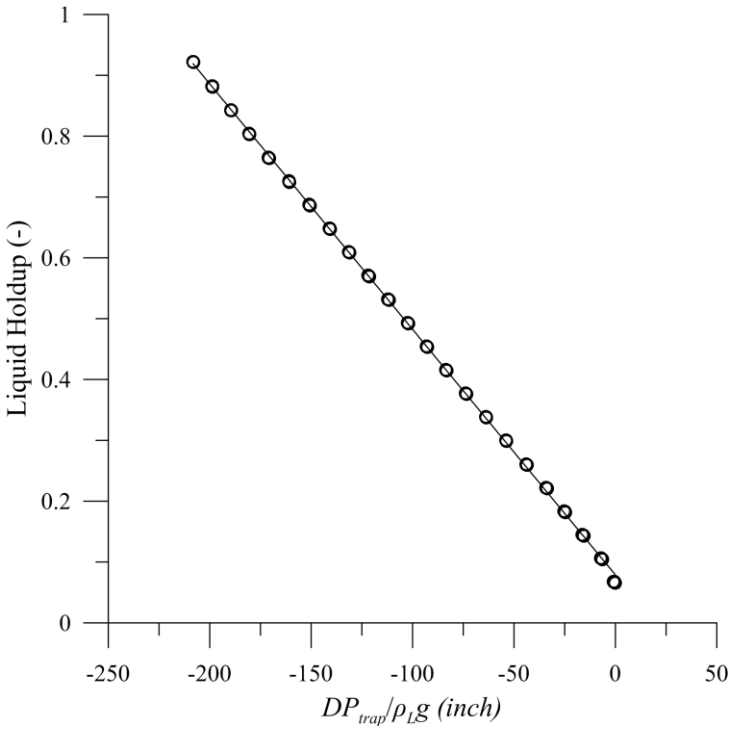

Figure 3.6 Average liquid holdup vs. $(DP_{trap}/\rho_L g)$.

3.3.3 Capacitance Sensors

In vertical downward flow with high viscosity oil, as dark-colored liquid film always exist along with the pipe wall, it is very difficult to identify flow patterns only with surveillance camera. Therefore, a pair of capacitance sensors are installed to identify flow patterns by analyzing liquid holdup Probability Distribution Function (PDF) of flow. Recorded capacitance sensor voltage signals converted into liquid holdup with the correlation from static calibration. Figure 3.7 and Figure 3.8 depict static calibration correlation curve for each capacitance sensor. Both of capacitance sensors are two-wire

type and have linear response as reported previously by other studies (Kora, 2010; Brito, 2012). Detailed explanations about characteristic of each flow pattern type will be treated in experimental results section.

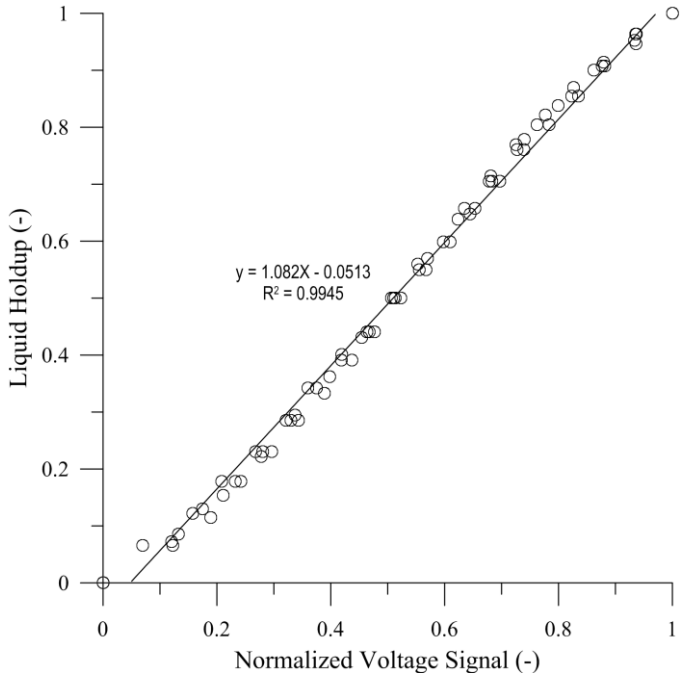

Figure 3.7 Static calibration correlation for Capacitance 1.

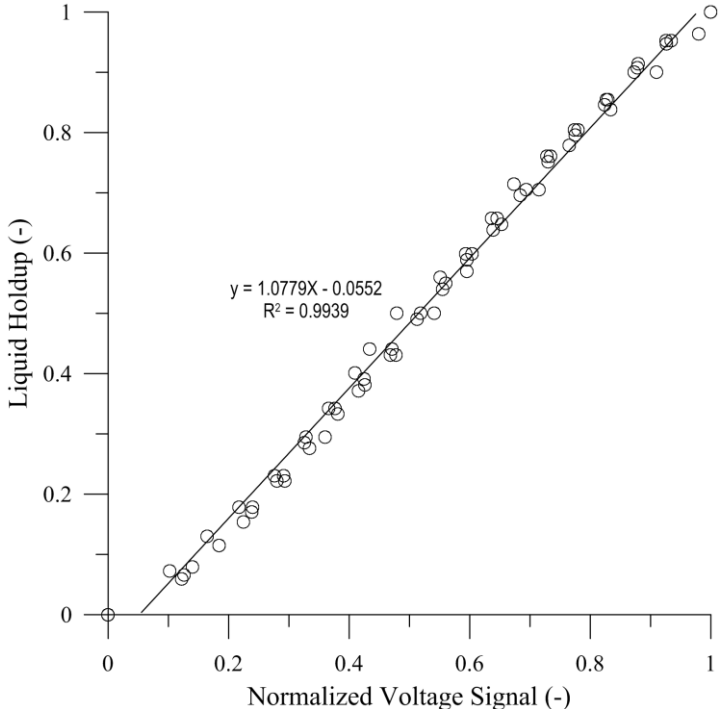

Figure 3.8 Static calibration correlation for Capacitance 2.

3.4 Experimental Procedure

An experimental procedure is for obtaining reliable experimental data; pressure drop, voltage signals from capacitance sensors and average liquid holdup. The procedure is given below.

1. Start air compressor.
2. Start data acquisition program, and monitor readings of all instruments.
3. Check all valves on test section to avoid operations problems.
4. Raise test section to vertical position
5. Check differential pressure transducer reading to examine DP zero correction is accurate.
6. Record empty pipe voltage reading for all capacitance sensors to obtained minimum voltage value. If for any capacitance sensor shows abnormally high values, lower the test section and adjust capacitance sensor readings to acceptable value.
7. Lower test section to horizontal position.
8. Check temperature of oil in main storage tank. Set-up heating system to adjust oil temperature should be done in previous day as it may take hours to reach required temperature.
9. Start oil pump, maintaining desired superficial oil velocity for testing.

10. Circulate single-phase oil until oil reaches back to oil tank.
11. Run single phase oil at two different v_{SL} values (0.2 m/s & 0.5 m/s) to check that all instruments display reasonable readings.
12. Check temperature transducers on test section for actual oil temperature in test section and adjust if necessary to desired temperature. The temperature should be kept constant during test for oil viscosity control.
13. Record voltage reading for single phase oil, to obtained maximum voltage value (horizontal position).
14. Raise test section to vertical position.
15. Close lower QCV and record voltage readings for single phase oil to obtained maximum voltage value in vertical position.
16. Open QCV and change QCV setting to capture entire trap section.
17. Open air valve and increase required superficial air velocity up to desired value.
18. Wait until the flow to be stabilized, monitoring temperature transducer and differential pressure transducer readings on test section.
19. Run low and high speed data acquisition system at a sampling frequency of 5 Hz for low speed data for 3 minutes (900 data points) and 1,000 Hz for high speed data for one minute (60,000 data points).
20. Run average liquid holdup measurement procedure:

a) Open bypass valve and close two QCVs simultaneously to trap fluid mixture

b) Wait for DP to be stabilized with the segregation of liquid and record it.

c) Calculate liquid holdup with average liquid holdup correlation.

d) Open two QCVs and then close bypass valve.

21. For each test point, repeat these steps (high/low speed data acquisition and average liquid holdup measurement) 3 times to confirm results.
22. Repeat there steps for different superficial air and oil velocities and viscosities which are listed in test matrix.
23. Shut down oil pump. Keep gas flowing to remove oil from the test section.
24. Lower test section to horizontal position.
25. Stop air flow.
26. Log out from data acquisition systems.
27. Shut down air compressor.
28. Set up heating system in oil tank for next day desired oil temperature.
29. Make backup copies of all the acquired data.

3.5 **Uncertainty analysis**

Since the true value can never be measured exactly, every measurement generates error, the difference between the true and measured values. Measurement uncertainty analysis is a numerical method for quantifying the potential error that exists in all data (Dieck, 2007). We can estimate the 95% confidence interval of the measurement that includes the true value.

Errors can be divided into 3 groups; random (precision), systematic (bias) and blunders (mistakes) errors. A random error is unpredictable fluctuation that is occurred among the measurements for the same test condition. Systematic error is the difference between a single true value and the average of measured values. Systematic error is a constant for all experiments. Blunders errors are occurred by improper performance of experimenter and assumed to be removed with good engineering practice.

Random Uncertainty: Random errors are values that affect test data in a random fashion from one reading to the next. Random uncertainty sources that cause scatter in the test results (Dieck, 2007). Experimental measurements are used to estimate random uncertainty. Random uncertainty is calculated by using the Student‘s t distribution. In these calculations, the random uncertainty is assumed to be normally distributed; therefore, the result is a symmetrical random uncertainty. Calculations related to uncertainty come from statistical methods. Scatter in samples is calculated by using the sample standard deviation definition (S_X),

$$S_X = \sqrt{\frac{\sum_{i=1}^{N}(X_i - \bar{X})^2}{N-1}} \quad (3\text{-}11)$$

where:

N = number of data points

X_i = the ith data point

$\bar{X}$ = the average of data points

(N-1) = the degrees of freedom for the data points

In order to find the error percentage in the average, the standard deviation of the average ($S_{\bar{X}}$) is estimated by:

$$S_{\bar{X}} = \frac{S_X}{\sqrt{N}}. \quad (3\text{-}12)$$

$S_{\bar{X}}$ is known as the random uncertainty with a confidence level of 68%. To determine the 95% confidence interval of a measurement, the student-t distribution t95 can be used. Therefore, the random uncertainty of measurement X is given by the uncertainty interval, $X = \bar{X} \pm t_{95} S_{\bar{X}}$. If several estimates of standard deviation are available, a better estimate of standard deviation is obtained by combining the individual estimates of the same standard deviation through a pooling process. The equation used to pool S_X is:

$$S_{X,pooled} = \left[\frac{\sum_{i=1}^{N} v_i \left(S_{X,i}\right)^2}{\sum_{i=1}^{N} v_i}\right]^{1/2} \quad (3\text{-}13)$$

where:

$S_{X,pooled}$ = the pooled standard deviation

N = number of standard deviation pooled

$S_{X,i}$= the ith standard deviation

v_i= the ith degrees of freedom

Systematic Uncertainty: Systematic error is constant for all experiments using a particular instrument and often provided by the manufacture. Systematic errors affect every measurement of a variable the same amount. The systematic uncertainty comes from various error sources. Each source of the elemental systematic uncertainty, b_i, needs to be combined by using the following equation,

$$b_R = \left[\sum_{i=1}^{N} (b_i)^2\right]^{1/2} \tag{3-14}$$

where b_R is the combined systematic uncertainty component of the uncertainty analysis. The systematic standard uncertainty is assumed to have infinite degrees of freedom. As such it represents 68% confidence interval. If systematic uncertainty is given as 95% confidence interval, the student-t would be 2 and we would divide our estimate of systematic uncertainty by 2.0 to use it in combined uncertainty equation. The systematic uncertainties of the measured parameters are listed in Table 3.1.

Table 3.1: Systematic Uncertainty of experimental instruments

Measured Parameters	**Instruments**		**Model**	**Systematic Uncertainty**
Gas Flow Rate	Micro Motion TM	MM3	83F08-DXW2/O	±0.1%
		MM4	83F08-DXW2/O	
Liquid Flow Rate	Micro Motion TM	MM1	RFT9739	±0.1%
Liquid Density	Micro Motion TM	MM1	RFT9739	±0.5 Kg/m3
Temperature	Rosemount Temperature Transducer	TT14	3144PD1A1E5B4 M5	±0.25^{o}C
Pressure	Rosemount Pressure Transducer	PT12	3051S2TA2A2E1 1A1AE5M5B4	±0.15% of Span
Differential Pressure	Rosemount Differential Pressure Transducer	DP15	3051S2CD2A2B1 2A1AB4E5M5	±0.15% of Span

Chapter 4 Experimental Results

This chapter covers the results of experimental works and their comparisons with experimental data for low viscosity vertical downward flow. Measured raw data were analyzed on the purpose of flow pattern identification, pressure drop measurement, and average liquid holdup measurement. Four temperature conditions, 70℉, 80℉, 100℉, and 120℉, are considered as test conditions. By equation (3-7), corresponding oil viscosities are estimated as 586 mPa·s, 401 mPa·s, 213 mPa·s, and 127 mPa·s, respectively. The superficial liquid and gas velocities vary with temperature conditions, having range of 0.05 to 0.7 m/s and 0.2 to 8 m/s, respectively. To estimate the uncertainty of average liquid holdup, each flow conditions has at least 3 measurements.

4.1 Flow Pattern

Considering the traditional flow pattern classification, all conditions can be categorized as annular flow. To describe more detailed physical phenomena, however, the Probability Distribution Function (PDF) are conducted from capacitance sensor signals and flow patterns were divided into three types: Falling Film (FF), Wavy Annular (WA) and Liquid Slip (LS). Videos for each flow condition were also utilized to help flow pattern distinction. Figure 4.1 shows typical PDF distributions and relating schematics for each flow pattern type which are observed in this study. Figure 4.2 depicts captured screenshot of video for each flow pattern.

Falling Film flow pattern occurs under low gas and liquid flow rate conditions. This flow pattern is frequently observed in previous researches (Oshinowo & Charles, 1974; Usui, 1989). Due to its low flow rates of each fluid, it shows low liquid entrainment into the gas core and small wave amplitude on liquid film (figure 4.2 (a)). PDF of Falling Film flow pattern are intensively distributed at relatively low value due to its thin film thickness and small wave amplitude (figure 4.1 (a)).

As liquid rate increases, liquid film starts getting thicker. Owing to combined effect of gravity and interfacial shear stress by gas flow, significant portion of liquid film near the liquid-gas interface starts to slip over the liquid film. This flow pattern is defined as Liquid Slip flow. A similar flow pattern was observed by Zadrazil et al. (2014a) for air-water downward flow at high liquid Reynolds numbers. As a result, a large and steady liquid entrainment is observed in the gas core region (figure 4.2 (c)). PDF of liquid slip flow pattern shows a long-tailed distribution towards high liquid holdup section, because of its large entrainment of liquid (figure 4.1 (c)).

With high gas rate, larger drag force acts on liquid film. It causes the erratic roll over waves with large amplitudes on liquid film surface as observed in figure 4.2 (b). Because the waves on liquid surface behave like roughness, high interfacial shear stress occurs between phases resulting in high pressure drop similar to an annular flow in vertical upward. PDF of wavy annular flow pattern shows wider distribution than Falling Film flow pattern, because waves occurs more frequently.

Figure 4.3 through 4.6 depicts the observed flow patterns for

different oil viscosities. As liquid viscosity decreases, liquid slip flow pattern is observed at higher v_{SG} and lower v_{SL} conditions. It means liquid slip are easy to slip at lower viscosity.

Each flow patterns can be distinguished using statistical parameter of PDF: skewness and kurtosis. PDF of Falling Film flow have relatively high kurtosis comparing other flow patterns because it has narrow and intensive distribution. For Wavy Annular flow, kurtosis is smaller than Falling Film flow due to the large role wave while Falling Film flow has small kurtosis owing to the large liquid droplet. Wavy Annular flow and Liquid Slip flow can be divided by skewness. Due to the small fraction of liquid entrainment, skewness of Wavy Annular flow is smaller than that of Liquid Slip flow. As Liquid Slip flow has irregular large liquid entrainment, PDF has a shape of long tail.

Figure 4.7 to 4.10 depict relationship between kurtosis and skewness depending on flow pattern for different oil viscosities. In same flow pattern group, kurtosis and have a positive correlation. When liquid viscosity increases, liquid tends to flow with small roll wave and small liquid entrainment. Consequently, both of skewness and kurtosis become small in Wavy Annular flow and Liquid Slip flow.

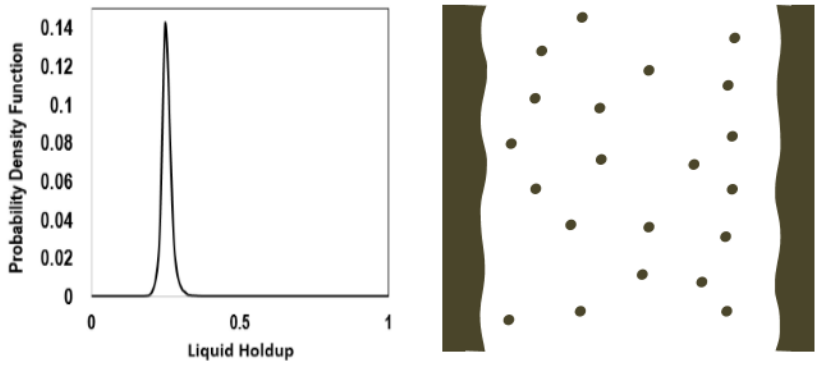

(a) type 1: Falling Film (FF)

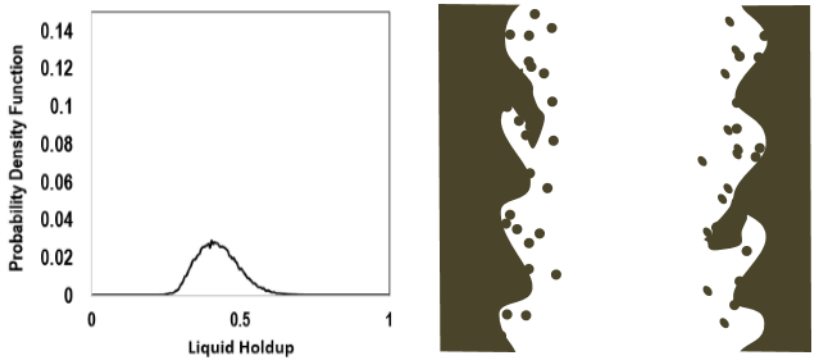

(b) type 2: Wavy Annular (WA)

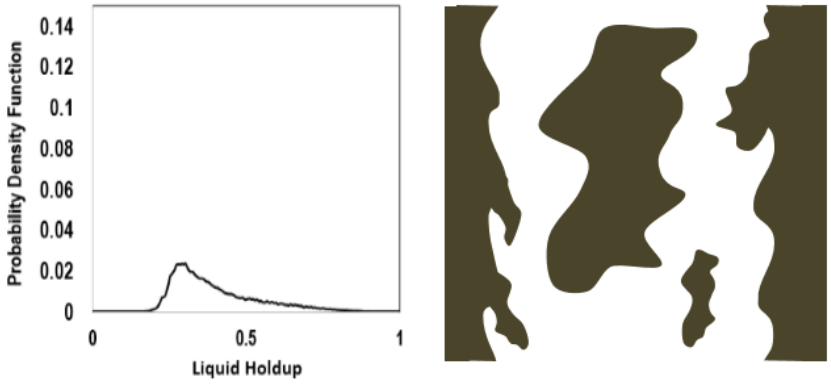

(c) type 3: Liquid Slip (LS)

Figure 4.1 Probabilistic Density Function (PDF) and schematics for each flow pattern type.

(a) Falling Film

v_{SL} = 0.06 m/s

v_{SG} = 0.64 m/s

(b) Wavy Annular

v_{SL} = 0.11 m/s

v_{SG} = 6.16 m/s

(c) Liquid Slip

v_{SL} = 0.7 m/s

v_{SG} = 0.7 m/s

Figure 4.2 Captured video screenshots for each flow pattern

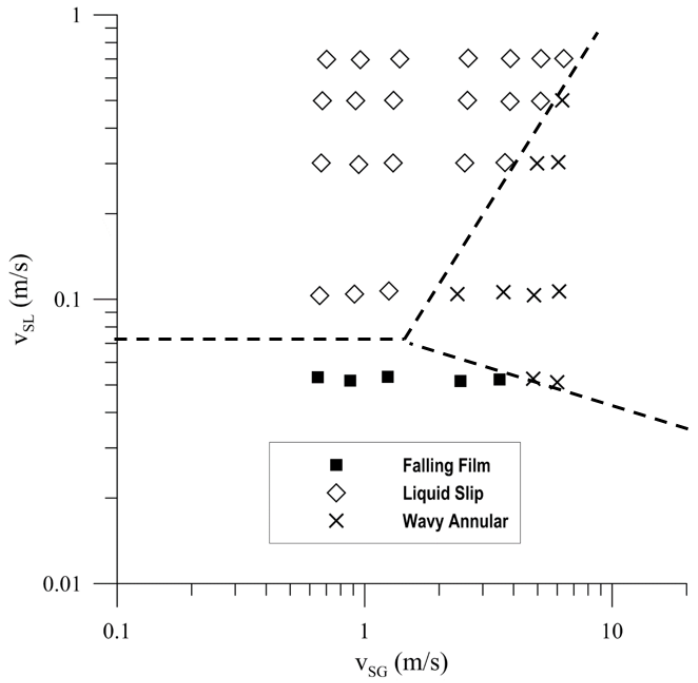

Figure 4.3 Observed flow pattern for μ_{oil} = 127 mPa·s

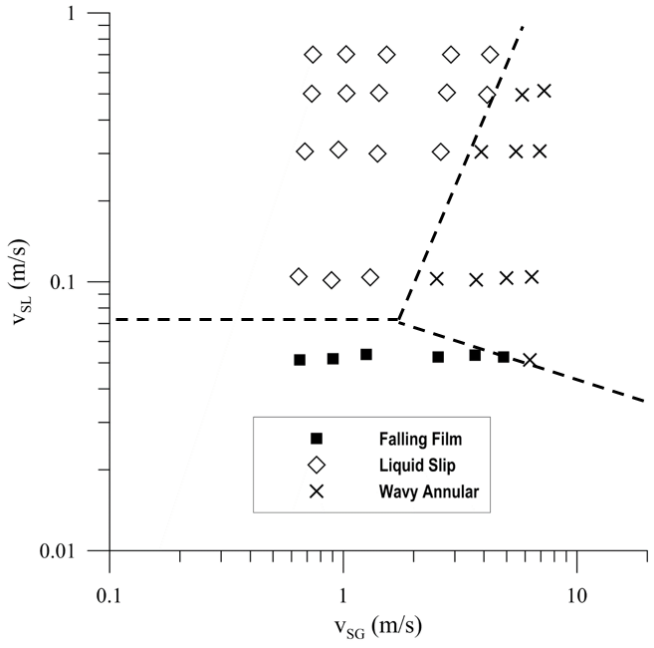

Figure 4.4 Observed flow pattern for μ_{oil} = 213 mPa·s

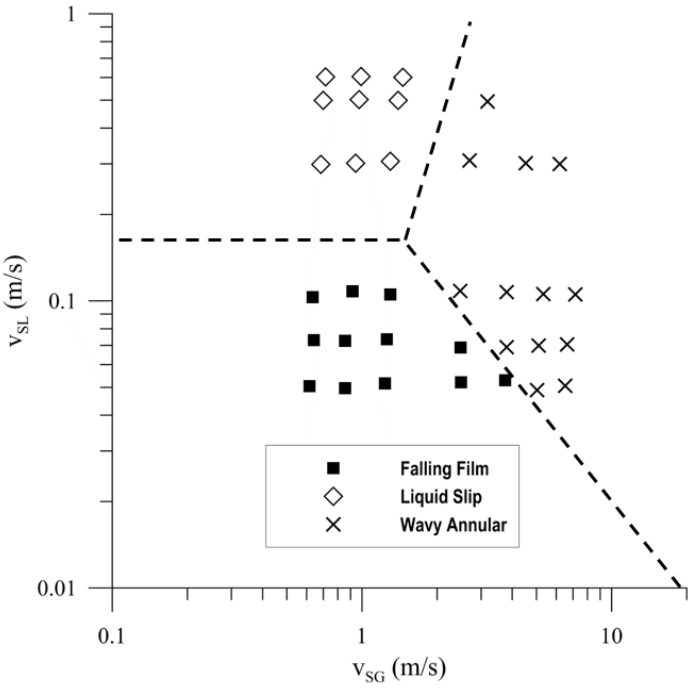

Figure 4.5 Observed flow pattern for μ_{oil} = 401 mPa·s

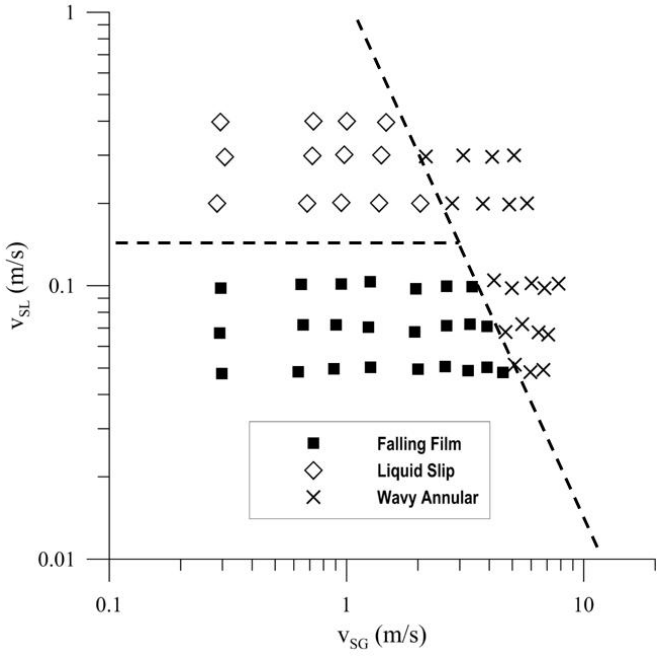

Figure 4.6 Observed flow pattern for μ_{oil} = 586 mPa·s

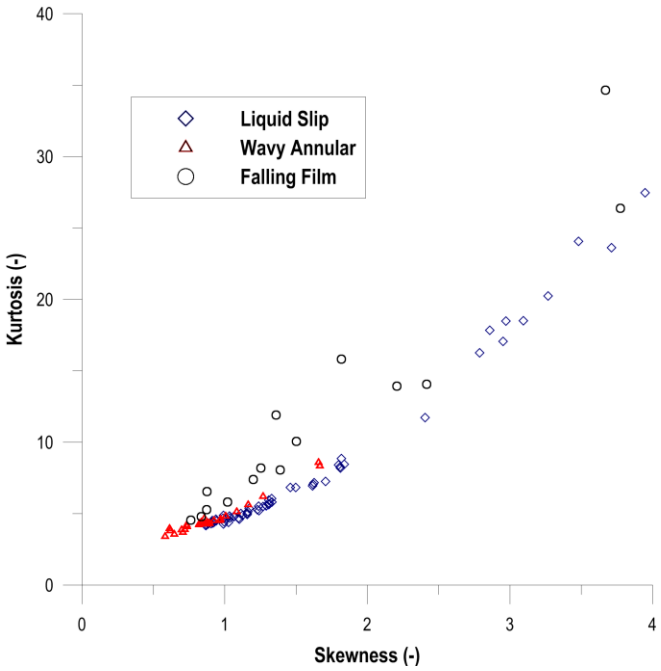

Figure 4.7 Skewness vs. kurtosis for μ_{oil} = 127 mPa·s

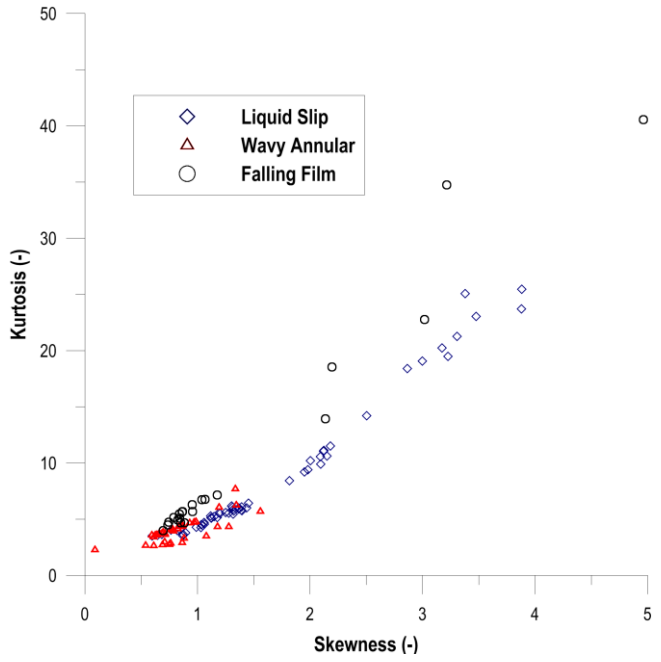

Figure 4.8 Skewness vs. kurtosis for μ_{oil} = 213 mPa·s

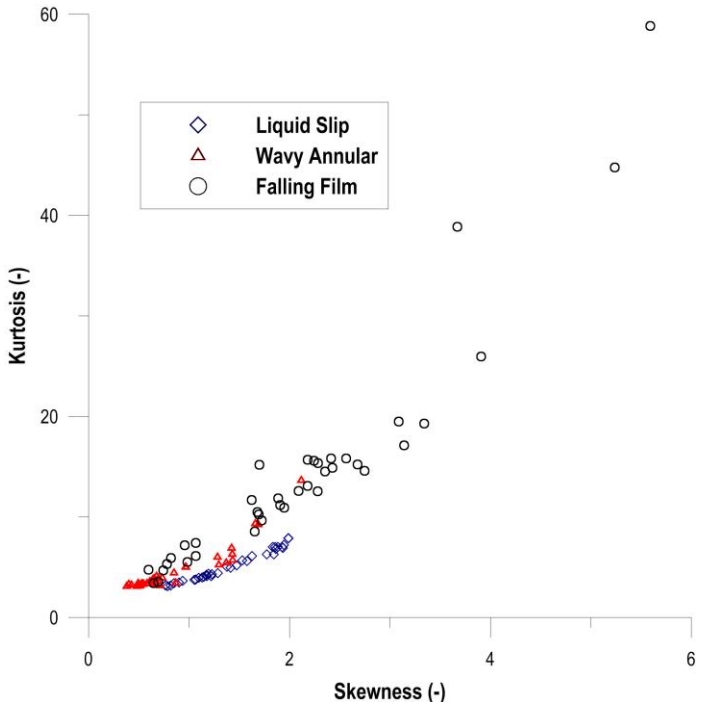

Figure 4.9 Skewness vs. kurtosis for μ_{oil} = 401 mPa·s

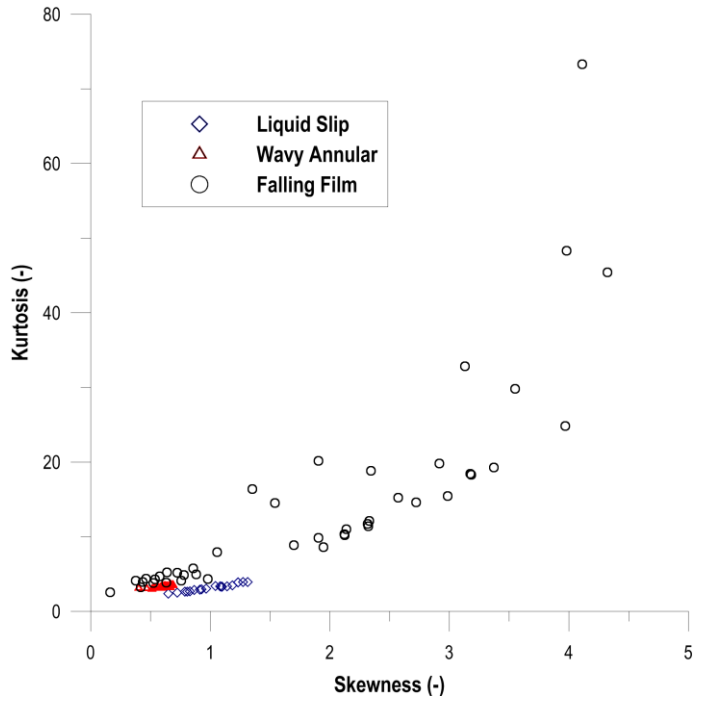

Figure 4.10 Skewness vs. kurtosis for μ_{oil} = 586 mPa·s

4.2 Pressure Gradient

Figures 4.11 to 4.14 show the measured pressure gradient vs. superficial gas velocity depending on oil viscosities. Pressure gradient significantly changes with the transition of flow pattern type. When Falling Film flow pattern occurs, as the liquid flows due to the gravity instead of pressure differences, pressure gradient is almost zero. For Liquid Slip flows, negative pressure gradient is observed for low gas rate conditions because of its high liquid flow rate. With the increase of gas rate, flow pattern changes to Wavy Annular flow. Pressure gradient increases sharply due to the high friction force. For wavy annular flow, pressure gradient increases linearly with increase of superficial gas velocity and its slope increases with higher v_{SL}.

Figures 4.15 compares pressure gradient for v_{SL}=0.3 m/s. Two features can be concluded from the figures. As liquid viscosity decreases, inflection point of pressure gradient positions at higher v_{SG} for same v_{SL}. This feature corresponds with which discussed in previous section; for lower liquid viscosity, annular wavy flow pattern occurs at higher gas rate condition. And slope of pressure gradient becomes larger for high liquid viscosity flow.

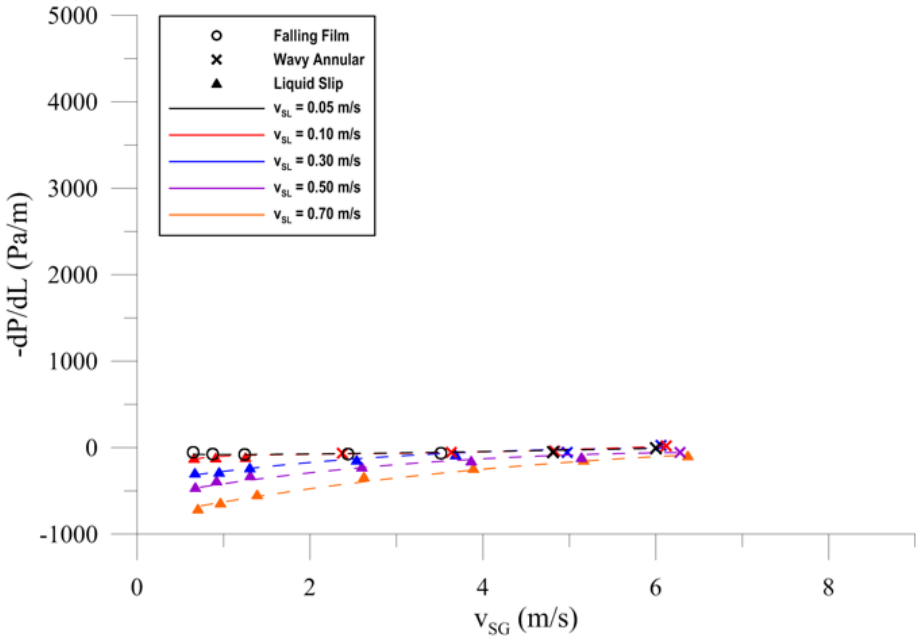

Figure 4.11 Pressure gradient vs. superficial gas velocity

for μ_{oil} = 127 mPa·s

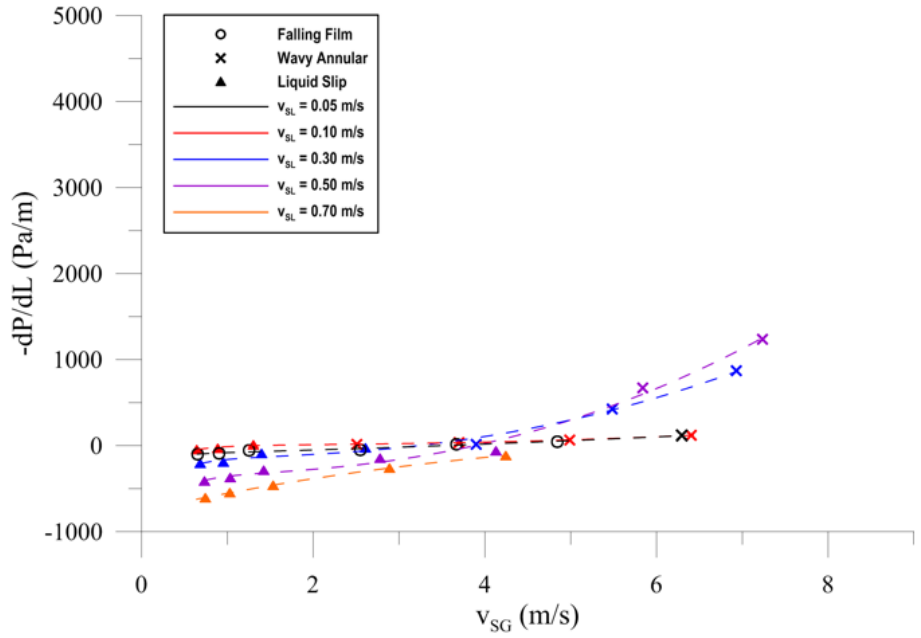

Figure 4.12 Pressure gradient vs. superficial gas velocity

for μ_{oil} = 213 mPa·s

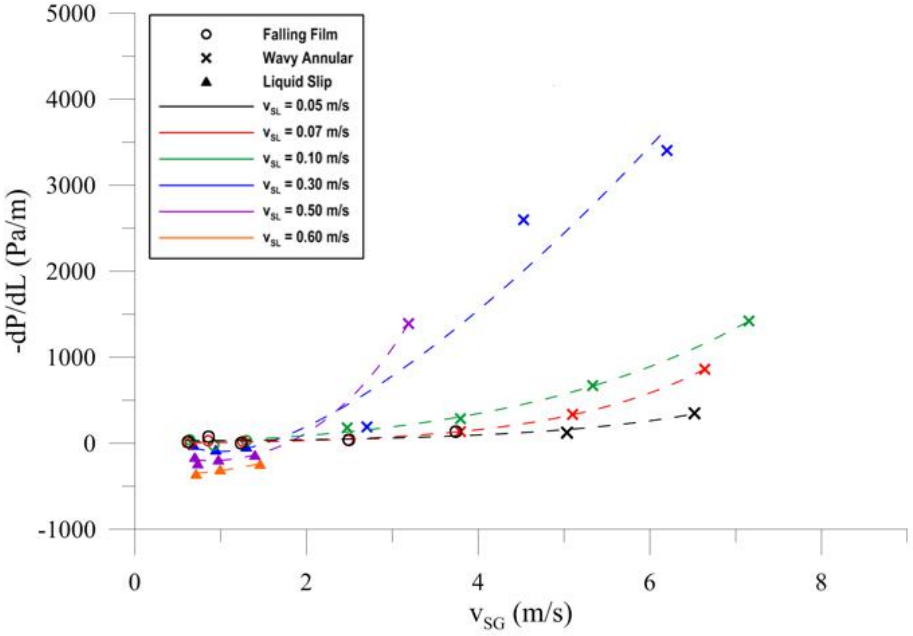

Figure 4.13 Pressure gradient vs. superficial gas velocity for μ_{oil} = 401 mPa·s

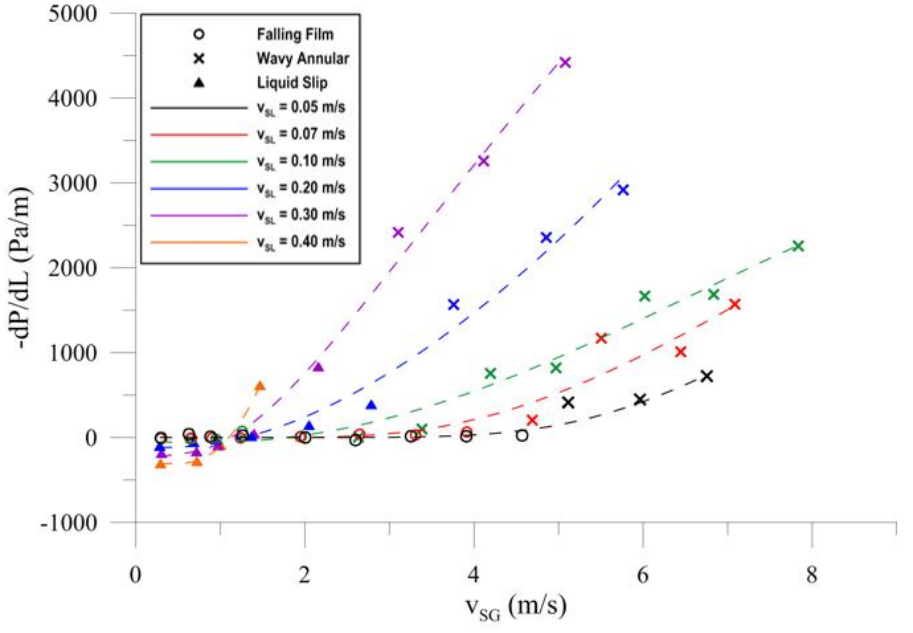

Figure 4.14 Pressure gradient vs. superficial gas velocity for μ_{oil} = 586 mPa·s

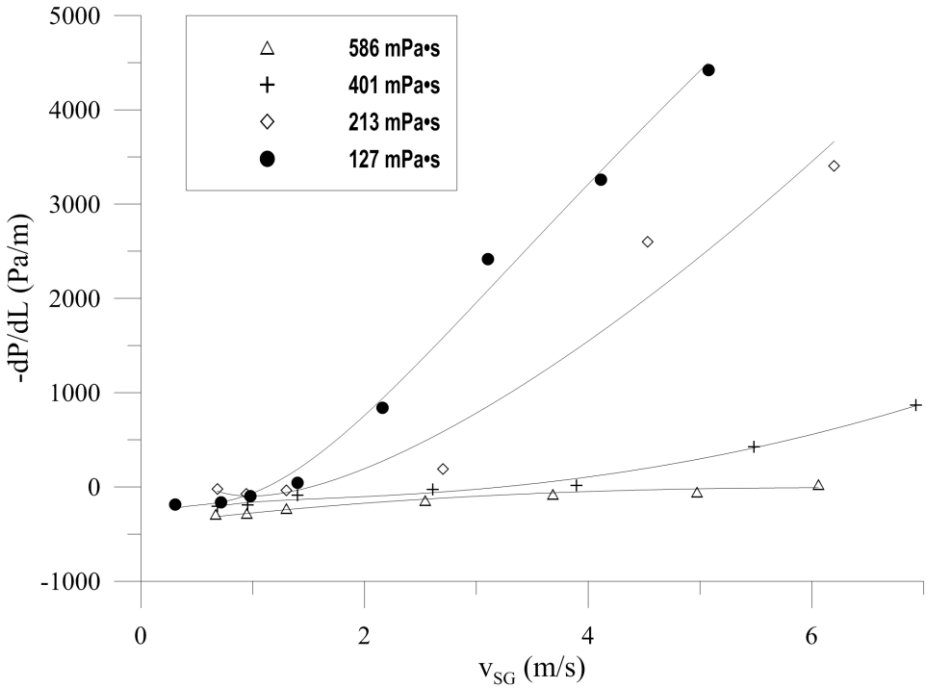

Figure 4.15 Comparison of pressure gradient for v_{SL}=0.3 m/s.

4.3 Average Liquid Holdup

Figures 4.16 to 4.19 show the average liquid holdup vs. superficial gas velocity depending on oil viscosities. Between Falling Film and Wavy Annular flow patterns, average liquid holdup shows no significant differences. For both flow patterns, most liquids flow in the liquid film region. On the other hand, average liquid holdup suddenly increases as the flow pattern changes from Liquid Slip to Wavy Annular for high viscosity condition. As flow pattern changes from liquid slip to wavy annular, gas tends to flow through center of the pipe pushing liquid droplet towards wall direction. Liquid droplets flow much faster than liquid film, and the deposition of liquid droplets to film region with flow pattern transition results in a decrease of average liquid velocity and an increase of average liquid holdup (Figure 4.20). However, liquid film can flow much faster in low viscosity condition, resulting large and clear role waves on liquid film surface. Consequently, as gas superficial velocity increases, liquid holdup decreases.

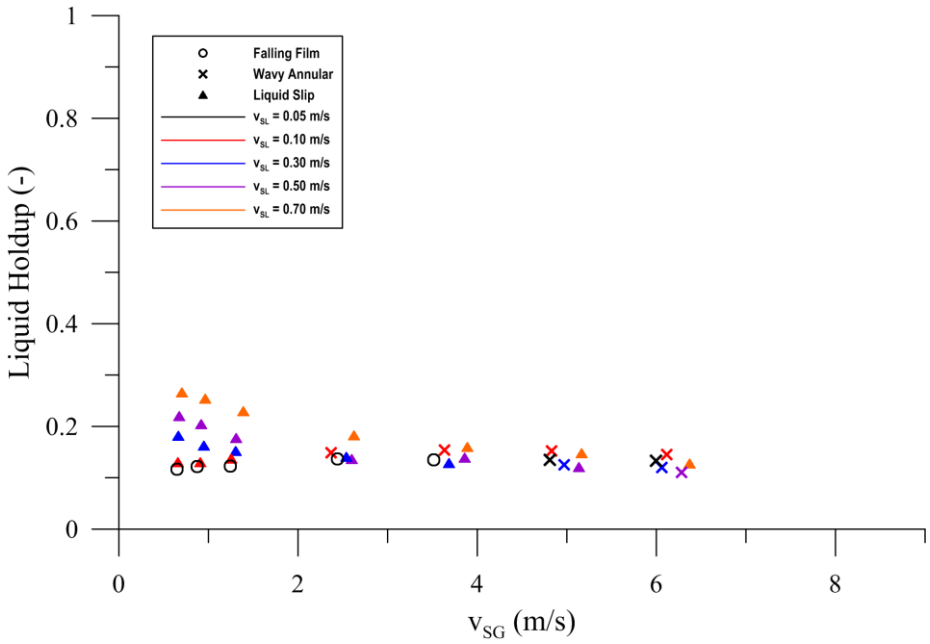

Figure 4.16 Liquid holdup vs. superficial gas velocity for μ_{oil} = 127 mPa·s

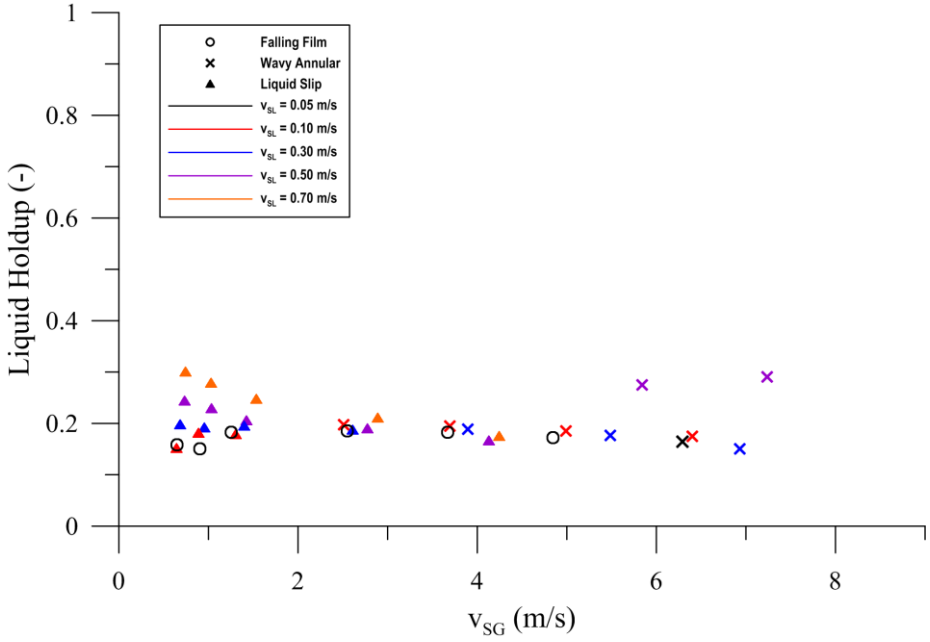

Figure 4.17 Liquid holdup vs. superficial gas velocity for μ_{oil} = 213 mPa·s

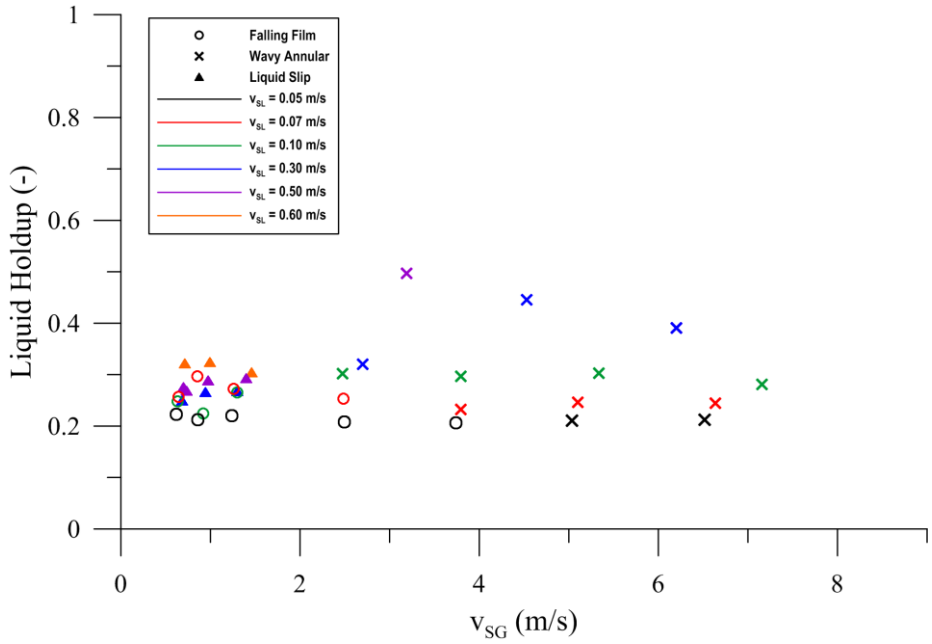

Figure 4.18 Liquid holdup vs. superficial gas velocity for μ_{oil} = 401 mPa·s

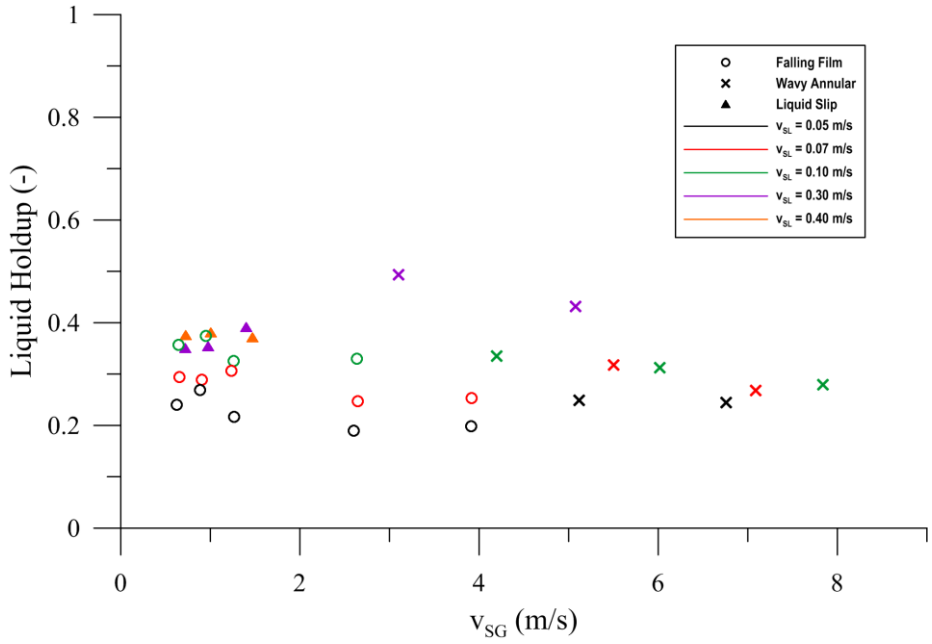

Figure 4.19 Liquid holdup vs. superficial gas velocity for μ_{oil} = 586 mPa·s

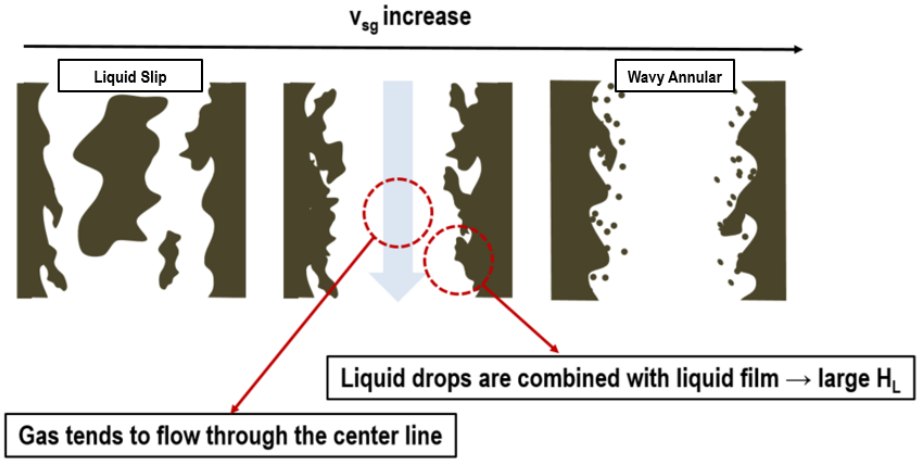

Figure 4.20 Schematic of sudden increase of liquid holdup between Liquid Slip and Wavy Annular flow patterns

Chapter 5 Discussions

5.1 Model Comparison

This section presents the evaluation of existing mechanistic models against the acquired two-phase flow data. The comparison is subdivided into sections of flow pattern, average liquid holdup, and pressure gradient.

5.1.1 Flow Pattern

Two models were considered for flow pattern prediction: Barnea et al. (1987), and TUFFP Unified (2011) model. Figure 5.1 through Figure 5.4 show the comparison between the observed flow patterns high oil viscosities and the predicted flow patterns map models of Barnea (1987), and TUFFP (2011) version 2011.

For most of the experimental conditions, the Barnea (1987) model and the TUFFP Unified (2011) model predict flow patterns as intermittent flow. For low viscosity condition, some of the point are included in annular flow in Barnea's (1987) model.

Transition criteria of annular flow and intermittent flow in Barnea's model is highly affected by slug liquid holdup. As the model was developed based on water-gas condition, it assumes slug liquid holdup as 0.7, while slug liquid holdup of high viscosity oil was reported as higher than 0.95. TUFFP unified model calculates transition criteria of annular flow and intermittent

flow based on slug flow parameters. As the film length goes infinite, slug flow changes to annular flow or stratified flow.

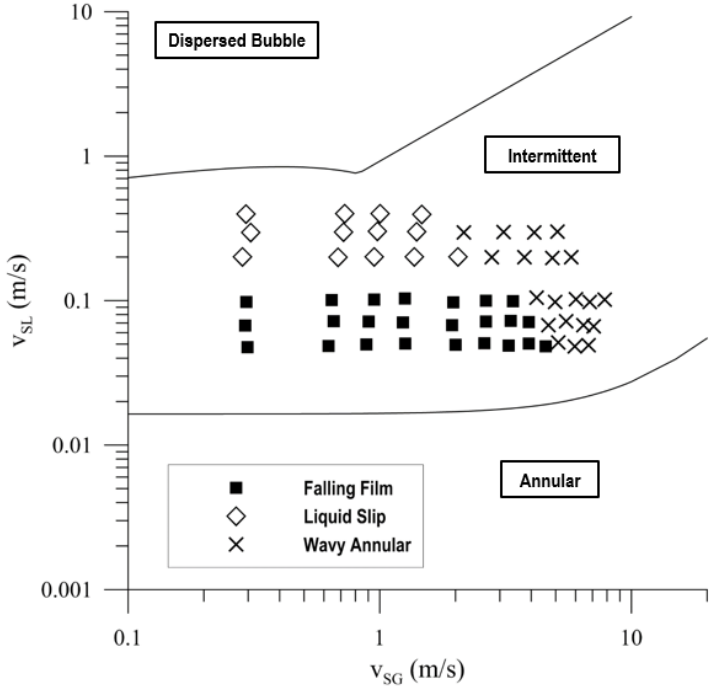

(a) Barnea's model (1987)

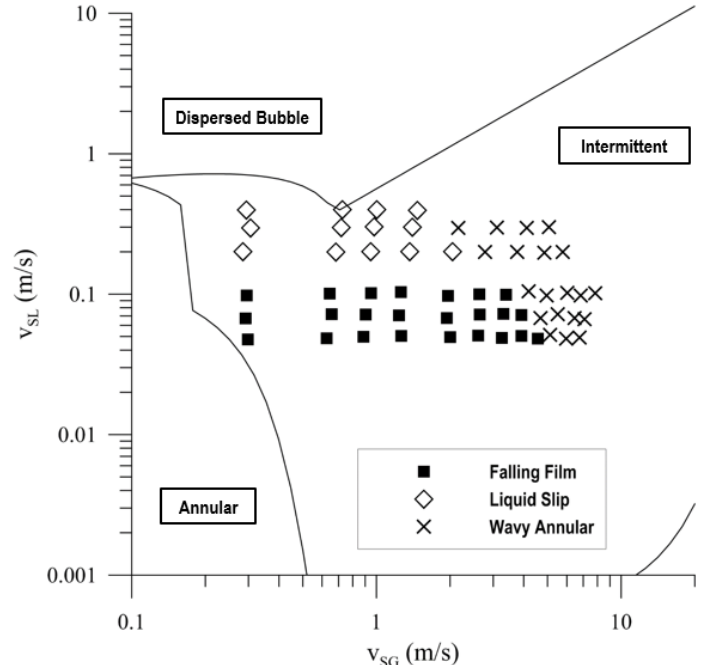

(b) TUFFP Unified (2011) model

Figure 5.1 Flow pattern map compared with observed flow patterns for μ_{oil} = 586 mPa·s

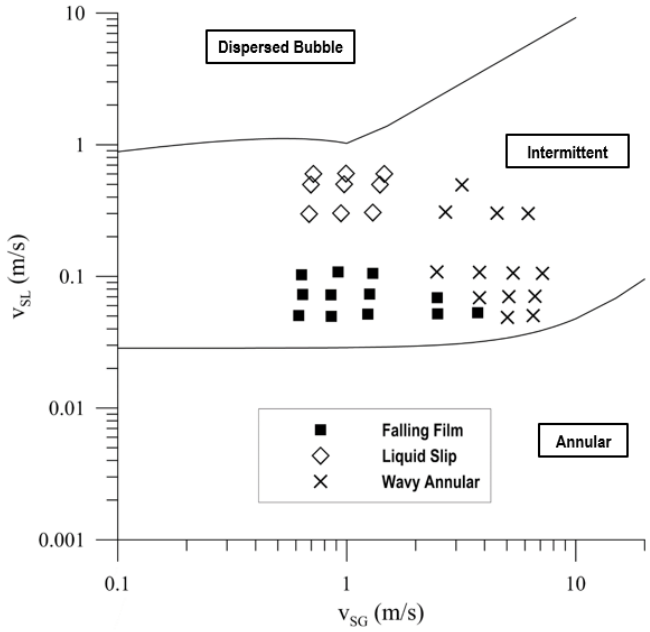

(a) Barnea's model (1987)

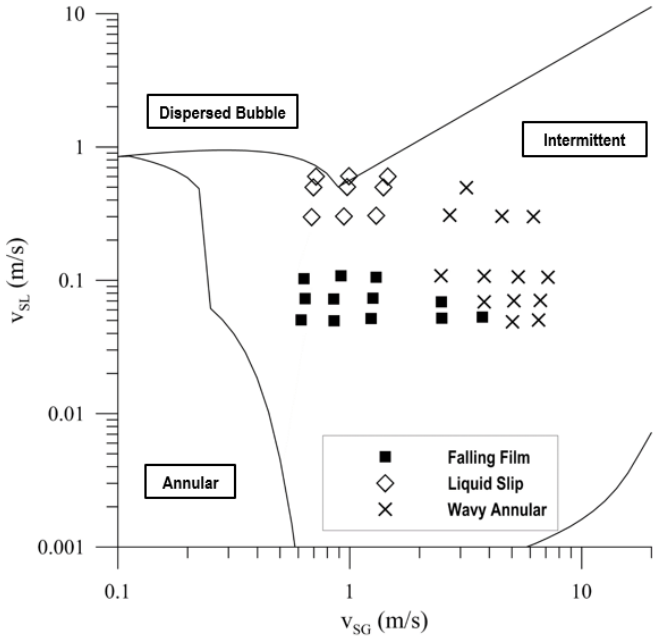

(b) TUFFP Unified (2011) model

Figure 5.2 Flow pattern map compared with observed flow patterns for μ_{oil} = 401 mPa·s

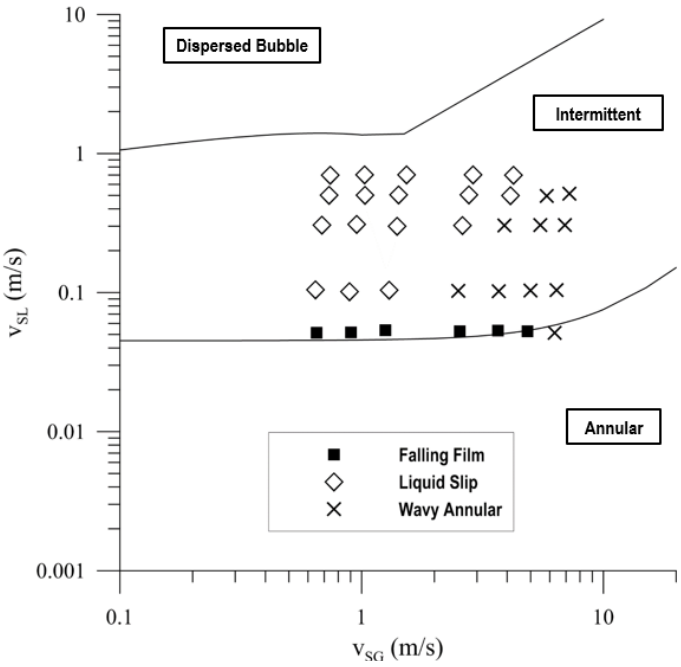

(a) Barnea's model (1987)

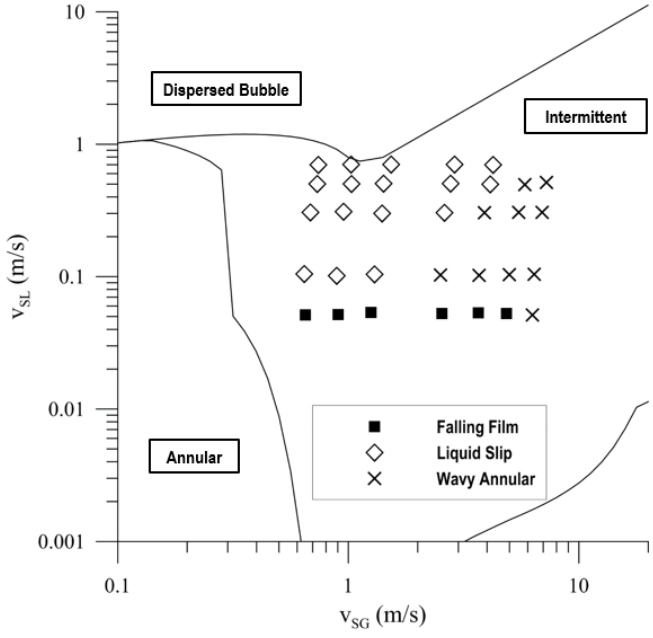

(b) TUFFP Unified (2011) model

Figure 5.3 Flow pattern map compared with observed flow patterns for μ_{oil} = 213 mPa·s

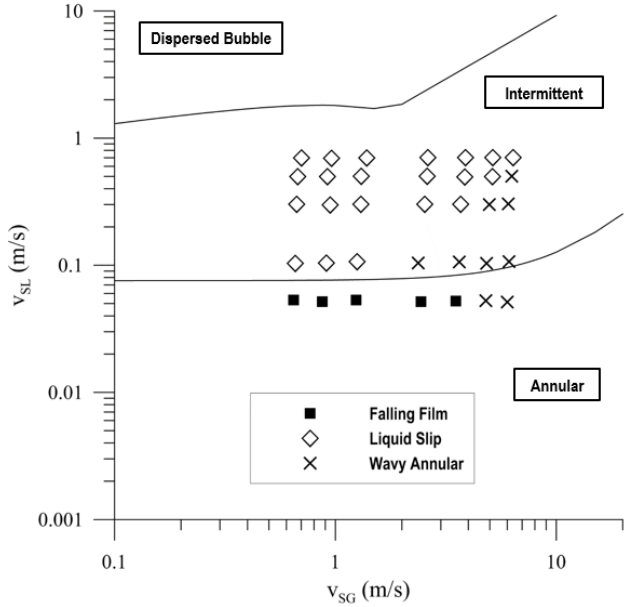

(a) Barnea's model (1987)

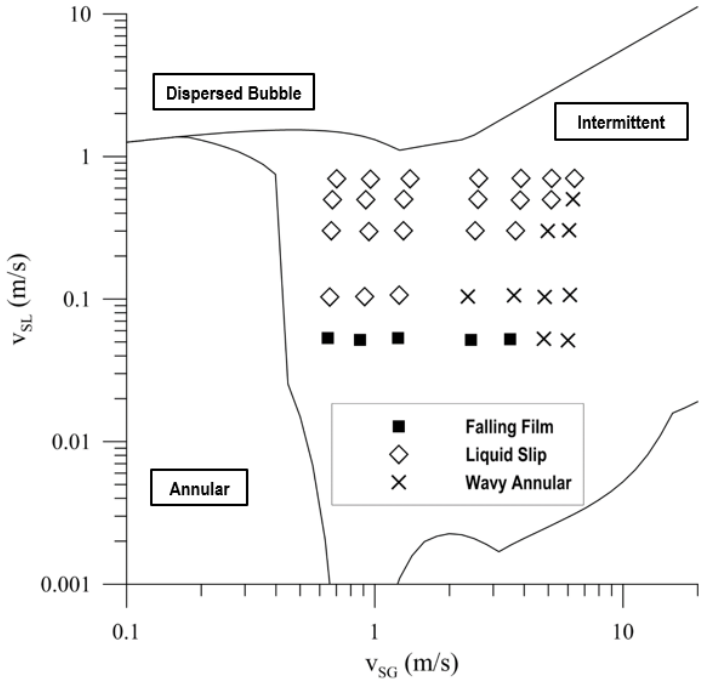

(b) TUFFP Unified (2011) model

Figure 5.4 Flow pattern map compared with observed flow patterns for μ_{oil} = 127 mPa·s

5.1.2 Pressure Gradient

Three models are compared against the experimental data for pressure gradient; TUFFP Unified (2011), OLGA version 7.2.3 steady-state model (OLGAS), and the annular model suggested by Alves et al. (1991). The correlations of Al-Sarkhi et al. (2011) and Wallis (1969) are used for liquid droplet entrainment fraction and interfacial friction factor, respectively. Figure 5.5 through Figure 5.8 show the comparison between the measured pressure gradient and the pressure gradient prediction of TUFFP (2011), OLGAS, and Alves's model.

When μ_{oil} = 586 mPa·s, Alves's annular model shows better prediction performance than others, especially for wavy annular flow. For other viscosity conditions, OLGA model shows better prediction performance than others, except it underestimates pressure gradients at μ_{oil} = 586 mPa·s. TUFFP model shows a tendency of overestimation over all viscosity conditions especially when the flow pattern is Falling Film or Liquid Slip. Alves model cannot predict negative pressure gradient over the all viscosities regardless flow patterns. Models show a tendency of over-prediction for all ranges of viscosity. Over-prediction of pressure gradients becomes severe for lower oil viscosities.

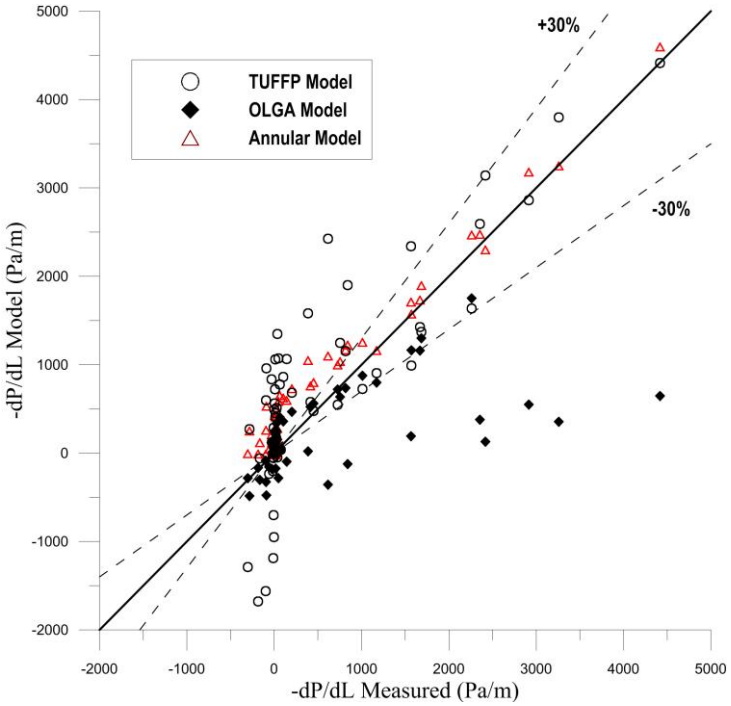

(a) Model prediction of pressure gradient

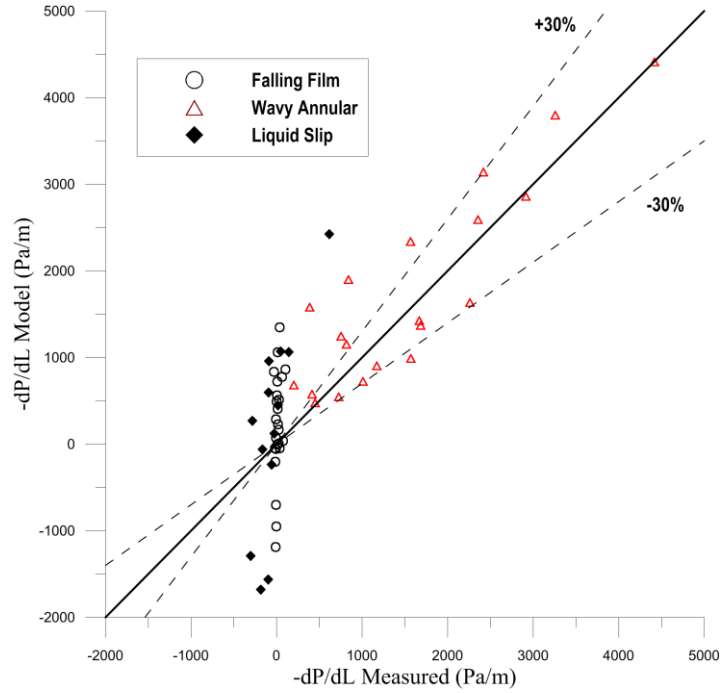

(b) TUFFP Unified (2011) model prediction marked with flow pattern

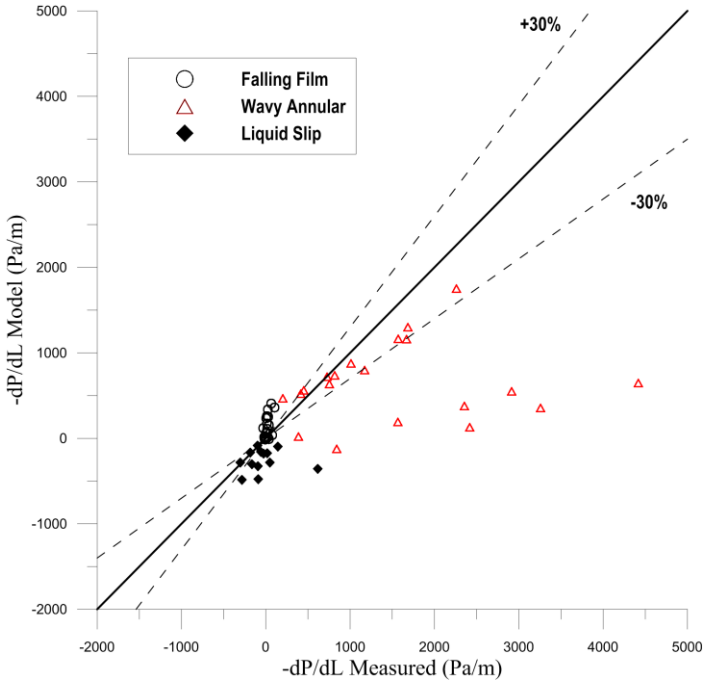

(c) OLGA model prediction marked with flow pattern

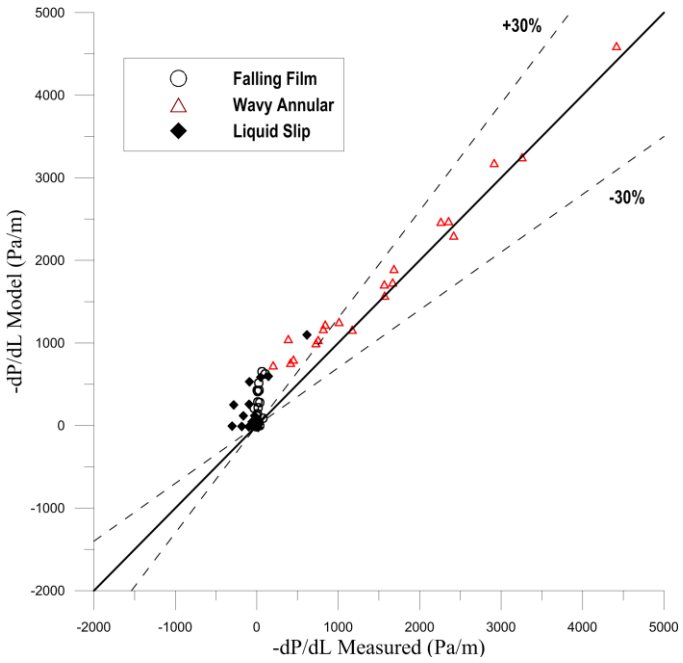

(d) Alves et al. (1991) model prediction marked with flow pattern

Figure 5.5 Pressure gradient prediction compared with measured data for μ_{oil} = 586 mPa·s

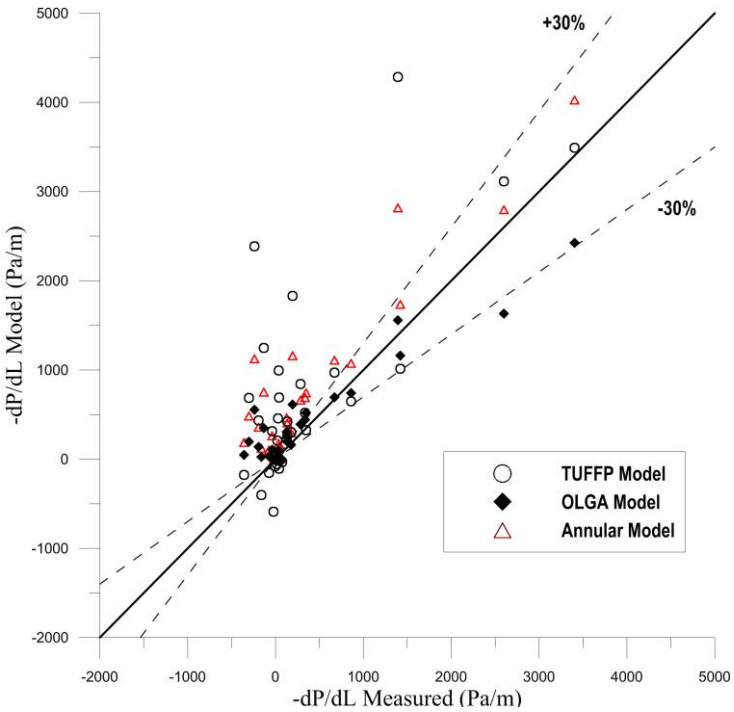

(a) Model prediction of pressure gradient

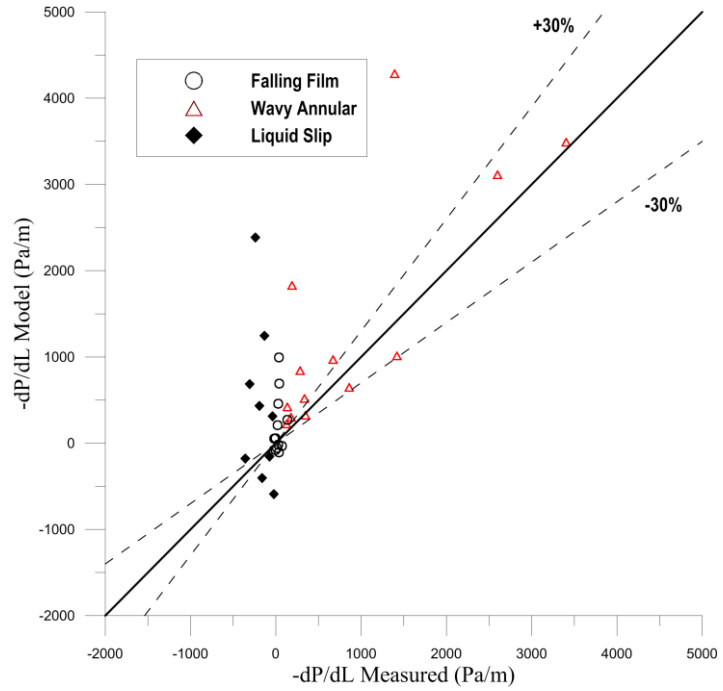

(b) TUFFP Unified (2011) model prediction marked with flow pattern

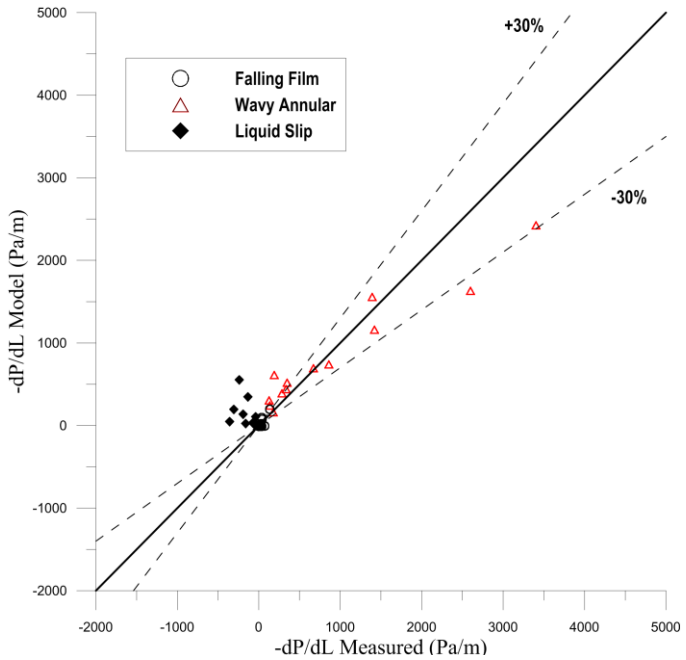

(c) OLGA model prediction marked with flow pattern

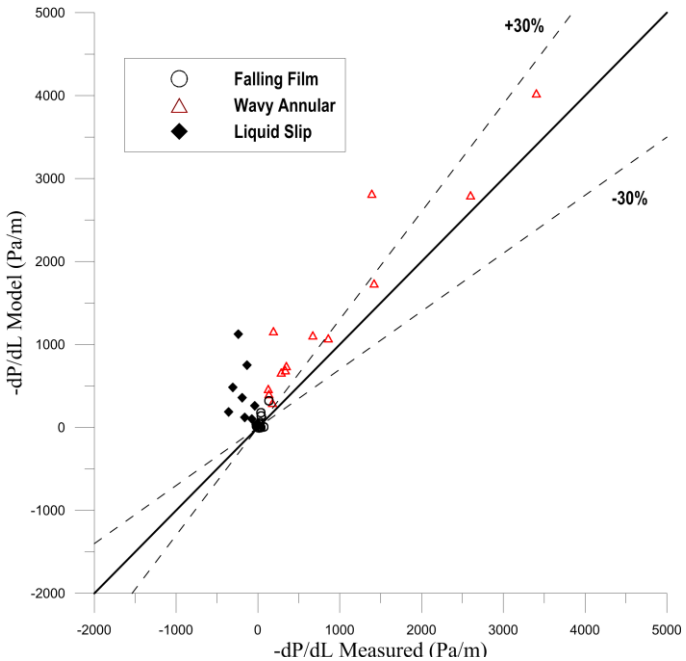

(d) Alves et al. (1991) model prediction marked with flow pattern

Figure 5.6 Pressure gradient prediction compared with measured data for μ_{oil} = 401 mPa·s

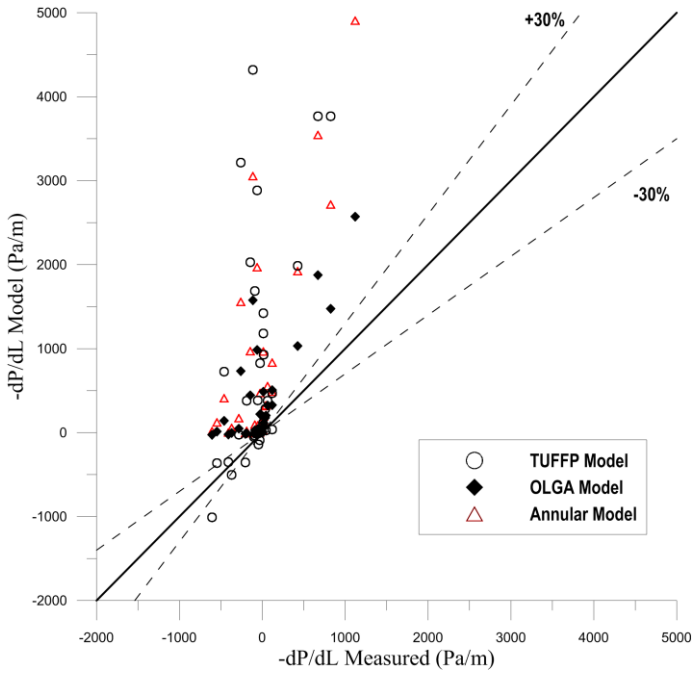

(a) Model prediction of pressure gradient

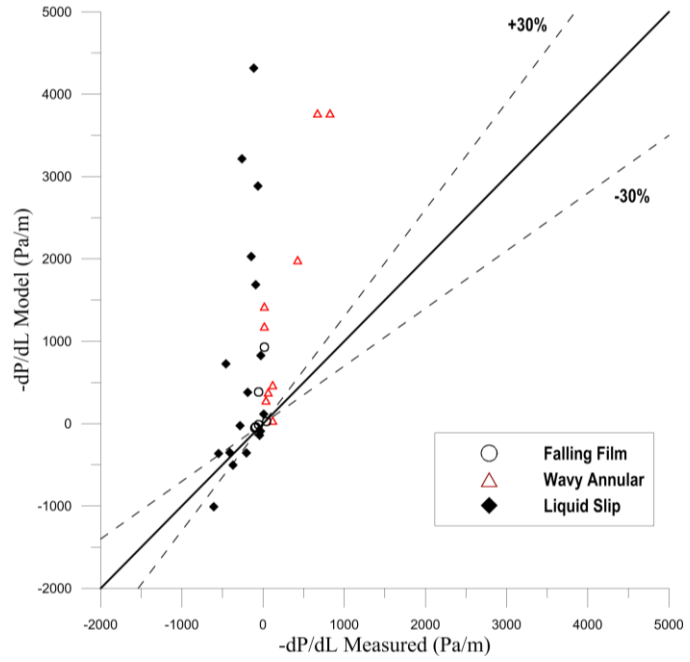

(b) TUFFP Unified (2011) model prediction marked with flow pattern

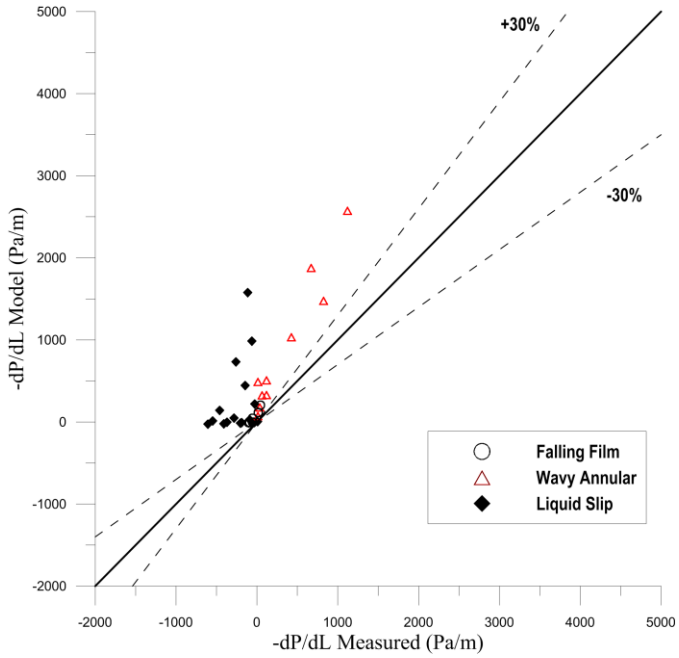

(c) OLGA model prediction marked with flow pattern

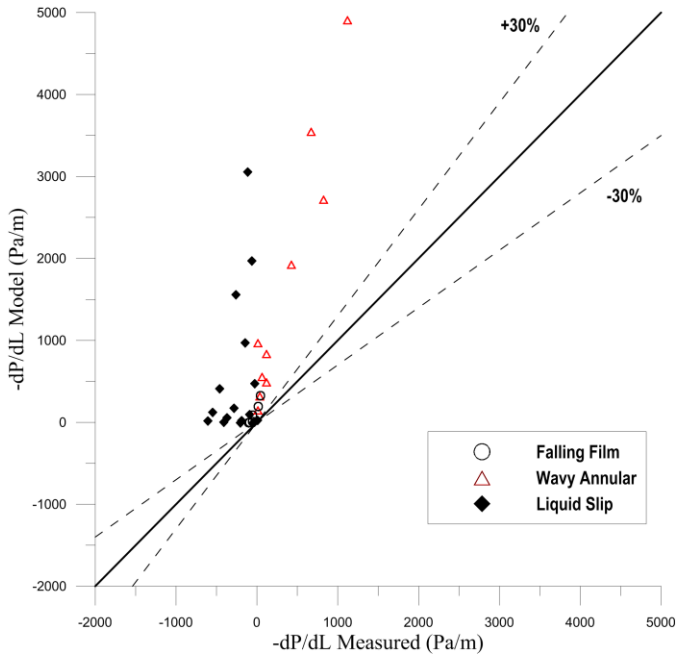

(d) Alves et al. (1991) model prediction marked with flow pattern

Figure 5.7 Pressure gradient prediction compared with measured data for μ_{oil} = 213 mPa·s

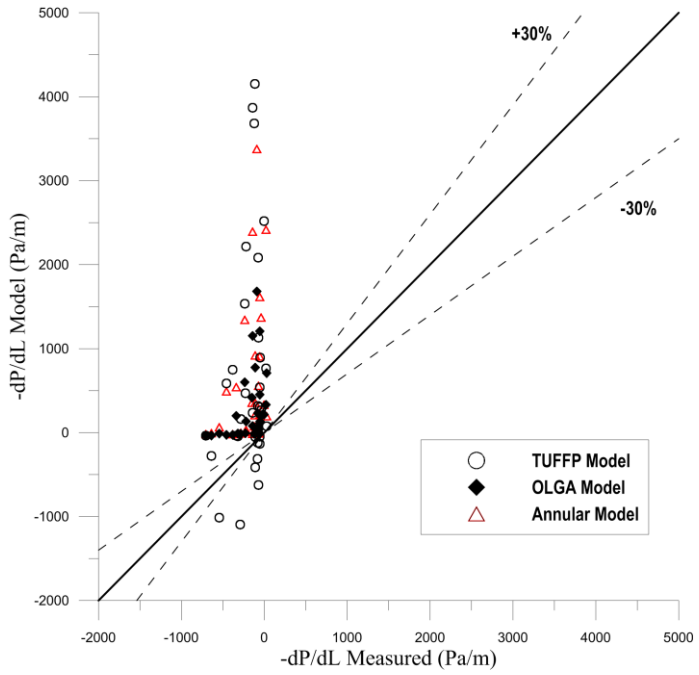

(a) Model prediction of pressure gradient

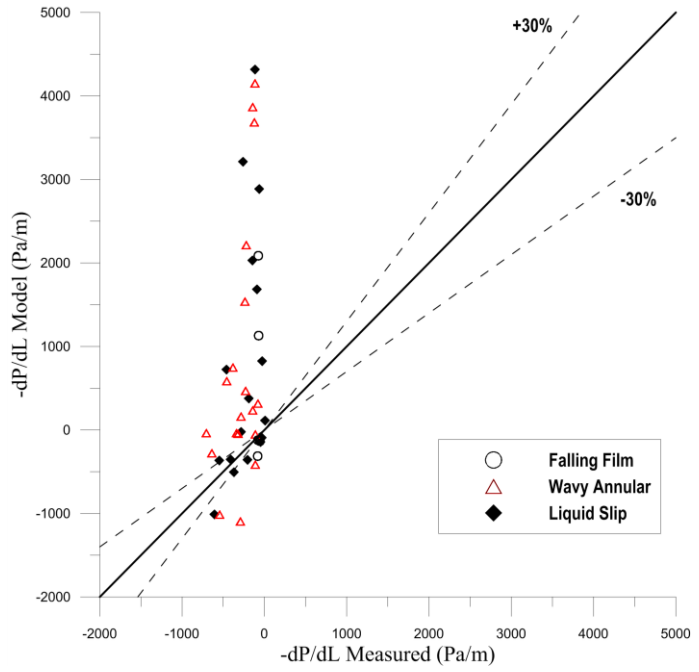

(b) TUFFP Unified (2011) model prediction marked with flow pattern

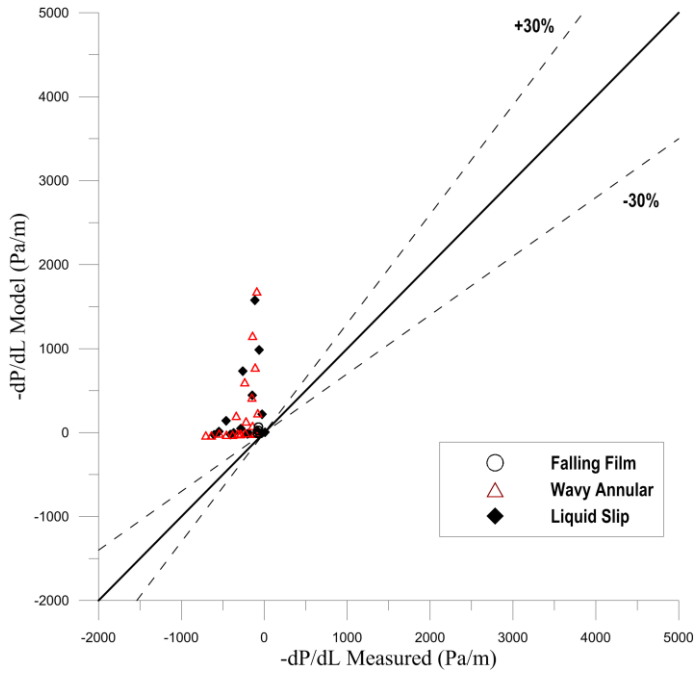

(c) OLGA model prediction marked with flow pattern

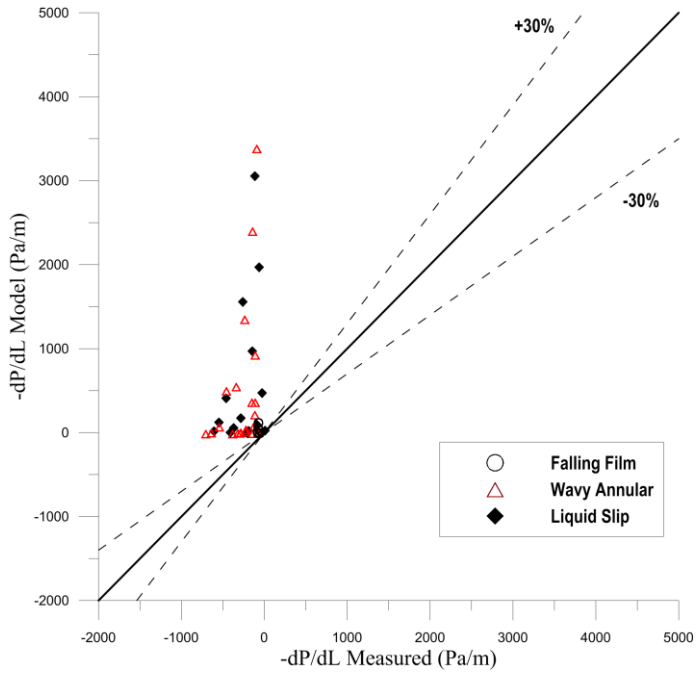

(d) Alves et al. (1991) model prediction marked with flow pattern

Figure 5.8 Pressure gradient prediction compared with measured data for μ_{oil} = 127 mPa·s

5.1.3 Average Liquid Holdup

Three models are compared against the experimental data for average liquid holdup; TUFFP Unified (2011), OLGA version 7.2.3 steady-state model (OLGAS), and the annular model suggested by Alves et al. (1991). The correlations of Al-Sarkhi et al. (2011) and Wallis (1969) are used for liquid droplet entrainment fraction and interfacial friction factor, respectively. Figure 5.9 through Figure 5.12 show the comparison between the measured average liquid holdup and the average liquid holdup prediction of TUFFP (2011), OLGAS, and Alves's model.

Liquid holdups are overestimated, especially for the liquid slip flow pattern. As Al-Sarkhi's (2011) liquid entrainment model was developed based on upward flow of low viscosity liquid, it underestimates the amount of liquid entrainment into the gas core. Actual average liquid holdup is much lower for liquid slip flow because liquid drops in the gas core flow very fast. As liquid viscosity decreases, roll waves on the liquid film surface transport liquid faster for all flow patterns, resulting in lower liquid holdup values without heavy liquid droplet entrainment.

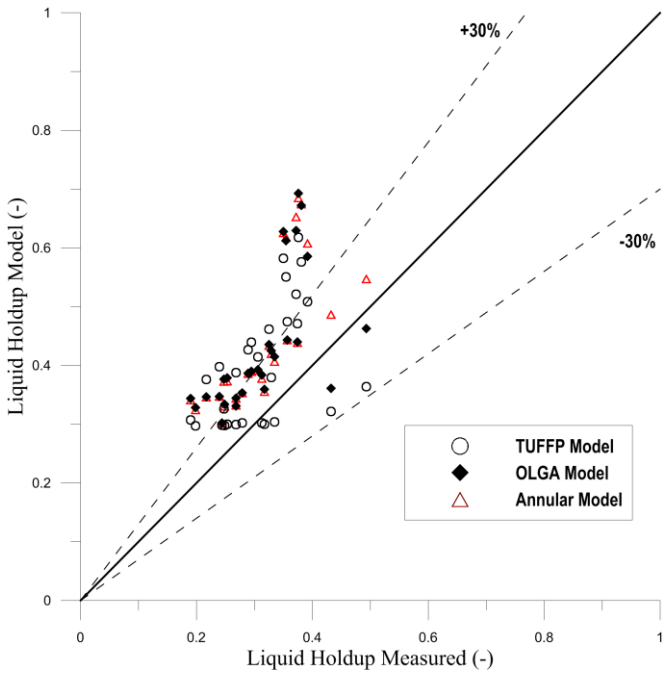

(a) Model prediction of average liquid holdup

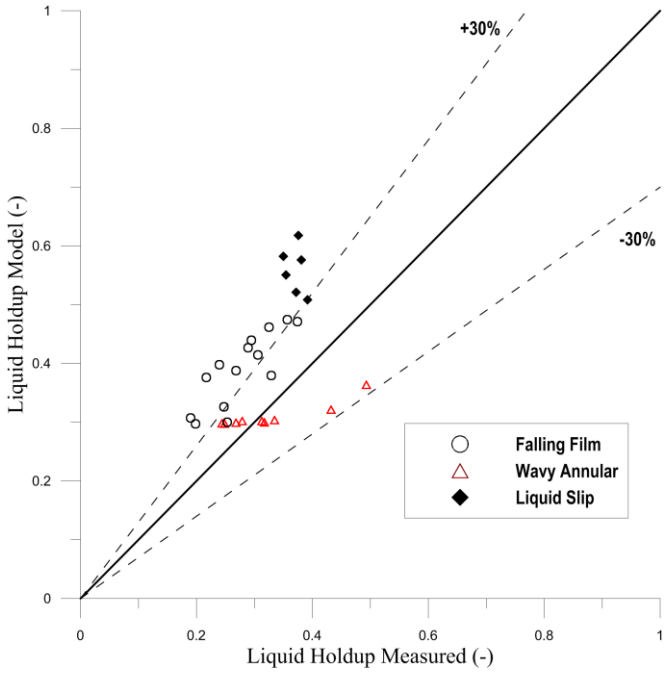

(b) TUFFP Unified (2011) model prediction marked with flow pattern

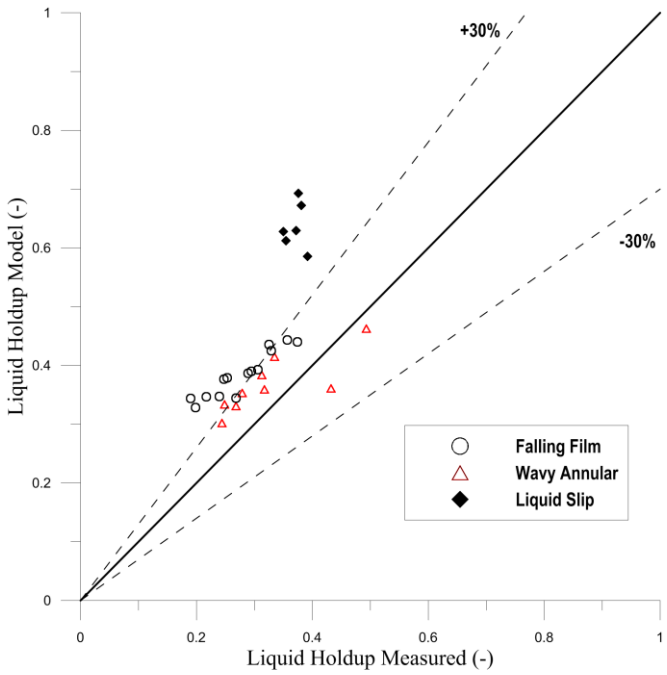

(c) OLGA model prediction marked with flow pattern

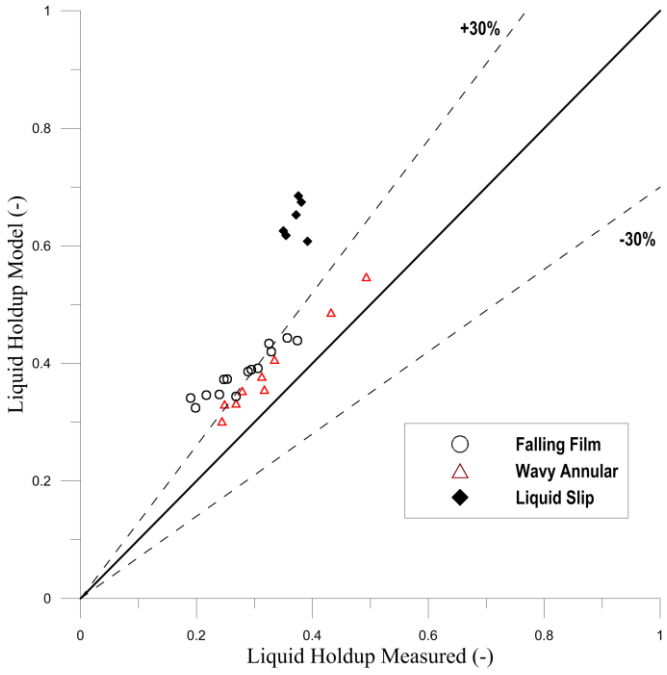

(d) Alves et al. (1991) model prediction marked with flow pattern

Figure 5.9 Average liquid holdup prediction compared with measured data for μ_{oil} = 586 mPa·s

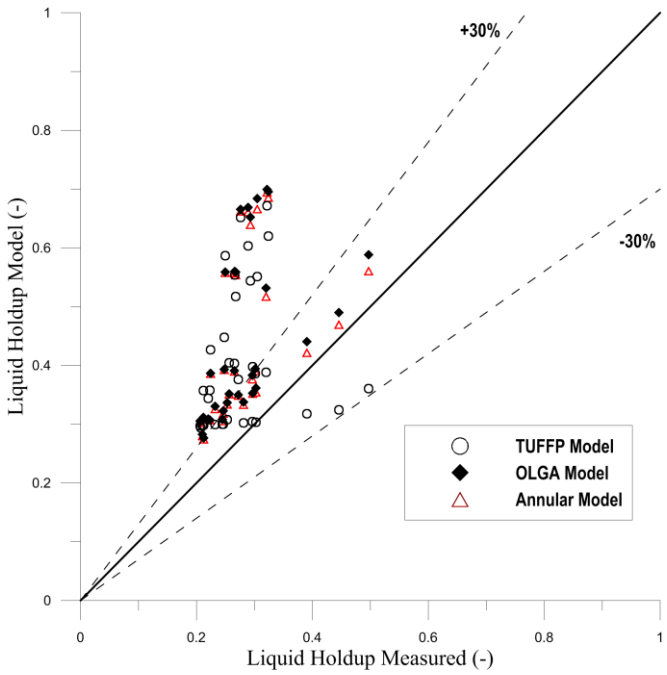

(a) Model prediction of average liquid holdup

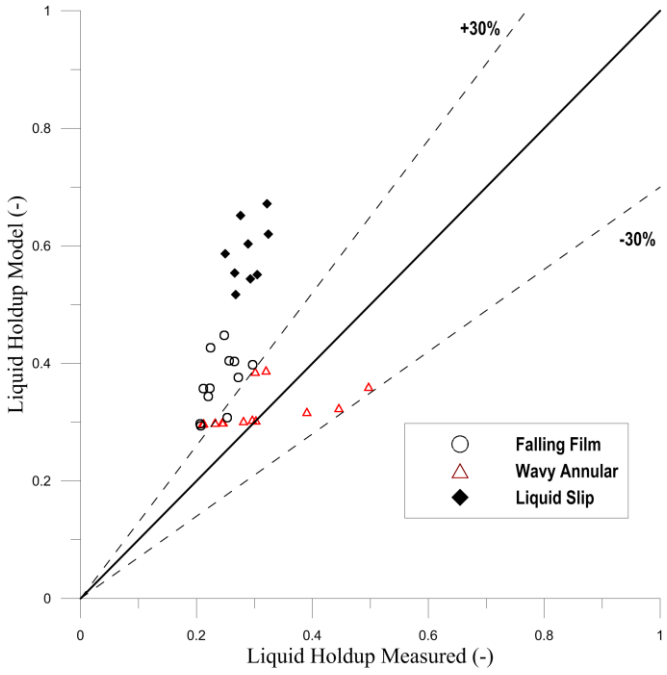

(b) TUFFP Unified (2011) model prediction marked with flow pattern

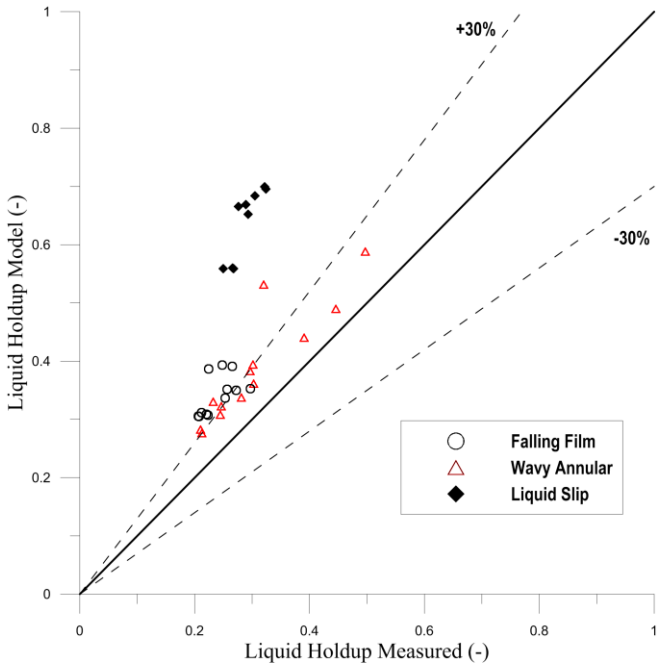

(c) OLGA model prediction marked with flow pattern

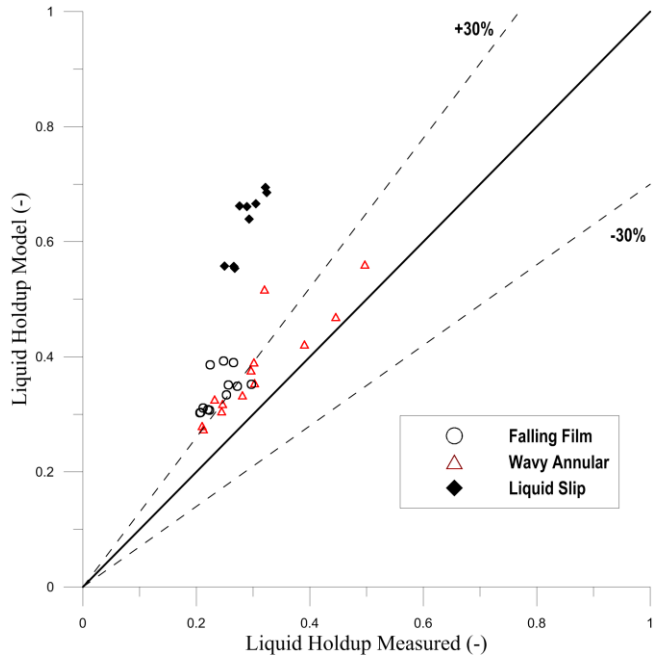

(d) Alves et al. (1991) model prediction marked with flow pattern

Figure 5.10 Average liquid holdup prediction compared with measured data for μ_{oil} = 401 mPa·s

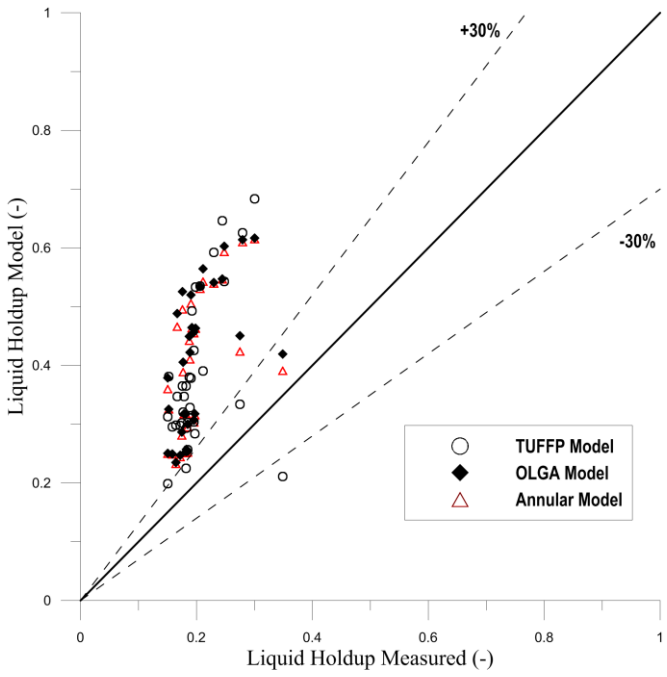

(a) Model prediction of average liquid holdup

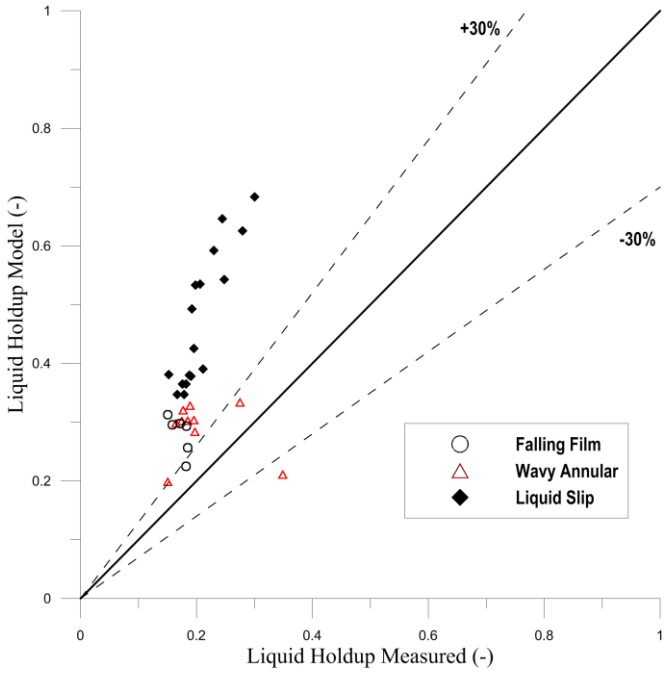

(b) TUFFP Unified (2011) model prediction marked with flow pattern

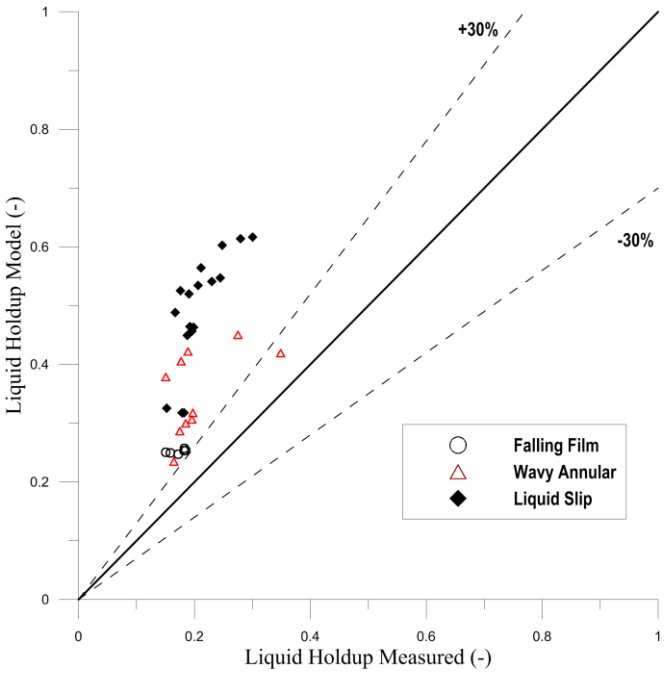

(c) OLGA model prediction marked with flow pattern

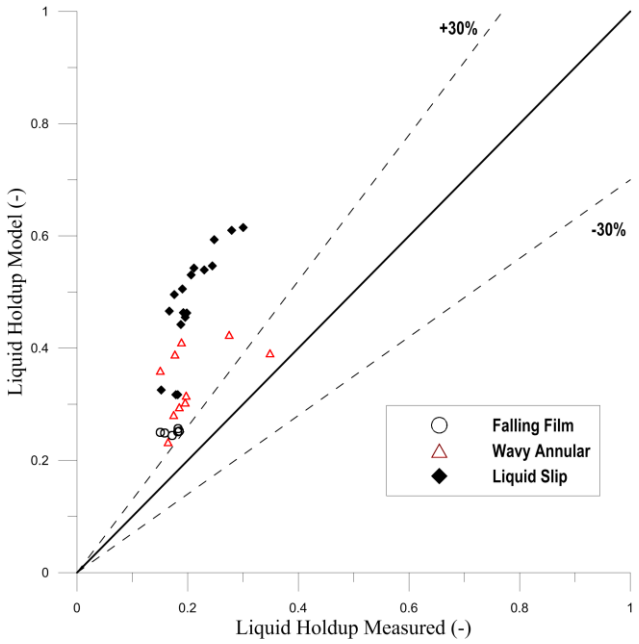

(d) Alves et al. (1991) model prediction marked with flow pattern

Figure 5.11 Average liquid holdup prediction compared with measured data for μ_{oil} = 213 mPa·s

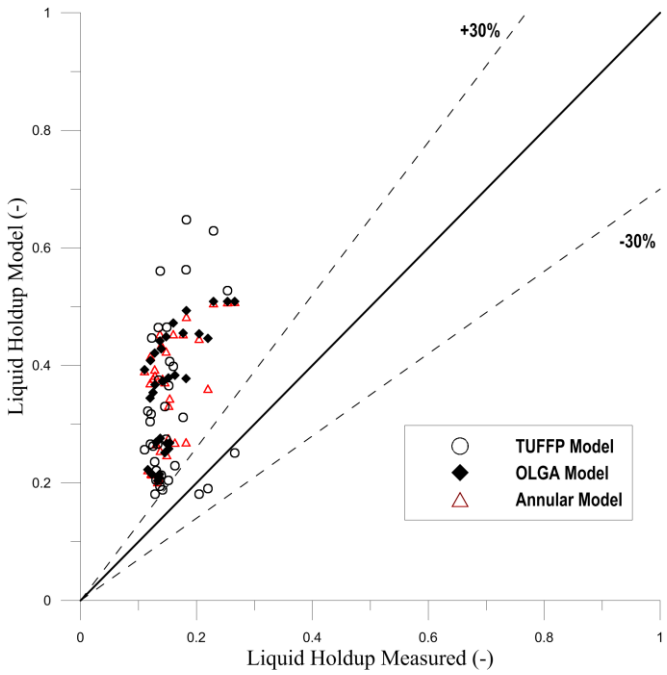

(a) Model prediction of average liquid holdup

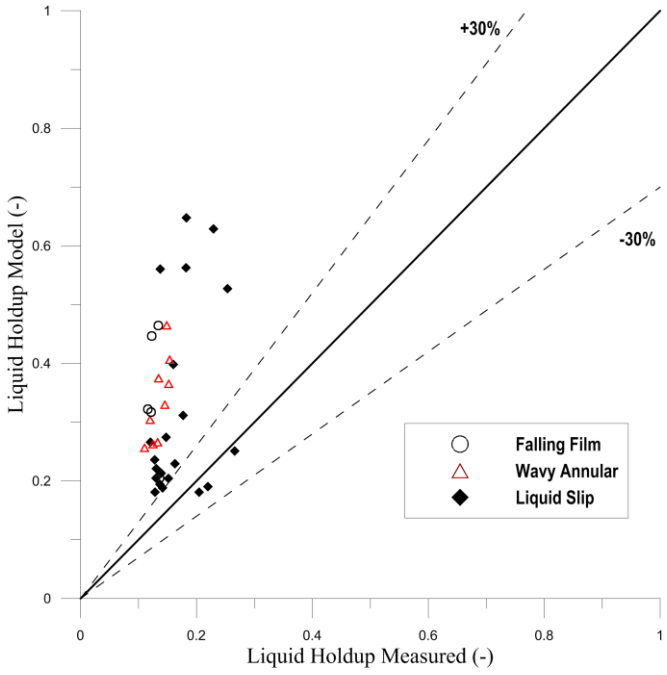

(b) TUFFP Unified (2011) model prediction marked with flow pattern

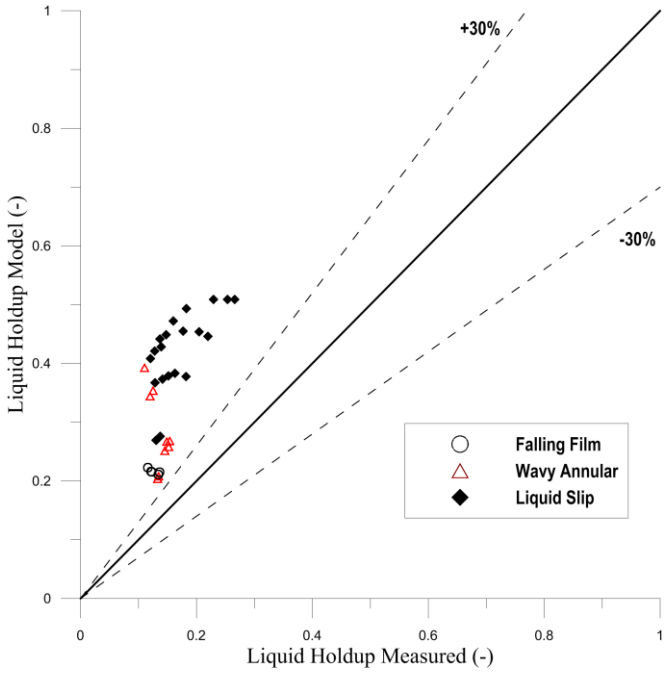

(c) OLGA model prediction marked with flow pattern

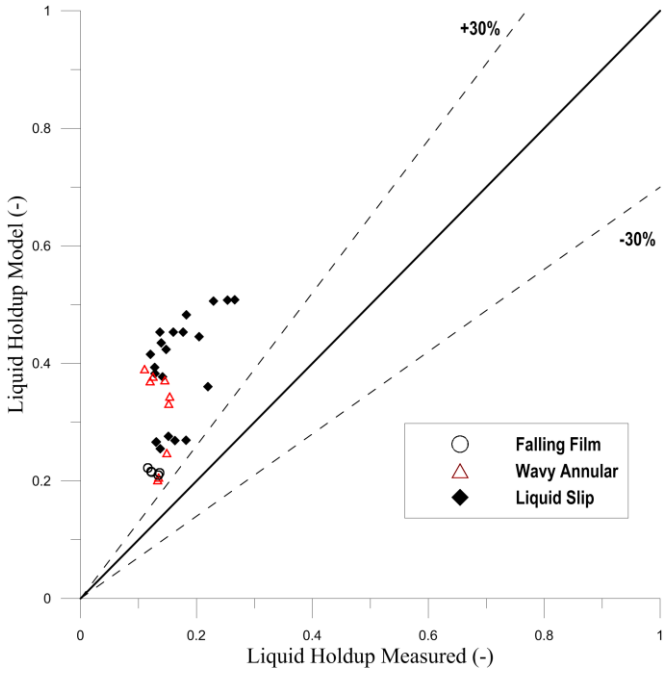

(d) Alves et al. (1991) model prediction marked with flow pattern

Figure 5.12 Average liquid holdup prediction compared with measured data for μ_{oil} = 127 mPa·s

5.2 Effect of Liquid Viscosity on Vertical Downward Flow

Mukherjee (1979) performed experimental study of inclined two-phase flow with low viscosity liquids including vertical downward flow. Kerosene and lube oil was used with the viscosity range of 1.0 ~ 2.5 mPa·s. Inner diameter of pipeline was 1.5 inch. Mukherjee's (1979) experimental data for low viscosity vertical downward flow are presented to discuss the effect of liquid viscosity on vertical downward flow.

The observed four flow patterns for vertical downward flow are, namely, stratified, annular mist, slug, and bubble flow. In his study, stratified (27 experimental points) and annular mist flow patterns (38 experimental points) correspond to Falling Film/liquid slip and wavy annular flow patterns, respectively. Stratified flow converted to annular mist flow as the superficial gas velocity increased (Figure 5.13).

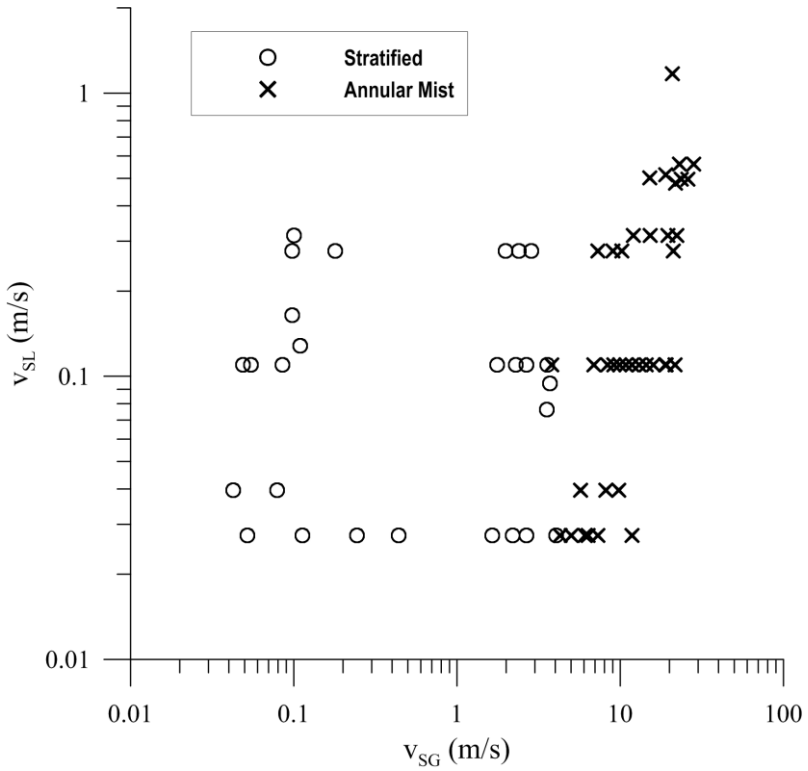

Figure 5.13 Observed flow pattern for vertical downward flow observed by Mukherjee (1979)

Figures 5.14 presents pressure gradient vs. superficial gas velocity from Mukherjee's study. Same as high viscosity case, pressure gradient sharply increase as the flow pattern changes from 'Stratified flow" to 'Annular Mist flow' with increase of gas velocity. As the flow pattern changes at higher v_{SG} comparing high viscosity case, the increase of pressure gradient occurs at higher v_{SG}.

Average liquid holdup is getting lower as superficial gas velocity increases. Rapid increase of liquid holdup was not observed as flow pattern changes from 'Stratified flow" to 'Annular Mist flow' due to low liquid viscosity (Figure 5.15).

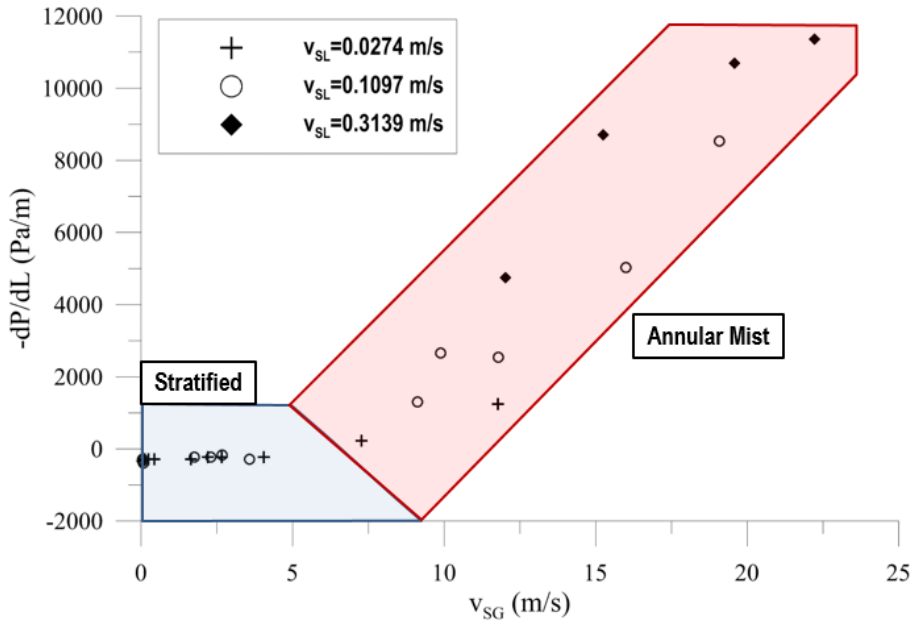

(a) μ_{oil} > 1.5 mPa·s

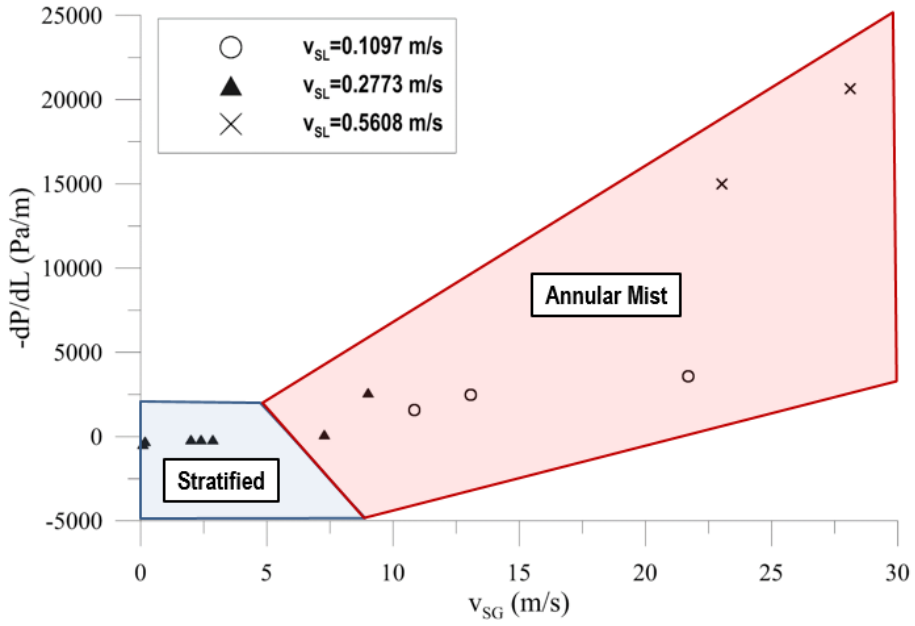

(b) μ_{oil} < 1.5 mPa·s

Figure 5.14 Pressure gradient vs. superficial gas velocity in Mukherjee's study

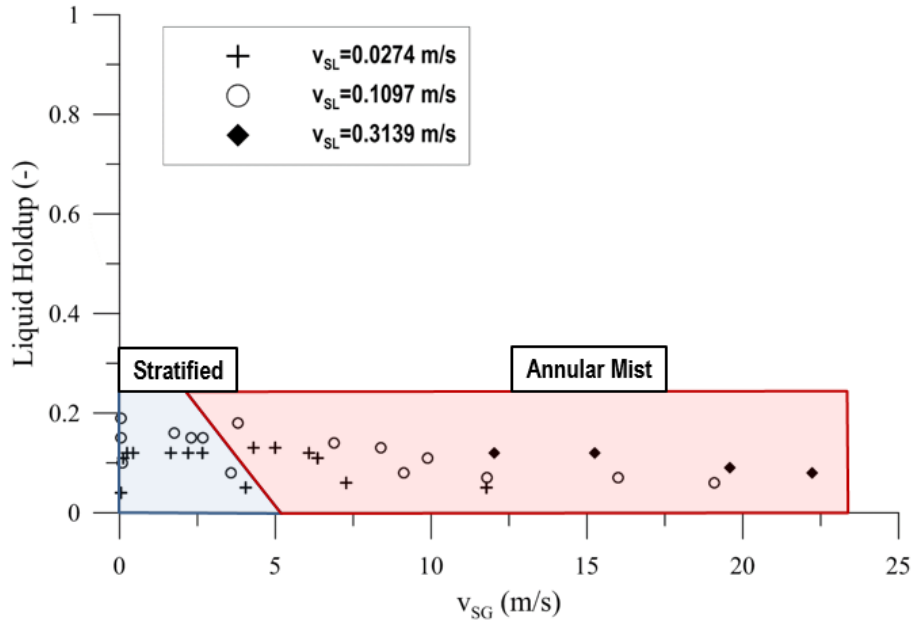

(a) μ_{oil} > 1.5 mPa·s

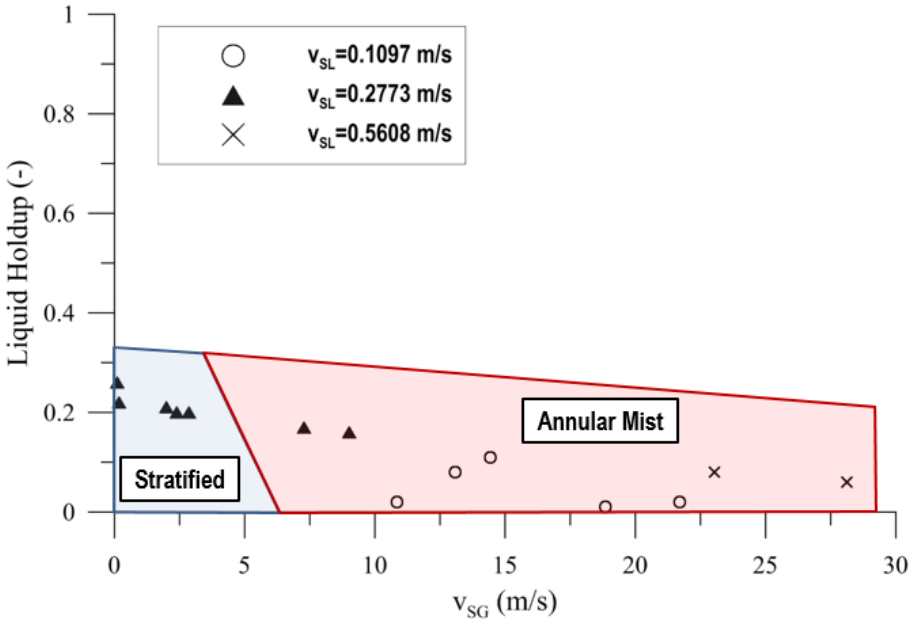

(b) μ_{oil} < 1.5 mPa·s

Figure 5.15 Liquid holdup vs. superficial gas velocity in Mukherjee's study

5.3 Closure Relationships for Annular Model

Two types of closure relationships are necessary in annular model; interfacial shear correlation and liquid entrainment fraction correlation. In section 5.1, Wallis (1969) and Al-sharkhi (2012)'s correlations are used. However, the prediction performance of model comparison results was dissatisfactory. In this section, performance of various closure relationships are examined for vertical annular flows. Two additional data was considered, Alruhaimani (2015) and Mukherjee (1979), to discuss the effects of flow direction and viscosity.

5.3.1 Liquid Entrainment Fraction Correlations

Two correlations were considered for liquid entrainment fraction correlation; Ishii & Mishima (1989) model and Al-Sarkhi's (2012) model. Ishii & Mishima (1989) is one of the common correlation for prediction of liquid entrainment in annular flow. It is based on a modified weber number defined as

$$We' = \frac{\rho_G v_G^2 d_F}{\sigma}\left(\frac{\rho_L - \rho_G}{\rho_G}\right)^{1/3} \tag{5-1}$$

where d_F is the hydraulic diameter of liquid film. Entrainment fraction can be

calculated from

$$f_E = \tanh\left[7.25 \times 10^{-7}(We')^{1.25} Re_F^{0.25}\right] \tag{5-2}$$

where Re_F is the liquid film Reynolds number.

Al-Sarkhi's (2012) model is modified from the model of Sawant et al. (2008). Entrainment fraction can be calculated as below:

$$f_E = f_{E,max}[1 - exp(-We_{SG}/We_{SG}^*)]$$

$$We_{SG} = \frac{\rho_G v_{SG}^2 D}{\sigma}\left(\frac{\rho_L - \rho_G}{\rho_G}\right)^{\frac{1}{4}},\ \alpha = 0.000231\ Re_{SL}^{-0.358} \tag{5-3}$$

$$We_{SG}^* = \left(\frac{f_{E,max}}{\alpha}\right)^{0.925},\ f_{E,max} = \left[1 - exp\left(-\left(\frac{Re_{SL}}{1400}\right)\right)^{0.6}\right]$$

5.3.2 Interfacial shear correlations

Three correlations were considered for liquid entrainment fraction correlation; Al-Sarkhi (2013), Whallet & Hewitt (1978), and Henstock & Hanratty (1976). Interfacial shear correlations can be expressed as equation (5-4)

$$I = \frac{f_I}{f_{SC}} \tag{5-4}$$

and each model calculates f_I. Liquid entrainment fraction correlations which are considered here are as below:

Al-Sarkhi (2013):

$$I = 1 + C\frac{\delta_L}{d} \tag{5-5}$$

C=750 (annular flow), 1270 (wavy annular), 21000 (slug and churn)

Whallet & Hewitt (1978):

$$I = 1 + 24\left(\frac{\rho_L}{\rho_G}\right)^{1/3}\left(\frac{\delta_L}{d}\right) \tag{5-6}$$

Henstock & Hanratty (1976):

$$I = 1 + 1{,}400F\left\{1 - exp\left[-\frac{(1 + 1{,}400F)^{1.5}}{13.2FG}\right]\right\} \tag{5-7}$$

$$F = \frac{(0.42Re_F^{1.25} + 2.8 \times 10^{-4}Re_F^{2.25})^{0.4}}{Re_{SG}^{0.9}}\frac{\mu_L}{\mu_G}\left(\frac{\rho_G}{\rho_L}\right)^{0.5}$$

$$G = \frac{\rho_L dg}{\rho_G v_{SG}^2 f_{SG}}$$

Al-Sarkhi's (2013) model is modified from the model of Wallis(1969). If C=300, it becomes Wallis's (1969) correlation.

5.3.3 Comparison with vertical upward annular flow experiment

For Alruhaimani's (2015) experimental data, vertical upward annular flow for

high viscosity oil, liquid holdup and pressure gradient prediction performances are presented in Figure 5.16 and Figure 5.17. As the liquid entrainment fraction is less than 1% due to the high viscosity, type of liquid entrainment correlations are not critical for average liquid holdup prediction. However type of interfacial shear correlation has an effect as it determines pressure gradient of fluid. Al-Sarkhi's correlation and Henstock & Hanratty's correlation show acceptable prediction performance.

However for vertical downward flow, liquid holdup is overestimated especially for Liquid Slip flow pattern. As we visually observed in the experiment, liquid entrainment fraction is much higher comparing vertical upward cases. Consequently, annular model shows disappointing prediction performances of pressure gradient and average liquid holdup.

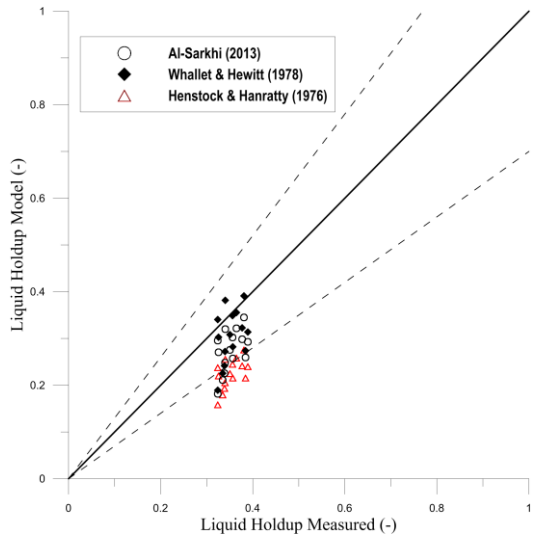

(a) Ishii & Mishima (1989)

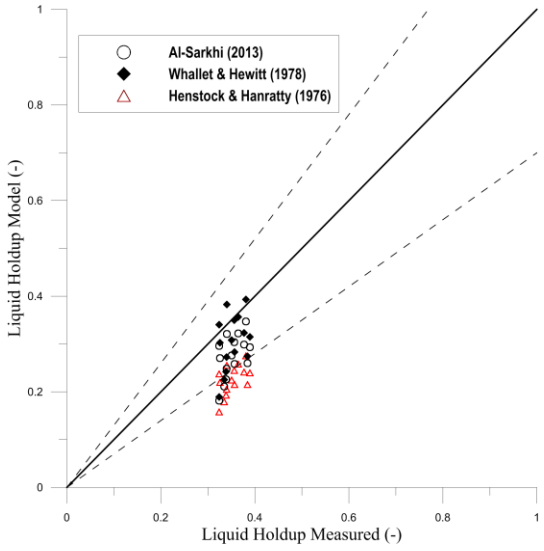

(b) Al-Sarkhi's (2011)

Figure 5.16 Average liquid holdup prediction for Alruhaimani's (2015) vertical upward annular flow

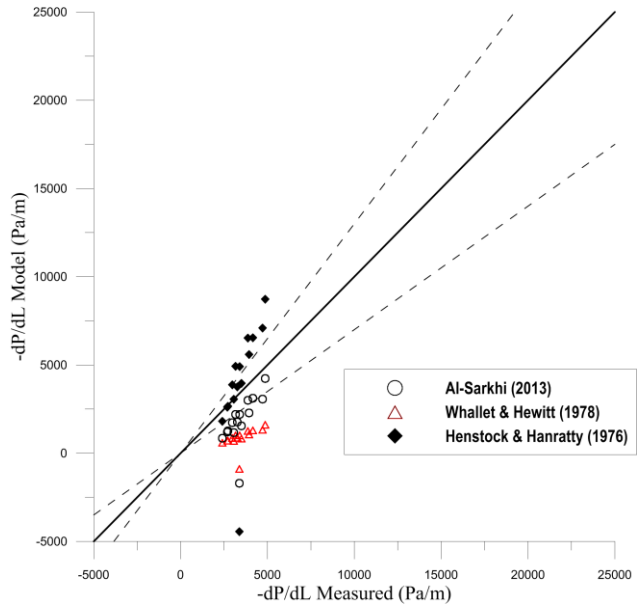

(a) Ishii & Mishima (1989)

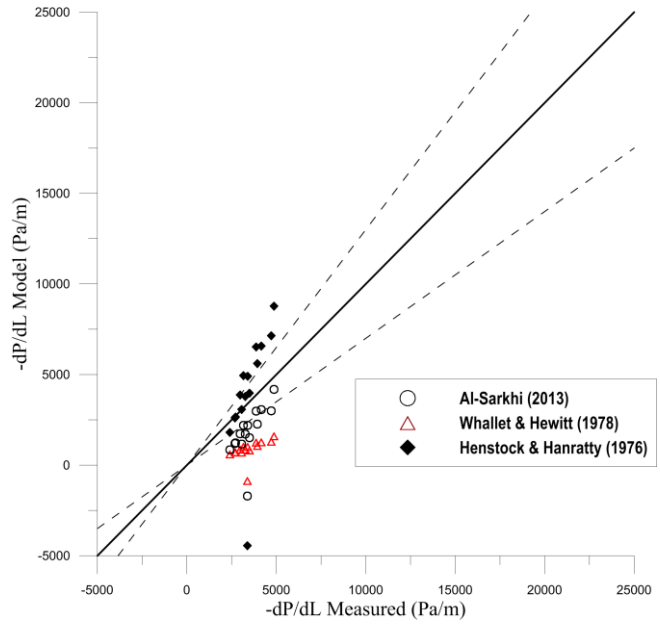

(b) Al-Sarkhi's (2011)

Figure 5.17 Pressure gradient prediction for Alruhaimani's (2015) vertical upward annular flow

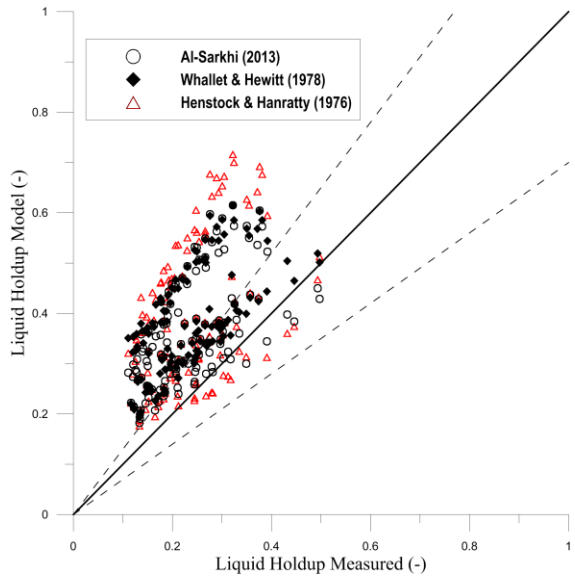

(a) Ishii & Mishima (1989)

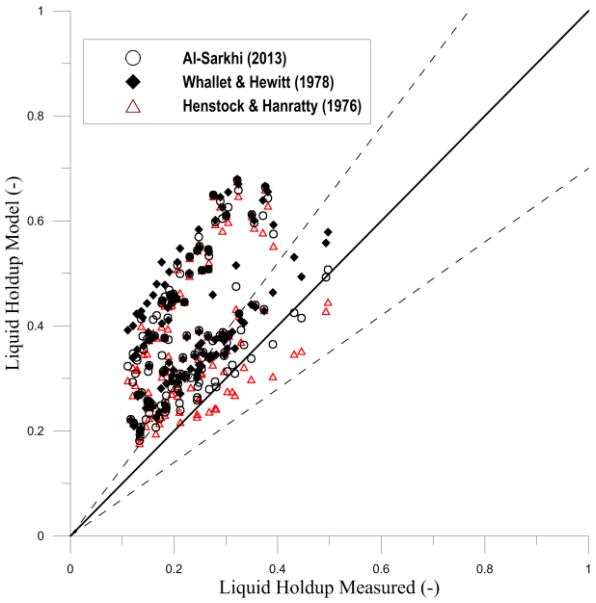

(b) Al-Sarkhi's (2011)

Figure 5.18 Average liquid holdup prediction for vertical downward annular flow

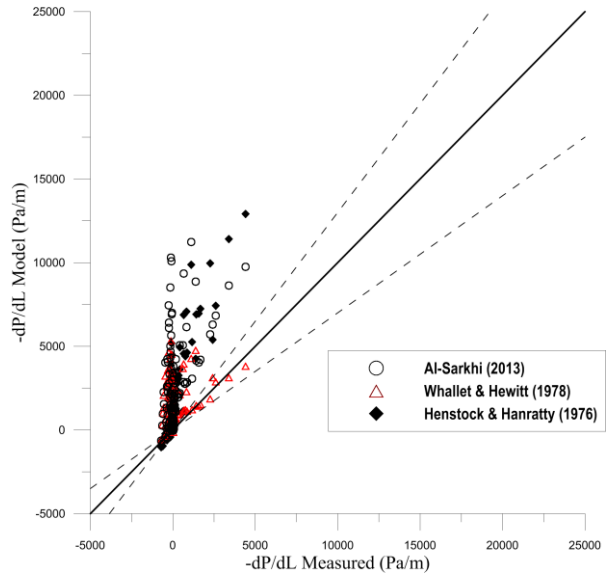

(a) Ishii & Mishima (1989)

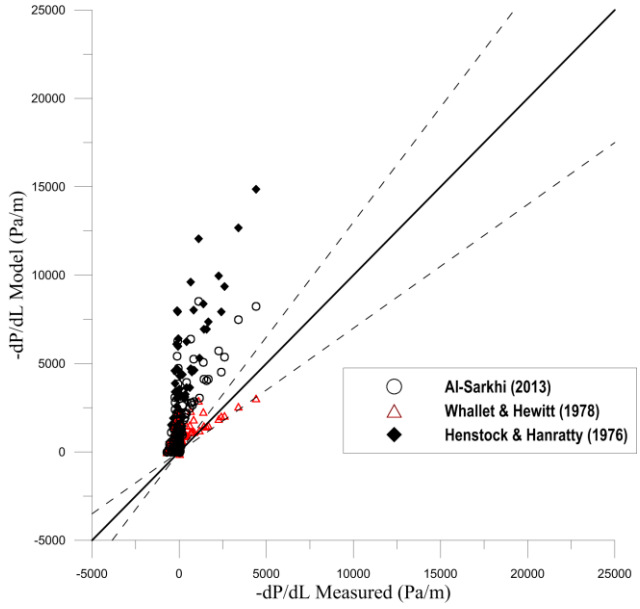

(b) Al-Sarkhi's (2011)

Figure 5.19 Pressure gradient prediction for vertical downward annular flow

Chapter 6 Conclusions and Future Works

6.1 Conclusions

Based on the experimental investigation and model evaluation conducted in this study, the following conclusions are reached:

(1) This study confirmed three different flow regime based on the Probability Distribution Function (PDF) from capacitance sensor signals: Falling Film (FF), Wavy Annular (WA) and Liquid Slip (LS). Flow patterns can be distinguished by skewness and kurtosis of PDF. Considering the traditional flow pattern classification, all conditions can be categorized as annular flow.

(2) When both of gas and liquid have low flow rate, Falling Film flows are observed with the pressure gradients near zero. Liquid Slip flows have negative pressure gradients and are observed in low gas and high liquid flow rate conditions. When gas flow rate increases, flow pattern changes to Wavy Annular flow and pressure gradient sharply increases due to the high shear forces.

(3) Between Falling Film and Wavy Annular flow patterns, average liquid holdup shows no significant differences. Average liquid

holdup suddenly increases as the flow pattern changes from Liquid Slip to wavy annular for high viscosities above 127 mPa·s.

(4) As the liquid viscosity increases, Liquid Slip flow patterns are observed in narrower range. Transition from Wavy Annular to Liquid Slip occurs at lower gas velocity. For higher oil viscosity condition, pressure gradient increases more sharply. And liquid droplet becomes hard to be entrained into the gas core, resulting higher average liquid holdup after flow pattern is changed from Liquid Slip to Wavy Annular.

(5) With high viscosity liquids, existing mechanistic model for annular flow shows poor performance for downward flow while vertical upward flow shows acceptable prediction performance. It comes from miscalculation of liquid droplet entrainment fraction. For vertical downward flow, different type of liquid entrainment correlation should be suggested, as the entrainment mechanism is quite different from upward annular flow.

6.2 Future Works

(1) Predicting thickness of liquid film is highly important as it could affect in determining the portion of liquid entrained into the gas core. There are some studies (Zhang et al, 2000; Mendoza, 2011) which investigate the characteristic of liquid film in vertical or deviated downward flow. The modified closure relationship for liquid film can be suggested.

(2) As aforementioned, closure relationship should about liquid entrainment can lead mispredicting of average liquid holdup. Also the measurement of liquid droplet velocity might lead to prediction of liquid holdup portion occupied by entrained liquid droplet.

(3) Using Computational Fluid Dynamics (CFD) software to simulate high viscosity liquid-gas two-phase flow in vertical pipes is highly recommended to study the effect of high viscosity on two-phase flow behavior.

References

Akhiyarov, D.T., Zhang, H.-Q., and Sarica, C. 2010. High-Viscosity Oil-gas Flow in Vertical Pipe. *Presented at Offshore Technology Conference*, Houston, TX, 3-6 May.

Al-Sarkhi, A., Sarica, C., and Qureshi, B. 2012. Modeling of Droplet Entrainment in Co-current Annular Two-phase Flow: A New Approach. *International Journal of Multiphase Flow* **39** (1): 21-28. http://dx.doi.org/10.1016/j.ijmultiphaseflow.2011.10.008

Alves, I.N., Cartano, E.F., Minami, K., and Shoham, O. 1991. Modeling Annular Flow Behavior for Gas Wells. *SPE Production Engineering* **6** (4): 435-440. SPE-20384-PA. http://dx.doi.org/10.2118/20384-PA

Barnea, D., Shoham, O., and Taitel, Y. 1982. Flow Pattern Transition for Vertical Downward Two Phase Flow. *Chemical Engineering Science* **37** (5): 741-744. http://dx.doi.org/10.1016/0009-2509(82)85034-3

Barnea, D. 1987. A Unified Model for Predicting Flow-pattern Transitions for the Whole Range of Pipe Inclinations. *International Journal of Multiphase Flow* **13** (1): 1-12. http://dx.doi.org/10.1016/0301-9322(87)90002-4

Bhagwat, S.M. and Ghajar, A.J. 2011. Flow Patterns and Void Fraction in Downward Two Phase Flow. *Paper presented at ASME Early Career Technical Conference*, Fayetteville, AR, 31 March-2 April.

Bhagwat, S. M. and Ghajar, A. J. 2012. Similarities and Differences in the Flow Patterns and Void Fraction in Vertical Upward and Downward Two Phase Flow. *Experimental Thermal and Fluid Science* **39**: 213-227. http://dx.doi.org/10.1016/j.expthermflusci.2012.01.026

Brito, R. 2012. *Effect of Medium Oil Viscosity on Two-phase Oil-gas Flow Behavior in Horizontal Pipes*. MS Thesis, University of Tulsa, Tulsa, OK.

Colmenares, J., Ortega, P., Padrino, J., and Trallero, J.L. 2001. Slug Flow Model for the Prediction of Pressure Drop for High Viscosity Oils in a Horizontal Pipeline. *Paper SPE 71111 presented at SPE International Thermal Operations and Heavy Oil Symposium*, Margarita Island, Venezuela, 12-14 March. http://dx.doi.org/10.2118/71111-MS

Dieck, R. 2007. *Measurement Uncertainty – Methods and Applications*, fourth edition. NC, USA: ISA.

Farsetti, S., Farisè, S., and Poesio, P. 2014. Experimental Investigation of

High Viscosity Oil–air Intermittent Flow. *Experimental Thermal and Fluid Science* **57**: 285-292. http://dx.doi.org/10.1016/j.expthermflusci.2013.12.004

Furukawa, T. and Fukano, T. 2001. Effects of Liquids Viscosity on Flow Pattern in Vertical Upward Gas-liquid Two-phase Flow. *International Journal of Multiphase Flow* **27**: 1109-1126. http://dx.doi.org/10.1016/S0301-9322(00)00066-5

Godbole, P.V., Tang, C.C., Ghajar, A.J. 2011. Comparison of Void Fraction Correlations for Different Flow Patterns in Upward Vertical Two Phase Flow. *Heat Transfer Engineering* **32** (10): 843–860. http://dx.doi.org/10.1080/01457632.2011.548285

Gokcal, B. 2008. *An Experimental and Theoretical Investigation of Slug Flow for High Oil Viscosity in Horizontal Pipes*. PhD Dissertation, University of Tulsa.

Gomez, L.E., Shoham, O., Schmidt, Z., Chokshi, R., Brown, A., and Northug, T. 2000. Unified mechanistic Model for Steady-State Two-Phase Flow: Horizontal to Vertical Upward Flow. *SPE Journal* **5** (3): 339-350. SPE-65705-PA. http://dx.doi.org/10.2118/65705-PA

Hibiki, T., Goda, H., Kim, S., Ishii, M., and Uhle, J. 2004. Structure of

Vertical Downward Bubbly Flow. *International Journal of Heat and Mass Transfer* **47** (8): 1847-1862. http://dx.doi.org/10.1016/j.ijheatmasstransfer.2003.10.027

Ishii, M. and Mishima, K. 1989. Droplet Entrainment Correlation in Annular Two-Phase Flow. *International Journal of Heat and Mass Transfer* **32** (10): 1835. http://dx.doi.org/10.1016/0017-9310(89)90155-5

Ishii, M., Paranjape, S. S., Kim, S., and Sun, X. 2004. Interfacial Structures and Interfacial Area Transport in Downward Two-phase Bubbly Flow. *International Journal of Multiphase Flow* **30** (7): 779-801. http://dx.doi.org/10.1016/j.ijmultiphaseflow.2004.04.009

Jeyachandra, B. 2011. *Effect of Pipe Inclination on Flow Characteristics of High Viscosity Oil-gas Two-phase Flow.* M.S. Thesis, University of Tulsa, Tulsa, OK.

Kim, S., Paranjape, S. S., Ishii, M., and Kelly, J. 2003. Interfacial Structures and Regime Transition in Co-current Downward Bubbly Flow. In ASME/JSME 2003 4th Joint Fluids Summer Engineering Conference, *American Society of Mechanical Engineers*, Honolulu, Hawaii, 6-10 July. http://dx.doi.org/10.1115/FEDSM2003-45541

Kora, C. 2010. *Effect of High Oil Viscosity on Slug Liquid Holdup in*

Horizontal Pipes. MS Thesis, University of Tulsa, Tulsa, OK.

Mukherjee, H. 1979. *An Experimental Study of Inclined Two-phase Flow.* PhD Dissertation, University of Tulsa, Tulsa, OK.

Mukherjee, H. and Brill, J.P. 1985. Empirical Equations to Predict Flow Patterns in Two-phase Inclined Flow. *International Journal of Multiphase Flow* **11** (3): 299-315. http://dx.doi.org/10.1016/0301-9322(85)90060-6

Nädler, M., and Mewes, D. 1995. Effects of the Liquid Viscosity on the Phase Distributions in Horizontal Gas-liquid Slug Flow. *International Journal of Multiphase Flow* **21** (2): 253-266. http://dx.doi.org/10.1016/0301-9322(94)00067-T

Nuland, S., Malvik, I., Valle, A., and Hende, P. 1997. Gas Fractions in Slugs in Dense-gas Two-phase Flow from Horizontal to 60 Degrees of Inclination. *Proceedings of the ASME Fluids Eng. Div. Summer Meeting*, 22-26 June.

Oshinowo, T. and Charles, M. E. 1974(a). Vertical Two-phase Flow: Part I. Flow Pattern Correlations. *The Canadian Journal of Chemical engineering* **52** (1): 25-35. http://dx.doi.org/10.1002/cjce.5450520105

Oshinowo, T. and Charles, M. E. 1974(b). Vertical Two-phase Flow: Part II. Holdup and Pressure Drop. *The Canadian Journal of Chemical Engineering* **52** (4): 438-448. http://dx.doi.org/10.1002/cjce.5450520402

Picard, A. Davis, R. S. Glaser, M. and Fujii, K. 2008. Revised Formula for the Density of Moist Air (CIPM-2007). *Metrologia* **45**: 149-155. http://dx.doi.org/10.1088/0026-1394/45/2/004

Ros, N.C.J. 1961. Simultaneous Flow of Gas and Liquid as Encountered in Well Tubing. *Journal of Petroleum Technology* **13** (10): 1037-1049. SPE-18-PA. http://dx.doi.org/10.2118/18-PA

Rosa, E.S. and Netto, J.R.F. 2004. Viscosity Effect and Flow Development in Horizontal Slug Flows. Paper 306 presented at 5th International Conference on Multiphase Flow, Yokohama, Japan, 30 May-4 June.

Taitel, Y., and Barnea, D. 1990. Two-phase Slug Flow. *Advances in Heat Transfer* **20**: 83-132.

Troniewski, L. and Spisak W. 1987. Flow Patterns in Two-phase Downflow of Gas and Very Viscous Liquid. *International Journal of Multiphase Flow* **13** (2): 257-260. http://dx.doi.org/10.1016/0301-9322(87)90033-4

Usui, K. and Sato, K. 1989. Vertically Downward Two-phase Flow, (I). *Journal of Nuclear Science and Technology* **26**(7): 670-680. http://dx.doi.org/10.1080/18811248.1989.9734366

Usui, K. 1989. Vertically Downward Two-phase Flow, (II). *Journal of Nuclear Science and Technology*, **26**(11): 1013-1022. http://dx.doi.org/10.1080/18811248.1989.9734422

Wang, S., Zhang, H.-Q., Sarica, C., and Pereyra, E. 2014. A Mechanistic Slug-liquid-holdup Model for Different Oil Viscosities and Pipe-inclination Angles. *SPE Production & Operations* **29** (4): 329–336. SPE-171563-PA. http://dx.doi.org/10.2118/171563-PA

Wallis, G.B. 1969. *One-dimensional Two-phase Flow.* NY, USA: McGraw-Hill Book Co. Inc.

Yamazaki, Y. and Yamaguchi, K. 1979. Characteristics of Cocurrent Two-Phase Downflow in Tubes: Flow Pattern, Void Fraction and Pressure Drop. *Journal of Nuclear Science and Technology* **16**(4): 245-255. http://dx.doi.org/10.1080/18811248.1979.9730898

Zadrazil, I., Matar, O. K., and Markides, C. N. 2014(a). An Experimental Characterization of Downwards Gas–liquid Annular Flow by Laser-induced Fluorescence: Flow Regimes and Film

Statistics. *International Journal of Multiphase Flow* **60**: 87-102. http://dx.doi.org/10.1016/j.ijmultiphaseflow.2013.11.008

Zadrazil, I. and Markides, C. N. 2014(b). An Experimental Characterization of Liquid Films in Downwards Co-current Gas–liquid Annular Flow by Particle Image and Tracking Velocimetry. *International Journal of Multiphase Flow* **67**: 42-53. http://dx.doi.org/10.1016/j.ijmultiphaseflow.2014.08.007

Zhang, H.-Q., Wang, Q., Sarica, C., and Brill, J.P. 2003(a). Unified Model for Gas Liquid Pipe Flow via Slug Dynamics – Part 1: Model Development. *J. Energy Res, Tech*. **125** (4): 266-273. http://dx.doi.org/10.1115/1.1615246

Zhang, H.-Q., Wang, Q., Sarica, C., and Brill, J.P. 2003(b). Unified Model for Gas Liquid Pipe Flow via Slug Dynamics - Part 2: Model Validation. *J. Energy Res, Tech*. **125** (4): 274-283. http://dx.doi.org/10.1115/1.1615618

요약 (국문초록)

이 연구는 수직 하방관에서 고점성도 오일-가스 2상 유동의 특징을 실험적으로 분석한다. 해상 중질유 처리시설의 해저 배관망에서 일어나는 해당 유동의 압력 구배, 평균 액체 점유율 등의 예측은 생산 시설 설계 및 용량 결정 과정에서 대단히 중요하다.

이전의 실험들은 대부분 저, 중점성도 유체에 대한 평가이므로 고점성도 오일의 경우 유동 특성 및 인자 예측의 정확도에 대한 검증이 필요하다. 따라서 본 연구에서는 수직 2인치 관과 고점성도 오일을 이용하여 오일 점성도에 따른 유동 패턴, 압력 구배, 평균 액체 점유율 등의 변화 양상을 실험하였다. 서로 다른 4가지 오일 점성도(586 mPa·s, 337 mPa·s, 213 mPa·s, 127 mPa·s)와 지정된 범위 내의 공탑 액체 속도(0.05 m/s ~ 0.7 m/s), 공탑 기체 속도(0.3 m/s ~ 8.0 m/s)를 사용하였다.

실험을 통해 세 종류의 유동 패턴(Falling Film, Wavy Annular, Liquid Slip)을 관찰하였으며 각각의 유동패턴이 갖는 압력구배 및 평균 액체 점유율 등의 특징과 이에 대한 점성도의 영향을 분석하였다. 나아가 본 연구에서는 측정된 결과와 기존의 2상 유동 예측 모델들을 통해 예측한 결과를 정량적으로 비교하였다. 기존 모델들은 대부분의 유동 조건에 대해 슬러그 유동 패턴을 예측하고,

낮은 점성도 오일 조건에서 평균 액체 점유율을 크게 과대평가하는 경향을 확인하였다.

기존 모델들의 적용성을 평가하기 위해 본 연구에서는 저점성도 수직 하방 환상유동 및 고점성도 수직 상방 환상유동 실험 데이터와의 비교를 통해 환상유동의 유동 예측 모델에 사용되는 관계식의 예측성능을 평가하였다. 연구 결과 기존 환상유동 모델에 사용되는 관계식들은 고점성도 유체의 수직 상방유동에 대해 만족할만한 결과를 보여주나 수직 하방 유동에 대해서는 가스 코어 내의 액체 침투율을 과소평가하는 결과를 보여주었다. 이 연구는 해상 중질유 필드의 원유 처리시설 설계 자료로 활용될 수 있는 기술로 기대된다.

주요어: 2상유동, 수직하방유동, 고점성도, 관내유동, 유동패턴, 압력구배, 평균액체점유율

학 번: 2010-30260